FORSCHUNGSZENTRUM ROSSENDORF FZR

WISSENSCHAFTLICH-TECHNISCHE BERICHTE
**FZR-303**
November 2000
ISSN 1437-322X



*Valery Nikolajevich* ***Chochlov***, *Andrej Vsjevolodovich* ***Duncev***,
*Vadim Vladimirovich* ***Ivanov***, *Vladimir Valentinovich* ***Kontelev***,
*Vladimir Ivanovich* ***Melnikov***, *Leonid Karlovich* ***Stoppel***,
*Horst-Michael* ***Prasser***, *Winfried* ***Zippe***,
*Jochen* ***Zschau***, *Robert* ***Zboray***

# Local and integral ultrasonic gauges for two-phase flow instrumentation in nuclear reactor and safety technology

***BMWi Project 150 1097***

Herausgeber:
FORSCHUNGSZENTRUM ROSSENDORF
Postfach 51 01 19
D-01314 Dresden
Telefon +49 351 26 00
Telefax +49 351 2 69 04 61
http://www.fz-rossendorf.de/

Als Manuskript gedruckt

FORSCHUNGSZENTRUM ROSSENDORF
WISSENSCHAFTLICH-TECHNISCHE BERICHTE
**FZR-303**
November 2000

*Valery Nikolajevich* ***Chochlov****, Andrej Vsjevolodovich* ***Duncev****,*
*Vadim Vladimirovich* ***Ivanov****, Vladimir Valentinovich* ***Kontelev****,*
*Vladimir Ivanovich* ***Melnikov****, Leonid Karlovich* ***Stoppel***[1)]*,*
*Horst-Michael* ***Prasser****, Winfried* ***Zippe****,*
*Jochen* ***Zschau***[2)]*, Robert* ***Zboray***[3)]

# Local and integral ultrasonic gauges for two-phase flow instrumentation in nuclear reactor and safety technology

**BMWi Project 150 1097**

[1)] *Technical State University of Nishny Novgorod, Russian Federation*
[2)]*Forschungszentrum Rossendorf e.V. Institute of Safety Research*
[3)]*Delft University of Technology, Interfaculty Reactor Institute*

**The reported work was carried out in the frame of a research project funded by the Federal Ministry of Education, Science, Research and Technology under the project number 150 1097. The authors are responsible for the content of this report.**

## Berichtsblatt

| 1. ISBN oder ISSN | 2. Berichtsart<br>Schlussbericht |
|---|---|

3a. Titel des Berichts
Local and integral ultrasonic gauges for two-phase flow instrumentation in the nuclear reactor and safety technology

3b. Titel der Publikation

4a. Autoren des Berichts (Name, Vorname(n))
**Chochlov**, Valery Nikolajevich, **Duncev**, Andrej Vsjevolodovich, **Ivanov**, Vadim Vladimirovich, **Kontelev**, Vladimir Valentinovich, **Melnikov**, Vladimir Ivanovich, **Stoppel**, Leonid Karlovich, **Prasser**, Horst-Michael, **Zboray**, Robert, **Zippe**, Winfried, **Zschau**, Jochen

4b. Autoren der Publikation (Name, Vorname(n))

5. Abschlussdatum des Vorhabens
31.05.2000

6. Veröffentlichungsdatum
November 2000

7. Form der Publikation
Broschüre

8. Durchführende Institution(en) (Name, Adresse)

Forschungszentrum Rossendorf e.V.
Institut für Sicherheitsforschung
Postfach 510119
01314 Dresden

9. Ber.Nr. Durchführende Institution

10. Förderkennzeichen *)
150 1097

11a. Seitenzahl Bericht
81

11b. Seitenzahl Publikation

13. Fördernde Institution (Name, Adresse)

Bundesministerium für Wirtschaft (BMWi)
11019 Berlin

12. Literaturangaben
25

14. Tabellen
2

15. Abbildungen
83

16. Zusätzliche Angaben

17. Vorgelegt bei (Titel, Ort, Datum)

18. Kurzfassung
Das vorliegende Projekt wurde im Rahmen einer Kooperationsvereinbarung zwischen dem Forschungszentrum Rossendorf (FZR) und der wissenschaftlichen Gruppe von Prof. Melnikov von der Technischen Universität Nishny Novgorod (TUNN) der Russischen Föderation durchgeführt. Es ist Teil des Wissenschaftsunterstützungsprogramms / FSU der Bundesregierung im Rahmen der Beratungshilfe für den Aufbau von Demokratie und sozialer Marktwirtschaft (TRANSFORM). Neue Methoden der Instrumentierung für Zweiphasenströmungen wurden entwickelt: Ultraschall-Wellenleitersonden können zur lokalen Gas- bzw. Dampfgehaltsmessung eingesetzt werden. Der neue Ultraschall-Gittersensor erlaubt eine Visualisierung der Zweiphasenströmung mit ca. 250 Bildern/ Sekunde. Sowohl die lokalen Sonden als auch der Ultraschall-Gittersensor können erfolgreich unter den Bedingungen von Wasser-Dampf-Gemisch bei hohem Druck und hoher Temperatur, sowie in anderen Fluiden, wie organischen Flüssigkeiten und Kältemitteln, eingesetzt werden. Darüber hinaus wurden berührungslos arbeitende Wellenleitersonden für die Durchschallung von Rohrleitungen und Dichtesensoren, die auf der Messung der Ausbreitungsgeschwindigkeit von Ultraschall in Wellenleitern beruhen, die sich im Messmedium befinden, entwickelt und getestet. Bei dem gegenwärtigen Stand der Entwicklung können die berührungslosen Sensoren als qualitativer Nachweis von Gas in einer Flüssigkeitsströmung dienen. Die Funktion der Dichtesensoren wurde anhand von Messungen in verschiedenen einphasigen Flüssigkeiten unterschiedlicher Dichte demonstriert. Für einen praktischen Einsatz ist die weitere Verbesserung der elektronischen Signalerfassung erforderlich. Die hauptsächliche Innovation wird durch den Ultraschall-Gittersensor verkörpert, dessen Auflösung mit der von schnellen elektrischen Gittersensoren und ultraschnellen Röntgentomographen vergleichbar ist, während das Gerät selbst sehr robust und preiswert ist.

19. Schlagwörter
Ultraschallsensoren, Zweiphasenmesstechnik, Gasgehalt, Dampfgehalt, Visualisierung

20. Verlag

21. Preis

## Document Control Sheet

| 1. ISBN or ISSN | 2. Type of Report<br>Final Report |
|---|---|

3a. Report Title
Local and integral ultrasonic gauges for two-phase flow instrumentation in the nuclear reactor and safety technology

3b. Title of Publication

| 4a. Author(s) of the Report (Family Name, First Name(s)) | 5. End of Project<br>31.05.2000 |
|---|---|
| **Chochlov**, Valery Nikolajevich, **Duncev**, Andrej Vsjevolodovich, **Ivanov**, Vadim Vladimirovich, **Kontelev**, Vladimir Valentinovich, **Melnikov**, Vladimir Ivanovich, **Stoppel**, Leonid Karlovich, **Prasser**, Horst-Michael, **Zboray**, Robert, **Zippe**, Winfried, **Zschau**, Jochen | 6. Publication Date<br>November 2000 |
| 4b. Author(s) of the Publication (Family Name, First Name(s)) | 7. Form of Publication<br>Booklet |
| 8. Performing Organisation(s) (Name, Address)<br>Forschungszentrum Rossendorf e.V.<br>Institut für Sicherheitsforschung<br>Postfach 510119<br>01314 Dresden | 9. Originator's Report No.<br>10. Reference No.)<br>150 1097<br>11a. No. of Pages Report<br>81<br>11b. No. of Pages Publication |
| 13. Sponsoring Agency (Name, Address)<br>Bundesministerium für Wirtschaft (BMWi)<br>11019 Berlin | 12. No. of References<br>25<br>14. No. of Tables<br>2<br>15. No. of Figures<br>83 |
| 16. Supplementary Notes | |
| 17. Presented at (Title, Place, Date) | |

18. Abstract

The present project was executed in the frame of a co-operation agreement between FZR and the scientific group of Prof. Melnikov of the Technical University of Nishny Novgorod (TUNN) in the Russian Federation. It is part of the Federal Government's programme for the provision of advice for Eastern Europe on the building up of democracy and social market economy (TRANSFORM Programme). New methods of two-phase flow instrumentation were developed: Intrusive wave-guide probes can be used for local void fraction measurements. The new ultrasonic mesh sensors allow a fast two-phase flow visualisation with about 250 frames per second. Experiments carried out at the test loop in Rossendorf, but also the tests at the DESIRE facility in Delft have shown that both local wave-guide probes and ultrasonic mesh sensors can be successfully applied under the conditions of high pressure and temperature steam-water mixture, as well as in organic liquids and refrigerants. Furthermore, non-intrusive wave-guide sensors as well as density sensors based on the measurement of the wave propagation velocity in wave-guides immersed into the measuring liquid were developed and tested. In the present stage of the development, the non-intrusive sensors can rather be used for a qualitative gas respectively level detection than for void fraction measurements. The wave-guide density sensor was successfully demonstrated that it is able to measure densities of single-phase liquids. It requires further development of the electronic circuitry. The main innovation was achieved by the development of the ultrasonic mesh sensor, the resoluting capability of which is comparable to methods like electrical wire-mesh sensors and ultra-fast X-ray tomography, while the device itself is robust and low expensive.

19. Keywords
Ultrasonic sensors, two-phase flow instrumentation, gas fraction, void fraction, visualisation

| 20. Verlag | 21. Preis |
|---|---|

V. N. Chochlov, A. V. Duncev, V. V. Ivanov, V. V. Kontelev, V. I. Melnikov,
L. K. Stoppel, H.-M. Prasser, W. Zippe, J. Zschau, R. Zboray

# Lokale und integrale Ultraschallsonden für Zweiphasenströmungen in der Reaktor- und Sicherheitstechnik

## Kurzfassung

## 1 Einleitung

Das vorliegende Projekt wurde im Rahmen einer Kooperationsvereinbarung zwischen dem Forschungszentrum Rossendorf (FZR) und der wissenschaftlichen Gruppe von Prof. Melnikov von der Technischen Universität Nishny Novgorod (TUNN) der Russischen Föderation durchgeführt. Es ist Teil des Wissenschaftsunterstützungsprogramms / FSU der Bundesregierung im Rahmen der Beratungshilfe für den Aufbau von Demokratie und sozialer Marktwirtschaft (TRANSFORM). Das wissenschaftliche Ziel der Vorhabens ist die Entwicklung von teils intrusiven, teils berührungslosen Ultraschallmessverfahren zur Charakterisierung von Zweiphasenströmungen. Die Messverfahren sollen für Forschungsarbeiten auf dem Gebiet der Kernenergie und der Sicherheitstechnik genutzt werden. Folgende neue Methoden der Instrumentierung für Zweiphasenströmungen wurden entwickelt:

- Dichtesensoren, die auf der Messung der Ausbreitungsgeschwindigkeit von Ultraschall in Wellenleitern beruhen,
- Ultraschall-Wellenleitersonden zur lokalen Gas- bzw. Dampfgehaltsmessung,
- Lokale Einpunktsonden, bei denen ein einzelner Wellenleiter gleichzeitig als Ultraschallsender und -empfänger fungiert,
- Berührungslos arbeitende Wellenleitersonden für die Durchschallung von Rohrleitungen
- Ultraschall-Gittersensoren zur Visualisierung der Zweiphasenströmung.

Die hauptsächliche Innovation wird durch den Ultraschall-Gittersensor verkörpert, dessen Auflösung mit der von schnellen elektrischen Gittersensoren und ultraschnellen Röntgentomographen vergleichbar ist, während das Gerät selbst sehr robust und preiswert ist.

Neben den unmittelbaren wissenschaftlich-technischen Ergebnissen gelang es, die Gruppe von Prof. Melnikov wesentlich zu unterstützen. So wurden innerhalb des Bearbeitungszeitraums wurden zwei Promotionen abgeschlossen, die mit den Arbeiten in Verbindung stehen. Diese sind:

Kontelev, Vladimir Valentinovitsch: Entwicklung und Untersuchung eines Ultraschall-Wellenleitersystems für die Visualisierung einer Zweiphasenströmung, Nishny Novgorod, Juni 1999,

Stoppel, Leonid Karlovitsch, Erarbeitung eines Systems für die Diagnose einer feindispersen Wasserdampf-Strömung in kerntechnischen Analgen, Nishny Novgorod, Juni 2000.

Weiterhin gelang es, flankierende Fördermittel einzuwerben. Herr Stoppel erhielt ein DAAD-Stipendium für einen 12-monatigen Arbeitsaufenthalt in Rossendorf, der von Oktober 1998 bis September 1999 im Vorfeld der Fertigstellung seiner Dissertation stattfand. Für einen dreimonatigen Studienaufenthalt von Herrn Kontelev wurde seitens der NATO über die Vermittlung durch DAAD ein Stipendium bewilligt. Dieser Aufenthalt wird vom September bis November 2000 stattfinden und die Weiterführung von Experimenten mit dem neuen Ultraschall-Gittersensor zum Gegenstand haben.

Ein weiterer dreimonatiger Gastaufenthalt wurde für Herrn Dunzev vermittelt, der am IPM, einem An-Institut der Hochschule für Technik, Wirtschaft und Sozialwesen Zittau/Görlitz stattfinden wird, und für den es gelang, Mittel vom Sächsischen Staatsministerium für Wissenschaft und Kunst zu erhalten. Dabei geht es um die Anwendung von Wellenleiter-Sensoren zur Füllstandsmessung in Druckbehältern.

Die Zusammenarbeit zwischen dem FZR und der Gruppe von Professor Melnikov haben zu weitergehenden fachlichen Kontakten geführt. Gemeinsam mit der Abteilung Magnetohydrodynamik des Instituts für Sicherheitsforschung wurde mit der Entwicklung von berührungslos arbeitenden Ultraschallverfahren zur Messung der Geschwindigkeitsverteilung in einphasigen Flüssigmetallströmungen begonnen. Es hat sich ein Kontakt mit dem Ingenieurbüro Robert Eschrich in Pirna bei Dresden entwickelt, bei dem es um den Nachweis und die Massenbestimmung von Staubpartikeln in Gasströmen mit Hilfe passiver Ultraschallaufnehmer geht.

Das Projekt hat im Sinne der Ziele des Wissenschaftsunterstützungsprogramms / FSU der Bundesregierung im Rahmen der Beratungshilfe für den Aufbau von Demokratie und sozialer Marktwirtschaft (TRANSFORM) zur sozialen Absicherung der Wissenschaftlergruppe um Professor Melnikov beigetragen.

## 2 Dichtesensor auf Basis von Wellenleitern

Der Dichtesensor arbeitet nach dem Prinzip der Messung der Ausbreitungsgeschwindigkeit von Transversalwellen in einem im Messmedium eingetauchten Ultraschall-Wellenleiter (Bild 1). Ein Wellenleiter wird hierzu durch einen Piezo-Umformer zu longitudinalen Schwingungen angeregt. Die Welle trifft auf eine T-Verbindung, wo eine Mode-Transformation zu Transversalwellen erfolgt, die ein schleifenförmiges sensitives Element umlaufen, um danach schließlich wieder in eine Longitudinalwelle umgeformt zu werden. Beide Mode-Umwandlungen an der T-Verbindung führen zu Signalreflektionen, die vom Piezokristall aufgenommen werden. Die nachfolgende Signalverarbeitung ermittelt die Zeitdifferenz zwischen den beiden Reflektionen, die sich aus der Laufzeit der Transversalwelle im sensitiven Element (Wellenleiter-Schleife) ergibt.

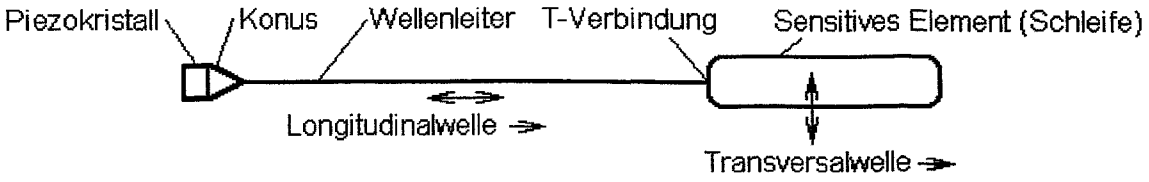


Bild 1 Prinzipskizze des Dichtesensors auf Basis von Wellenleitern

Wird das sensitive Element in das Messmedium eingetaucht, dann verringert sich die Ausbreitung der Transversalwellen in der Wellenleiter-Schleife. Die Zeitdifferenz ist damit ein direktes Maß für die Dichte. Die Funktion des Sensors wurde durch Kalibrierung mit verschiedenen Flüssigkeiten nachgewiesen.

## 3 Invasive lokale Gasgehaltssensoren auf Basis von Wellenleitern

Die lokale Wellenleitersonde besteht aus zwei parallel in das Messmedium eingeführte Wellenleiter (Bild 2), deren Enden sich in einem geringen Abstand gegenüberstehen und die das sensitive Element (Messvolumen) darstellen. Einer der Wellenleiter wird durch einen Piezo-Umwandler angeregt. Der Ultraschall wird in das Messmedium emittiert und vom zweiten Wellenleiter aufgenommen, wenn sich flüssige Phase im Messvolumen befindet. Bei Vorhandensein der Gasphase wird das Ultraschallsignal unterbrochen. Durch Auswertung der Signalunterbrechungen (s. Bild 2, typische Signalform) wird im Fall einer Zweiphasenströmung der lokale volumetrische Gasanteil ermittelt.

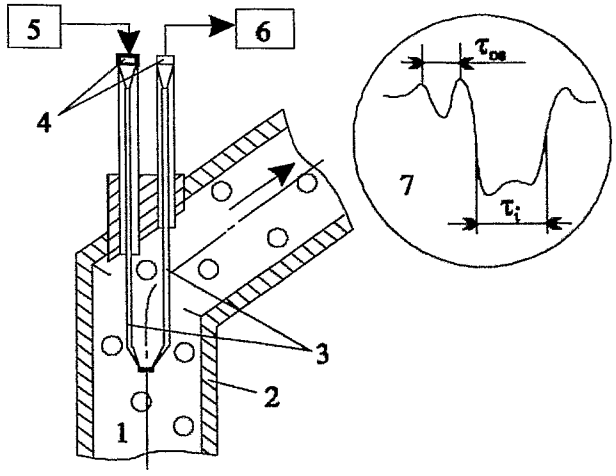


Bild 2 Lokale Gasgehaltssonde auf Basis von Ultraschall-Wellenleitern

1 - Zweiphasenströmung, 2 - Rohrwand, 3 - Wellenleiter, 4 - Piezo-Umformer, 5 - Pulsgenerator, 6 - Signalverarbeitungseinheit, 7 - typische Impulsform

Der Sensor wurde an der Zweiphasen-Testschleife des FZR umfangreichen Tests unterzogen. Dabei wurde in weiten Bereichen der Volumenstromdichten von Wasser und Luft eine gute Übereinstimmung der Messwerte mit anderen Messverfahren festgestellt (Gittersensoren, Gamma-Durchstrahlung). Der Sensor wurde weiterhin in Kältemittel (R12) getestet. Hierzu wurden erfolgreich Messungen im Zugschacht der DESIRE-Anlage des IRI Delft durchgeführt.

Für die lokale Wellenleitersonde wurde weiterhin eine neuartige Signalauswertungsmethode entwickelt, die die Messung von Gasgehalten und Blasendurchmessern in sehr feindispersen Zweiphasenströmungen ermöglicht. Die Methode wurde an der mit einem Generator für kleine Blasen (< 1 mm) ausgestatteten Testschleife erprobt.

Die Wechselwirkung der Sonde mit Gasblasen wurde mit Hilfe einer Hochgeschwindigkeits-Videokamera studiert. Die Signale wurden mit den Messergebnissen eines Laser-Doppler-Anemometers und eines Phasen-Doppler-Partikelanalysators verglichen.

Für die Messung von Gasanteilen mit der lokalen Wellenleitersonde stehen folglich zwei Signalverarbeitungsmethoden zur Verfügung: Bei Blasen, deren Abmessungen die der Sondenspitze übersteigen, werden die einzelnen Ereignisse ausgewertet, bei denen eine Blase die Sondenspitze umschließt und zu einer Unterbrechung des Ultraschallsignals führt. Bei kleinen Bläschen, deren Abmessungen die der Sonde wesentlich unterschreiten, ist es möglich, Gasgehalt und mittlere Blasengröße durch eine statistische Auswertung der Fluktuationen des Ultraschallsignals zu ermitteln. Beide Verfahren wurden hinsichtlich ihrer Genauigkeit und der Beeinflussung der Strömung durch die invasive Sonde detailliert untersucht.

## 4 Lokale Ultraschall-Einpunktsonde

Der Versuch, eine Wellenleitersonde zur lokalen Messung von Gasgehalten zu entwickeln, die mit nur einem Wellenleiter auskommt, der sowohl als Sender als auch als Empfänger arbeitet, hat bislang nicht zum Erfolg geführt. Im Rahmen des Vorhabens gelang zunächst die Geschwindigkeitsmessung in einer Einphasenströmung mit einer solchen Sonde. Die Experimente hierzu wurden an der Natrium-Testschleife NATAN des FZR durchgeführt. Dabei wurde der Dopplereffekt zur Bestimmung des Geschwindigkeitsprofils in der Flüssigmetallströmung angewandt. Die Verwendung einer neuartigen Wellenleiterkonstruktion erlaubt die Verwendung hoher Ultraschallfrequenzen unter günstigen Ankoppelbedingungen an die Rohrleitung.

## 5 Nichtinvasive Durchschallungssensoren

Eine nichtinvasive Überwachung der Strömungsverhältnisse in einer Rohrleitung ist durch Ankopplung von Ultraschall-Wellenleitern von außen an die Rohrwand möglich. Durch die Verwendung der Wellenleiter ist der Einsatz weitgehend unabhängig von den Parametern des Messmediums, wodurch z.B. eine Anwendung bei hohen Temperaturen möglich wird. Die Gasgehaltsmessung beruht auf der Schwächung der Ultraschallamplitude entlang der Durchstrahlungssehne zwischen zwei schräg gegenüberliegend angebrachten Aufnehmern.

Die Testmessungen mit diesen Sensoren zeigten, dass das Ultraschallsignal bereits bei Gasgehalten um 10-12 % vollständig abgeschirmt wird. Damit ist das Verfahren nur bei kleineren Gasgehalten zur quantitativen Bestimmung des Gasanteils geeignet. Hierbei muss jedoch auch eine gewisse Abhängigkeit der Dämpfung von der Blasengröße in Kauf genommen werden, was zu zusätzlichen Messfehlern führt. Bei dem gegenwärtigen Stand der Entwicklung können die berührungslosen Sensoren lediglich als qualitativer Nachweis von Gas in einer Flüssigkeitsströmung empfohlen werden.

## 6 Ultraschall-Gittersensoren zur Strömungsvisualisierung

Aufbauend auf der lokalen Wellenleitersonde wurde ein neuartiger Gittersensor entwickelt, der den Strömungsquerschnitt einer Rohrleitung der NW50 mit einer Auflösung von 8 x 8 Punkten überwacht (Bild 3a). Er erlaubt die Bestimmung der Gasgehaltsverteilung im Strömungsquerschnitt. Eine tomographische Bildrekonstruktion ist beim verwendeten Meßprinzip nicht erforderlich. Der Ultraschall-Gittersensor wurde an der Zweiphasen-Testschleife des FZR in einer Luft-Wasser- und einer Dampf-Wasser-Strömung erprobt. Die Signale wurden mit dem elektrischen Gittersensor des FZR verglichen. Der Ultraschall-Gittersensor kann mit einer Messfrequenz von 250 Hz betrieben werden. Der Sensor zeigt im Vergleich zum elektrischen Drahtgittersensor qualitativ vergleichbare momentane Gas- bzw. Dampfgehaltsverteilungen. So werden z.B. die Gaspfropfen in einer Pfropfenströmung gut wiedergegeben. Die Auflösung ist jedoch deutlich geringer, als beim elektrischen Gittersensor. Der Hauptvorteil besteht darin, daß der Ultraschallsensor auch in elektrisch nichtleitenden Fluiden (z.B. in Versuchsanlagen mit Kältemittel) eingesetzt werden kann. Eine quantitative Aussage über die Messgenauigkeit wurde durch Vergleich der mittleren volumetrischen Gas- bzw. Dampfgehalte erhalten. Hierbei zeigte es sich, dass der Ultraschall-Gittersensor die tatsächlichen Gasgehalte unterbewertet. Dies wird hauptsächlich durch Wassertropfen verursacht, die zwischen den Sender- und Empfängerwellenleitern festsitzen. Der Messfehler wurde in entsprechenden Kalibrierversuchen ermittelt.

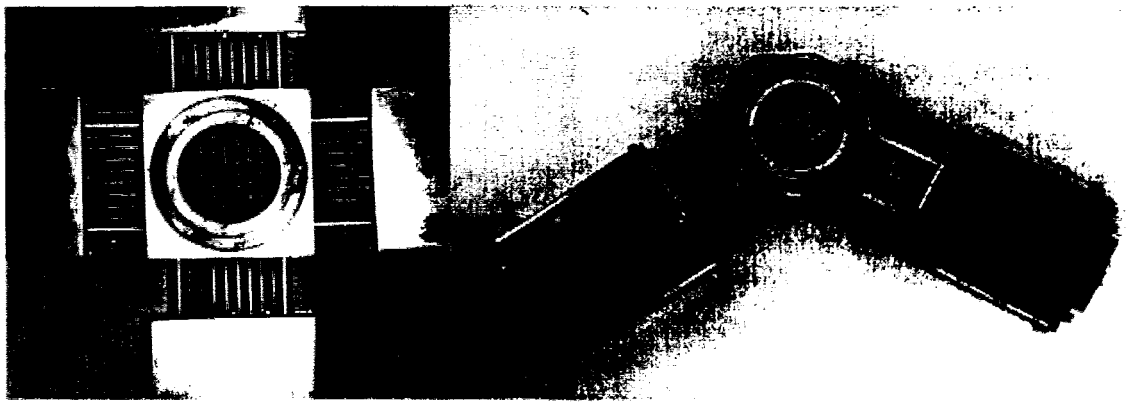

**A** **B**

Bild 3 Ultraschall-Gittersensoren, A - Prototyp, B - verbesserte Variante

Bereits am ersten Labormuster wurde die volle Funktionsfähigkeit des Gerätes nachgewiesen. Im weiteren wurde eine zweite Variante für die Konstruktion der Wellenleiter erarbeitet (Bild 3b), die eine Verbesserung des Be- und Entnetzungsverhaltens ermöglicht und somit zu einer Verringerung der Messfehler führt. Es wurde eine Erprobung des verbesserten Ultraschall-Gittersensors an der Zweiphasen-Testschleife im FZR in einer Wasser-Dampf-Strömung bei 225 °C und 2.5 MPa vorgenommen. Der Sensor war im gesamten Parameterbereich voll funktionsfähig.

Mit dem Sensor wird eine beachtliche Strömungsvisualisierung erreicht, die derzeit nur durch die Leitfähigkeits-Gittersensoren des FZR und die in Japan entwickelte, sehr aufwendige Hochgeschwindigkeits-Röntgentomographie überboten wird. Der Sensor hat bei bestimmten Anwendungen eine Reihe von Vorzügen gegenüber dem Leitfähigkeits-Gittersensor: (1) geringer Aufwand, (2) hohe Druck- und Temperaturfestigkeit, (3) Beständigkeit gegenüber vielen aggressiven Fluiden, (4) Anwendbarkeit bei elektrisch nichtleitenden Fluiden (Kohlenwasserstoffe, Öl o.ä.).

Zur Demonstration der Leistungsfähigkeit des Sensors zeigt Bild 4 eine Visualisierung einer Pfropfenströmung in der vertikalen Testsektion der Zweiphasen-Testschleife des FZR bei Luft-Wasser-Betrieb. Verglichen werden sogenannte virtuelle Schnittbilder, die durch Abtragen von momentanen, radialen Gasgehalteverteilungen als Zeitsequenzen entstehen. Zum Vergleich wurde eine virtuelle Schnittansicht hinzugefügt, die mit einem elektrischen Gittersensor des FZR erhalten wurde (im Bild rechts).

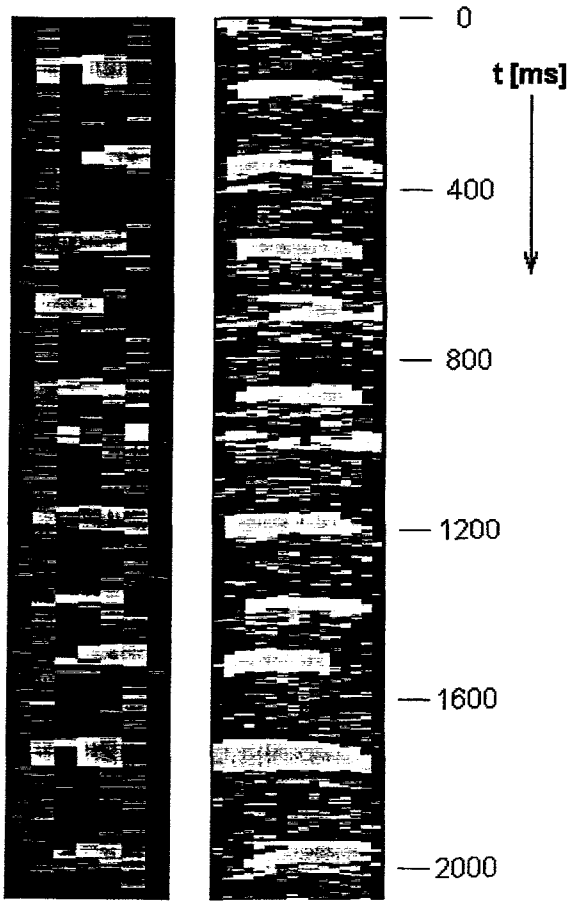


Bild 2: Visualisierung einer Pfropfenströmung, Ultraschall-Gittersensor (links), Leitfähigkeits-Gittersensor (rechts)

## Content

# 1. Introduction

The scientific goal of the project was to develop intrusive and non-intrusive measuring methods for the characterisation of a two-phase flow, which are based on the application of ultrasound. The developed measuring techniques shall be used for scientific work in the field of nuclear reactors and safety technology.

The project was executed in the frame of a co-operation agreement between FZR and the scientific group of Prof. Melnikov of the Technical University of Nishny Novgorod (TUNN) in the Russian Federation. It is part of the Federal Government's programme for the provision of advice for Eastern Europe on the building up of democracy and social market economy (TRANSFORM Programme).

In particular, three different ways of applying ultrasound to obtain measuring information from a two-phase flow (gas-liquid dispersion) were planned to be investigated: (1) a density measurement by registering the speed of transversal waves travelling along a wave guide submerged into the flowing medium, (2) local void probes based on acoustic impedance and (3) ultrasound through-transmission of the flow channel by external transducers (non-intrusive method).

In the course of the execution of the project, the work was concentrated on the use of local probes based on wave guides that have to be emerged into the fluid. These probes were tested in air-water, steam-water and a two-phase freon (R12) flow. Advanced statistic signal processing allows to measure not only bubbles with dimensions greater than the sensitive part of the probe, but also small bubbles in the range of micrometers.

One of the most important results is an ultrasonic mesh sensor for a high-speed visualisation of a two-phase flow. The sensor effectively combines several local ultrasonic probes to an array surveying the entire cross section of a pipe. It delivers sequences of two-dimensional gas fraction distributions with a rate of 200 - 250 frames per second. The use of the ultrasound wave guide technology allows to manufacture all parts of the sensor which contact the fluid from stainless steel. Compared to the electrical wire-mesh sensors developed by Forschungszentrum Rossendorf, the sensor has the advantage that it can be operated in non-conducting fluids, such as refrigerants, but also in alkanes and similar organic compounds in chemical facilities.

The attempts to create non-intrusive instrumentation for a two-phase flow did not show the expected success. After tests at the two-phase flow loop in the Institute of Safety Research, some measurements using an ultrasonic through-transmission were performed in the frame of another project [1.1] with a limited success. An application of a new type of high-frequency wave-guides, on the other hand, offers a promising possibility to a non-intrusive measurement of velocity distributions in a single-phase liquid metal flow.

The TRANSFORM project contributed significantly to strengthen the capabilities of the scientific group of Professor Melnikov. It provided an important social support to the scientists participating on the Russian side. Furthermore, it helped to educate young scientists and to deepen the scientific co-operation between the group of Professor Melnikof and the Institute of Safety Research of FZR. In the course of the project, two PhD thesis works were completed and successfully defended [1.2, 1.3]. One of the PhD students was working for a year in the Forschungszentrum Rossendorf,

where he performed experiments to calibrate local ultrasonic wave-guide probes. This stay was funded by a DAAD grant. The co-operation between the group of Professor Melnikov and FZR will be continued. The next joint activity is a three-months post-graduated study of one of the staff members of the group of Professor Melnikov funded by NATO to continue the development of the ultrasonic mesh sensors to finalise the device.

**References:**


[1.1] H.-M. Prasser, A. Böttger, J. Zschau: Development of two-phase measuring techniques for comparative investigations of transient flows in pipelines (in German), final report FZR-233, BMBF reserach project 11ZF9504/1, August 1998.

[1.2] V. V. Kontelev: Development and investigation of an ultrasonic wave-guide system for the visualisation of a two-phase flow (in Russian), PhD thesis work, Nishny Novgorod, June 1999

[1.3] L. K. Stoppel: Elaboration of a diagnostic system for a finely dispersed steam-water flow in nuclear installations (in Russian), PhD thesis work, Nishny Novgorod, June 2000.


## 2. Waveguide density sensor

This part of the report is dedicated to development of new wave-guide density sensor. It is applicable to measure the density of aggressive liquids as well as the density of a two-phase flow. The sensor is based on the change of the acoustic impedance of a wave-guide emerged into the measuring fluid. The sensor is made with specially adapted technology (wave-guide acoustic transducers technology). The paper tackles: principle of operation of the transducers, methods of testing under laboratory conditions, calibration of the sensor for different liquids and experience in foams.

### 2.1 Principle of operation the wave-guide density sensor

The operation of the sensor is based on the determination of the propagation velocity of ultrasound waves in the sensitive element. This acoustic impedance method uses bending waves. The sensitive element geometry and

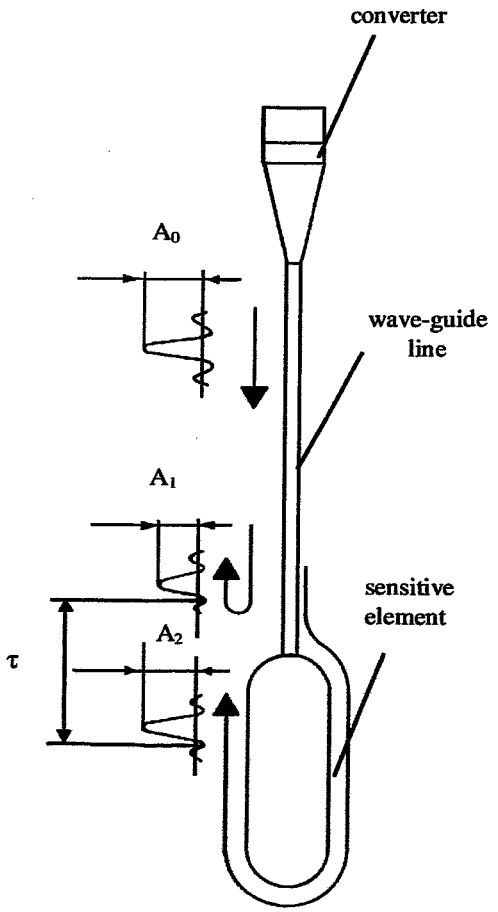


*Fig. 2.1.Scheme illustrating the working principle of the wave-guide density sensor.*

the ultrasound frequency are chosen in such a way, that the wave propagation velocity $c_b$ is less than the speed of sound in the liquid phase, and therefore ultrasound is not radiated from the wave-guide into the liquid. The coefficient of attenuation $\alpha$ is imaginary. The influence of liquid has an inertial character, that is, speed of sound in the sensitive element is reduced:

$$\Delta c = \frac{\rho_l c_b}{2\rho}; \qquad (2.1)$$

where $\rho_l$, $\rho$ -densities of liquid and of the wave-guide material correspondingly.

The theoretical calculation has shown that the relative change of the wave propagation velocity may reach up to 10%. In practice, the time delay between two reflection impulses is measured. The first reflection is generated, when the wave from the piezoelectric crystal arrives at the connection between wave-guide line and the sensitive element, the second after the wave has passed through the sensitive element and returned to that connecting point (Fig. 2.1). The time delay between these two reflections is measured. The change of this time delay in comparison to the dry sensor, $\Delta\tau$, is in the range of 1-2 ms. It is measured by using relatively simple technical means with an error less than 1%. The time delay change is proportional to the density of the liquid:

$$\Delta\tau = b\rho_l \qquad (2.2)$$

where b is a coefficient of proportionality, subject to calibration.

## 2.2 Functional elements of the sensor and its physical characteristics

The density sensor consists of three main parts which determine its operational capability and technical characteristics: sensitive element, wave-guide communication line and acoustic converter (Fig. 2.1).

For generating the necessary longitudinal waves, an acoustic converter with disc-shaped piezoelectric crystal and damping lap was proposed (Fig. 2.2). The piezo-crystal (Fig. 2.2a) is based on zirconate-titanate of lead-19. The diameter of the piezo-crystal disk and the lap from steel X6CrNiTi18.10 are equal to 2.5 mm. The heights of the piezo-crystal and the lap are 0.8 mm and 2.5 mm correspondingly. An increase of the height of the piezo-crystal - lap system and a covering by elastic sealing compound reduce the operating frequency. An increase of their diameter also lower the operating frequency. The transmission coefficient for the double conversion electric impulse - acoustic signal - electric impulse is equal to 0.3. The piezo-crystal disk is placed on the base of a connective

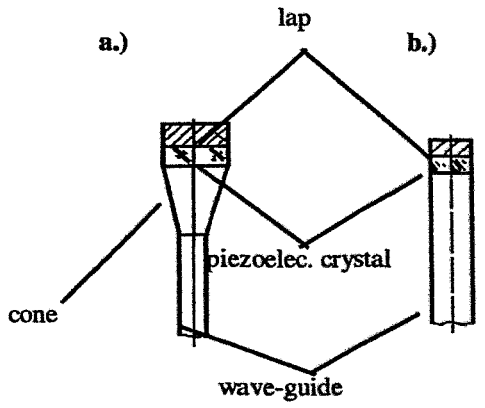


*Fig. 2.2. Acoustic converter for longitudinal waves*

cone, which is realising the matching between the large diameter of the piezo-crystal and the small diameter of wave-guide. The operating frequency of converter is 250 kHz. It is defined by the choice of the converter geometry (Fig. 2.3). For wave-guides of greater diameter, the acoustical converter without cone is used (Fig. 2.2b).

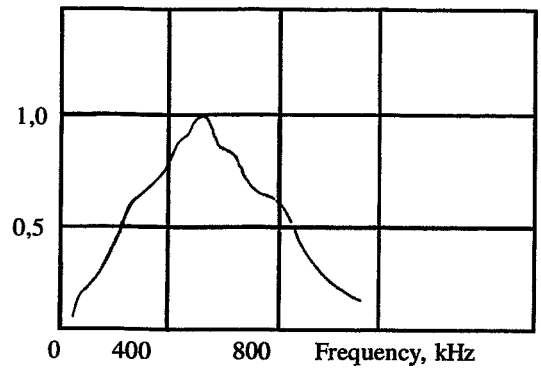


*Fig. 2.3 Amplitude-frequency characteristics of the acoustical converter.*

For producing the wave-guide cylindrical wires are used. The ultrasound attenuation in a wave-guide with a given length x is described by:

$$B = B_0 \exp(-\alpha x); \qquad (2.3)$$

where - $\alpha$ is the attenuation coefficient, which depends on the properties of the wave-guide material, as well as on the operating frequency and temperature.

It was discovered, that annealing a wave-guide, made of chromium - nickel steel, results in a decrease of the attenuation constant by 5-7 times (Fig. 2.4). A thermal processing is therefore very advantageous for long wave-guides. A temperature within the range of 20 - 350$^0$ C has only little influence on the attenuation coefficient, however, with rising temperature losses of ultrasonic energy increased considerably (Fig. 2.5). The wave-guide diameter has practically no influence on the attenuation of the longitudinal waves of zero order. To protect the wave-guide from ambient influences, and above all from damping by direct contact with the measuring fluid, it is put into a protective tube, which is sealed at both ends and filled with air. Inside, the wave-guide is fixed using heat-resistant rubber plugs. There is no radiation of acoustic waves into the gas fill because the gas has a very low wave impedance. Wave-guide, sensitive element and acoustic converter are welded together.

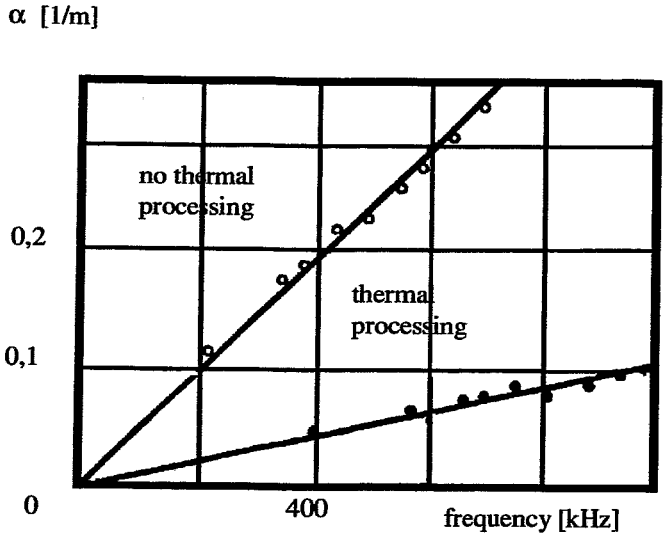


*Fig. 2.4. Attenuation coefficient as a function of frequency.*

The geometry of the sensitive element is determined by the propagation velocity of the bending wave, Fig. 2.6. Sensitive elements of circular or fork shapes are preferred. The circular sensitive element is usually made from a wire with a diameter of about 0.2 mm. Fork-shaped sensitive elements are cut from a monolith piece of

metal. It is very important to ensure the symmetry of the fork element. An accurate perpendicular T-junction between sensitive element and wave-guide guarantees an effective excitation of bending waves.

Two versions of sensitive elements were manufactured: (1) a circular sensitive element made from a chrome-nickel wire of 0.4 mm diameter and 20 mm length, (2) a fork-shaped element made from a titanium block of rectangular cross section with the dimensions of 2,5 × 0,5 mm.

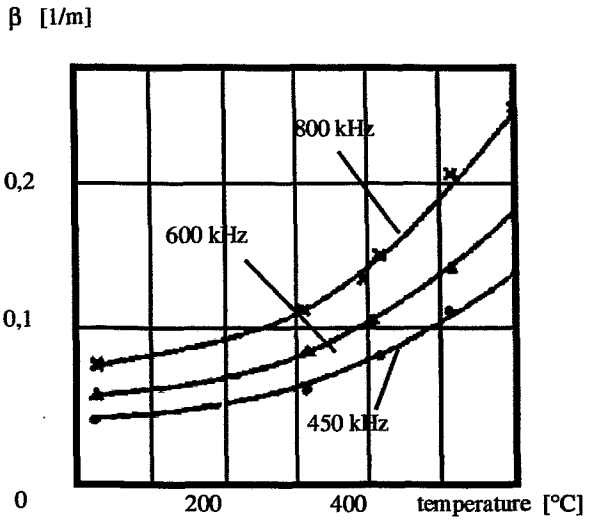


*Fig. 2.5 Attenuation as a function of temperature.*

## 2.3 Design and field of application

The design of a wave-guide density with a circular sensitive element is shown in Fig. 2.7a. The sensor was made from steel X6CrNiTi18.10 and consists of a case, a circular sensitive element (first model), wave-guide communications line with a diameter of 0.8 mm and a length of 2.5 m. The piezoelectric converter was made from zirconate-titanate of lead-19, the operating frequency is 250 kHz, the pulse frequency is 200 Hz.

The sensor functions as follows: acoustic pulses, created by the crystal, travel along the communications wave-guide to the sensitive element. They are partially reflected at the T-junction formed by the wave-guide - sensitive element joint. The reflection occurs twice: first, when the primary pulse arrives at the junction, second when the pulse reappears after travelling through the sensitive element.

The delay between this impulses is measured (Fig. 2.8). The delay between first and second reflection is independent of the pulse delay in the

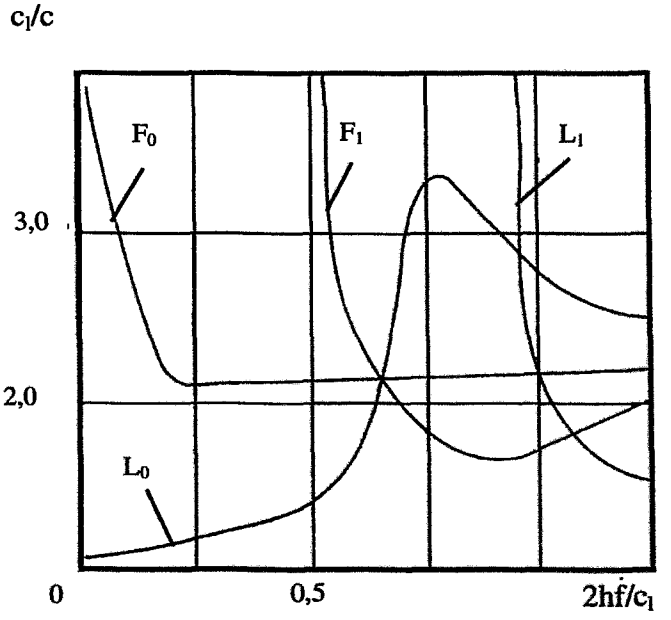


*Fig. 2.6 Wave propagation velocity as a function of geometry and frequency*
*$F_0$, $F_1$-bending wave*
*$L_0$, $L_1$-longitudinal wave*

wave-guide itself. The matching to the electrical impedance of the connecting line and a protection against electromagnetic disturbances is realised by using a differential transformer. The shift in delay time caused by liquid phase is shown in Fig. 2.10.

The second modification of a wave-guide density sensor is shown in Fig. 2.7b. The fork-shaped sensitive element of rectangular cross section (2.5×0.5 mm) and the wave-guide with a diameter of 3 mm are made from a massive block of titan. The length of wave-guide is 300 mm.

Experimental tests of the transducer and the measurement methods were performed at the facility of the Physical laboratory of Physical-Technical Department of the TUNN. Control measurements were carried out in the following cases: the sensitive element of the first modification was completely immersed in liquids with different densities and the time delay was registered correspondingly. The obtained calibration characteristics are given in Fig. 2.9.

## 2.4 Application experience in a two-phase flow

### 2.4.1 Level measurement in a steam generator heat exchanger tube

The wave-guide sensor with circular sensitive element (Fig. 2.7a) was used to measure the water level in a single heat exchanger tube model for horizontal steam generators of Russian VVER type reactors. The work was carried out in frame of thermal hydraulic investigations of the Hochschule für Technik, Wirtschaft und Sozialwesen Zittau/Görlitz (HTWS FH) concerning the decay heat removal capacity of these steam generators. Five probes were mounted to the heat exchanger tube of the HORUS test facility located in Zittau. The circular wave-guide loop was placed under an angle of 45° into the tube of 13 mm inner diameter. The probes were able to record the transient water level behaviour with an accuracy in the range of a millimetre in the small tube at pressures up to 8 MPa at the primary side and 6.4 MPa at the secondary side, with the corresponding thermal loads caused by the saturation temperatures. Especially the access to the inner space of the tube via the also pressurised secondary side was a challenge of these experiments. Results are published in [2.1].

### 2.4.2 Gas fraction measurements in experiments with hydrogen peroxide decomposition on catalyst surfaces

FZR has carried out measurements of the axial gas fraction distribution in the anode chamber of alkaline chloride membrane electrolysis cells. A catalytic $H_2O_2$ decomposition on a platinum-covered anode model was used as a substitute of the chlorine evolving anode reaction. The fork-shaped density sensor (Fig. 2.7b) was traversed over the height of the anode chamber model. It was found that the measured gas fraction is strongly biased by gas bubbles growing at the sensor surface due to the catalytic decomposition even in contact with Titanium. It is recommended to use this kind of probe only if a gas evolving reaction at the probe surface can be excluded.

## References

[2.1] S. Alt, W. Lischke, V.I. Melnikov: Anwendung einer neuartigen Ultraschallmesstechnik zur Bestimmung von Strömungsregimen und Füllständen in Wasser/Dampf-Systemen, Workshop "Messtechnik für stationäre und transiente Mehrphasenströmungen, Rossendorf, 06.-07.11.1997, FZR-204, S. 78-90.

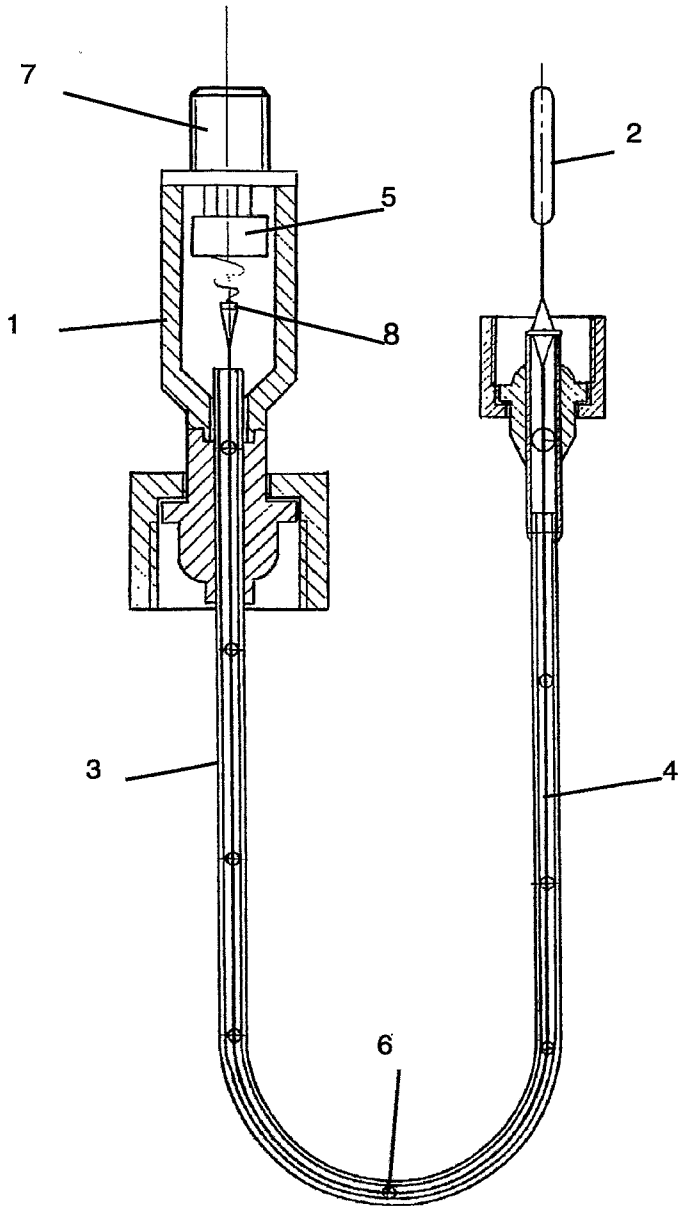


*Fig. 2.7a Design of the wave-guide density sensor with a circular sensitive element*

1 - case; 2 - sensitive element; 3 - protective tube;
4 - wave-guide; 5 - differential transformer;
6 - rubber plug; 7 - connector; 8 - acoustical converter

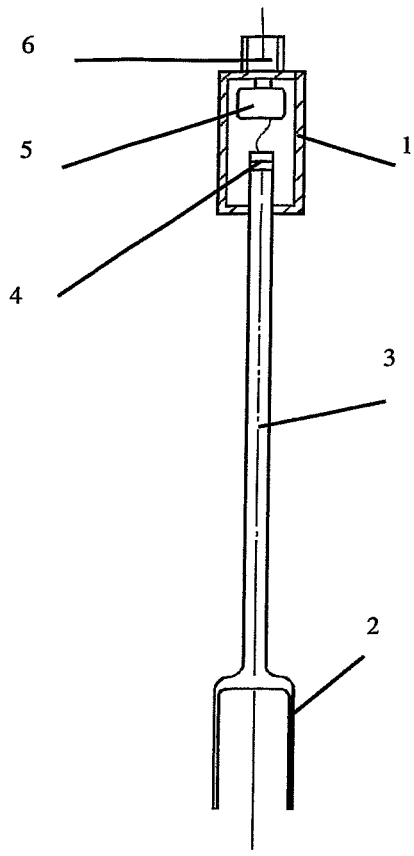


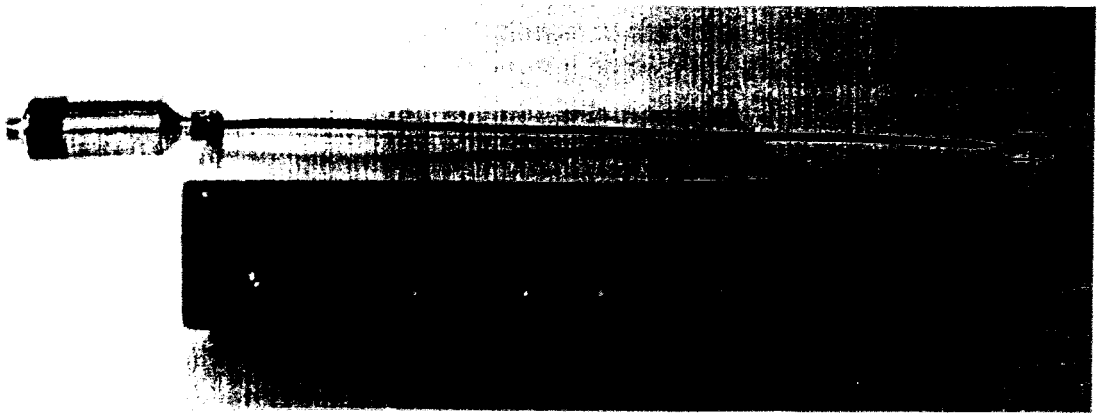

*Fig. 2.7b Design of the wave-guide density sensor with fork-shaped sensitive element*

1 - case; 2 - sensitive element; 3 - wave-guide; 4 - acoustical converter; 5 - differential transformer; 6 - connector.

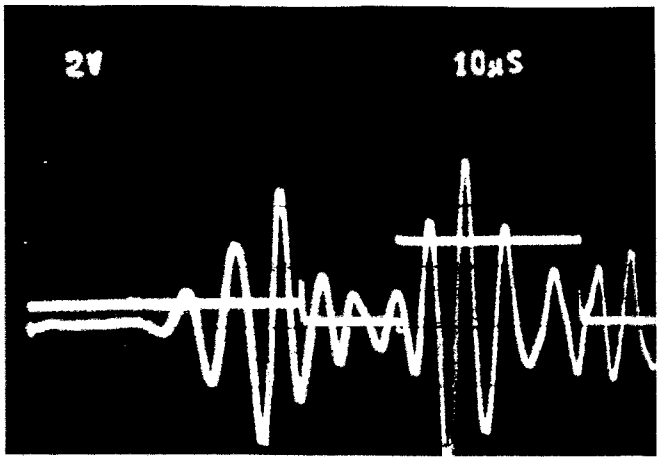


*Fig. 2.8 Electrical signal of the wave-guide density sensor*

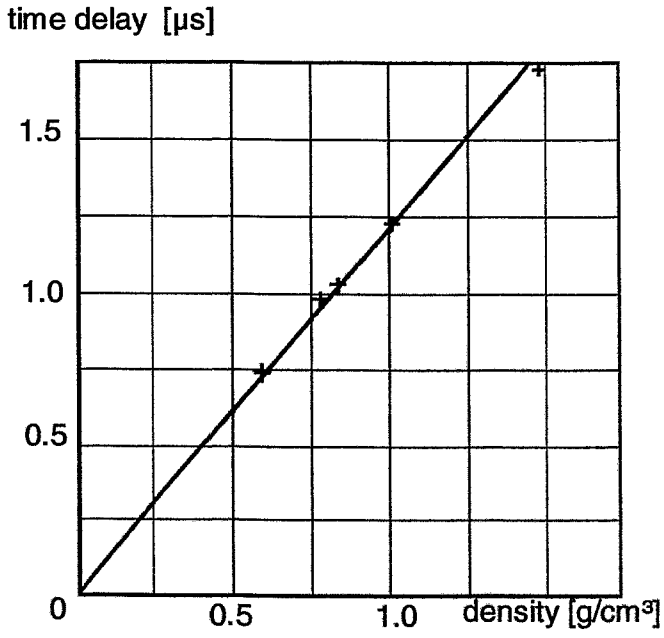


*Fig. 2.9 Calibration characteristic of a wave-guide density sensor*

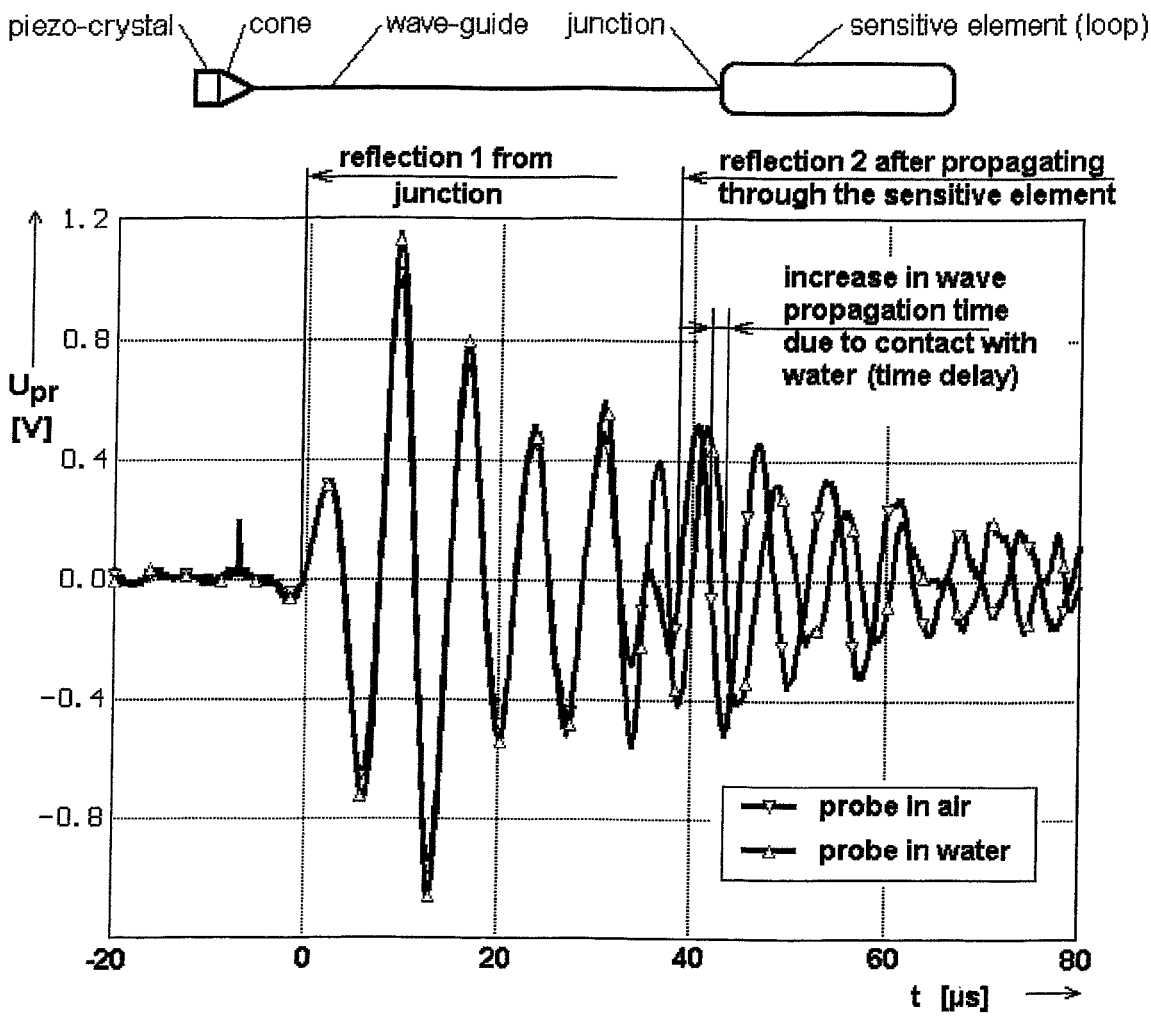


*Fig. 2.10 Probe signals recorded with an analogue transient recorder for illustrating the shift in time delay when the probe is immersed into the liquid phase*

# 3. Intrusive local void fraction probes based on wave-guides

## 3.1 General description

The intrusive ultrasonic void probe consists in two wave-guides for longitudinal waves, which are put into the two-phase flow (Fig. 3.1). The ends of the wave-guides are located in a small distance from each other. Both are equipped with piezoelectric crystals at their back ends outside the flow. One of the crystals is operated as a ultrasonic transmitter. The pulse propagates through the connected transmitting wave-guide. Finally, the ultrasound is partially irradiated into the fluid at the end of the wave-guide. The second wave-guide receives that pulse, correspondingly a signal is generated in the receiver crystal. The signal reflects the presence of the liquid phase in the immediate vicinity of the tips of both wave-guides, thus the ultrasound can only transfer from one tip to the other, if the acoustic impedance of the fluid is not too much different from the acoustic impedance of the wave-guide material. Therefore, the presence of a gas bubble covering the ends of the wave-guides leads to a complete interruption of the received signal. A characteristic signal shape caused by a bubble, the diameter of which is sufficiently greater than the control volume formed by the ends of the wave-guides, is shown in Fig. 3.1, too. The received signal shows characteristic pulse amplitude, when the probe is in the liquid phase. A bubble leads to a decrease of the pulse amplitude for a so-called contact period ($\tau_i$). As a matter of rule, the amplitude decreases to almost zero, because the gas phase has a too much different acoustic impedance compared to the steel of the wave-guides. Often there is an influence of an approaching bubble still before it contacts the probe. This is illustrated in Fig. 3.1 by the oscillating period ($\tau_{os}$).

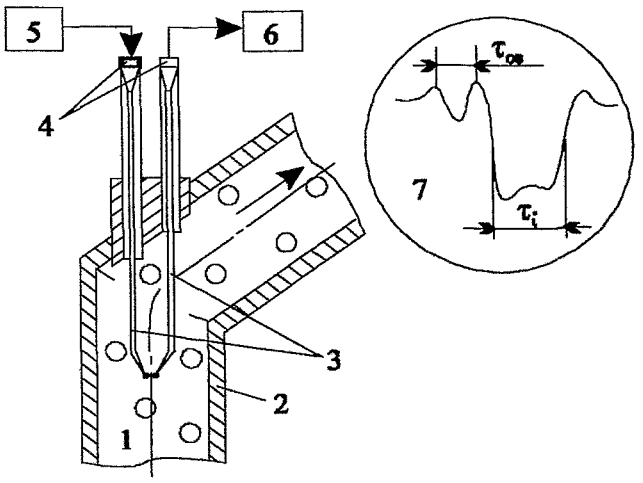


*Fig. 3.1 Local acoustic probe and typical output signal*

1 - two-phase flow; 2 - tube; 3 - wave-guides; 4 - piezo-ceramics; 5 - generator; 6 - signal processing unit; 7 - typical output signal

In case of small bubbles, the tips of the wave-guides cannot be covered and a complete interruption of the ultrasound transfer is not observed. Bubbles that travel through the gap between the ends of the wave-guides cause a gradual decrease of the ultrasound pulse amplitude. Bubble sizes can be evaluated if the relative signal decrease is measured. In a real two-phase flow, it must be expected, that more than one bubble resides in the gap in the same time. In this case, statistical methods must be applied to evaluate the signal.

In the following chapters, the described two cases of (1) bubbles larger than the control volume, and (2) bubbles smaller than the control volume will be discussed individually.

The main advantage of the local void probes is given by the fact, that they can be designed in a way, that all materials contacting the fluid are made from materials resistive against corrosion and high temperature. The piezoelectric crystals are located outside the region of high temperature. This allows to build very robust measuring gauges, which can be applied to solve many different experimental and industrial measuring tasks (high temperature and pressure, chemically aggressive fluids, explosion safety).

## 3.2 Design of the probe

The design is shown in Fig. 3.2. The wave-guides with a diameter of 0.8 mm are made of stainless steel (X6CrNiTi18.10). The sensible ends are equipped with cone-shaped concentrators (6 mm long) with a sphere of 0.5 mm diameter at each end. For the realisation of the described acoustic methods the gauge shown in Fig. 3.2 was developed. The ultrasound is passed through sealings inside the protection tube without essential losses. They are based on double-conical elements working as sound diffusers and collectors. The sealing itself is located at the widest part of these double-conical elements. The top parts of the wave-guides are shielded by capillaries. The surfaces of capillaries is wrapped with a wire serving as a damper. Thus by a varying of the length of the damper, the covering capillaries can be adjusted to the necessary level of suppression of the parasitic signals travelling on their surfaces.

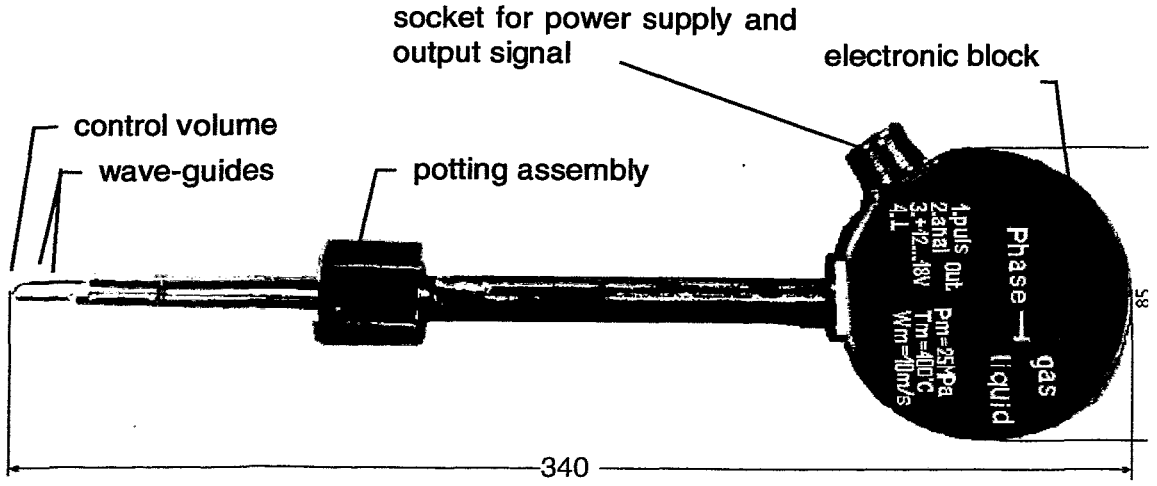


*Fig. 3.2 View of the acoustical gauge*

The piezoelectric transducers are placed onto the back ends of the wave-guides. The difference in diameter is compensated by cone-shaped elements (concentrators). Electrically, the crystals are connected to the cable through a matching transformer. This allows to suppress electromagnetic noise and optimise the coupling with the input cascades of the signal amplifiers. The transformers are located directly inside the gauge. It allows to transfer signals over a distance of up to 100 m, if this should be necessary. In case of the probe shown in Fig. 3.2, an electronic circuit solving the tasks of transmitter excitation, receiver pre-amplification and time-gated peak detection is located directly inside the casing of the probe (see next chapter).

The gauges are designed for steam fraction measurements at pressures of up to 25 MPa and temperatures of up to 400 $^0$C. The amplifier of the gauge can operate at an environmental temperature of up to 100 $^0$C. The length of the wave-guides must not exceed 0.5 - 0.7 m.

### 3.3 Signal acquisition

The excitation of the transmitting piezoelectric crystal is done by supplying the driving transformer with a short voltage pulse. The pulse frequency determines the measuring rate. Usually a frequency of 1-2 kHz is used. The limit for the pulse sequence frequency is given by the decay of the oscillations inside the wave-guide, which must calm down before the next pulse is applied.

The frequency of the transmitted ultrasound is given by the resonance frequency of the system driving transformer - piezo-crystal - wave-guide. It is in the range of 600-700 kHz. The transmitted pulse is received by the second wave-guide and transformed into a voltage signal by the receiver crystal. After an amplification, the signal is supplied to a peak-value detector. The peak value is obtained inside a given gate time, in which the useful signal has to be expected under consideration of the wave propagation velocity in the wave-guides. The result of the peak detection is the analogue output signal of the sensor, shown in Fig. 3.1. It is further processed to obtain either void fractions or bubble sizes.

### 3.4 Detection of large bubbles

The control volume of the probe is given by the dimensions of and the distance between the ends of the two wave-guides. If a bubble is larger than these dimensions, it can cover the control volume completely. In the consequence, the received signal decreases to a value close to zero. By an evaluation of the duration of the signal decrease it is possible to determine the size of the given individual bubble. For the decision whether gas or liquid is present in the control volume, the analogue signal can be compared to a threshold. The resulting binary signal is analysed by integrating the contact periods of each detected bubble. This is carried out by the summation of all contact periods related to the measuring period supplies the local void fraction [3.1]:

$$\alpha = \frac{\sum \tau_i}{T} \tag{3.1}$$

The average steam fraction in a cross section can be measured either by the use of several local probes or by traversing a single probe. The readings obtained at different radial positions must be averaged as follows [3.8]:

$$\varphi = \sum a_i \alpha_i \tag{3.2}$$

where $a_i$ - weight coefficients assigned to each measuring position. It is further possible to perform statistical analyses of the contact periods, e.g. a probability density distribution of the contact periods obtained during a certain measuring period supply information about the flow regime. The statistical distribution of contact periods can be transformed into a bubble size distribution, when the velocity of the bubbles is known. The latter can be approximated by the mixture velocity. In this way, information about the flow pattern can be obtained.

An important question is the right definition of the discriminating threshold. A possible solution is a determination of the threshold using a probability density distribution of the analogue probe signal, Fig. 3.3. In case of a fully developed two-phase flow, the distribution has two maxima, the first, at low output voltage, corresponds to the contact with the gas phase, the second, at high output voltage, to the contact with the liquid. The best value for the discriminating threshold $U_{level}$ is given by the position of the minimum between the two maxima. After defining the threshold, the probability density distribution W(U) can also be used to calculate the void fraction:

$$\alpha = \frac{\int_0^{U_{level}} W(U)\cdot dU}{\int_0^{\infty} W(U)\cdot dU} \qquad (3.3)$$

Usually, the probability density distribution is calculated as a histogram, in this case the integrals in eq. (3.3) are approximated by the sums over the corresponding histogram classes. Another possibility is the definition of a threshold set to a constant ratio of the signal difference between plain liquid and pure gas, for example to 50 %.

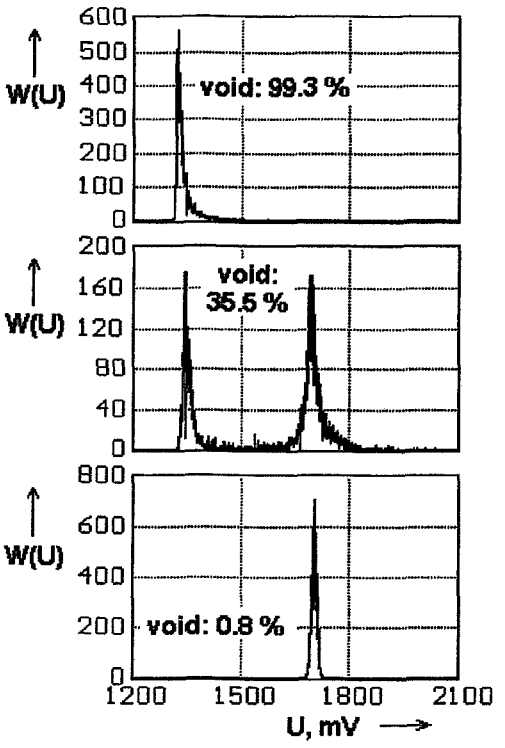


*Fig. 3.3 Histograms of the output voltage of the local probe for different void fractions*

The third approach to obtain volumetric gas fractions is to treat the instantaneous signal level as an analogue information proportional to the instantaneous gas fraction in the control volume:

$$\alpha_{lin}(t) = \frac{U_L - U(t)}{U_L - U_G} \qquad (3.4)$$

Here, $U_L$ - signal level for plain liquid, $U_G$ - signal level for pure gas. As the signal in the phase of the bubble approach often oscillates and shows amplitudes greater than the typical values for liquid, these instantaneous values must obviously be cut off, because they other wise would lead to negative gas fractions:

$$\alpha(t) = \begin{cases} 0 & \text{if} \quad \alpha_{lin}(t) < 0 \\ \alpha_{lin}(t) & \text{if} \quad 0 \le \alpha_{lin}(t) \le 1 \\ 1 & \text{if} \quad 1 < \alpha_{lin}(t) \end{cases} \qquad (3.5)$$

These instantaneous gas fractions can be averaged to obtain the local void fraction. If the physical properties of the measuring fluid are constant, the acoustic impedance is constant, too. In this case, the signal levels for pure liquid $U_L$ and pure steam respectively gas $U_G$ are very stable values. The ultrasonic local probe is much less sensible to changes of the fluid qualities, as electrical probes, because their signal

amplitude depends on the instantaneous conductivity, which is strongly influenced by temperature and content of foreign ions and corrosion products. During practical measurements with the ultrasonic probes it is therefor often possible to perform only one calibration run at the beginning of the experiment series, where the signal levels for both plain liquid and pure gas have to be recorded, while electrical probes require adaptive methods to determine instantaneous calibration values.

The use of a fixed threshold ratio as well as the linear method using constant calibration values have the advantage, that false measurements at gas fractions close to 0 % respectively 100 % are excluded. Close to these values, the probability density distribution often does not show the necessary two maximums (see Fig. 3.3).

Beside the gas fraction measurement, it is possible to estimate the bubble velocity by evaluating the signal oscillations appearing before the bubble contacts the probe. The observed maximum of the amplitude of the received ultrasound during this oscillation is caused by a positive superposition of the direct sound travelling from the transmitter wave-guide to the receiver with the sound reflected at the surface of the bubble. The distance between bubble and probe, at which the maximum appears, can be defined by the wavelength of the ultrasound $\lambda=c/f$, taking into account the geometry of the probe:

$$L_{max} = \sqrt{\left(\frac{l}{2}+\frac{c}{2\cdot f}\right)^2 - \left(\frac{l}{2}\right)^2}, \tag{3.6}$$

where l - distance between the ends of the wave-guides, c - sound propagation velocity, f - ultrasound frequency.

The bubble velocity $w_{bub}$ can be obtained by relating the length $L_{max}$ to the time difference between the appearance of the maximum and the contact of the bubble with the probe $\Delta t$:

$$w_{bub} = \frac{L_{max}}{\Delta t} \tag{3.7}$$

## 3.5 Detection of small bubbles

### 3.5.1 General remarks

If the size of the bubbles is less than the extension of the control volume of the probe (< 500 µm), then the ultrasonic wave-guide probe works as an integral detector. In this case, several bubbles may reside in the control volume at the same time. The amplitude of the signal is then the result of the attenuation of sound energy due to harmonic oscillations of the bubbles caused by an excitation in the sound field. The attenuation depends on the number and the diameter of the bubbles. Due to the fact that the instantaneous number of bubbles found in the control volume is a random number, the attenuation performs statistical fluctuations. The parameters of the two-phase flow can be determined by a statistical analysis of these fluctuations.

The intensity of the ultrasonic wave, passed through a layer of two-phase mixture with the thickness l and a bubble concentration of $n_0$ is, according to [3.5], given by:

$$J = J_0 \exp(-q n_0 l) \tag{3.8}$$

where **q** - effective cross-section of absorption of the sound by the bubbles.

The main contribution to the absorption cross-section is caused by bubbles, the radius of which is close to the resonance wavelength at the given frequency of the excitation. Therefore, by measuring the sound attenuation at different frequencies it is possible to determine both the bubble size distribution and their common concentration.

Other methods are based on the measurement of the sound velocity. In the liquid, the latter is defined by the compressibility $\gamma$ and density $\rho$ [3.5]:

$$c = 1/\sqrt{\gamma \rho} \tag{3.9}$$

When the concentration of bubbles in the liquid is small, the density is not effected significantly. However, the influence of the bubbles to the compressibility is large, making it possible to determine the bubble concentration.

Depending on the frequency of excitation, the sound velocity can grow or decrease. Usually, frequencies of excitation less than the resonance frequencies of the bubbles are applied. In this case the compression of the bubbles is large, the attenuation of the sound is low, and the sound velocity does not depend on bubble size distribution. The sound velocity in the bubble flow can be estimated as follows [3.7]:

$$c = c_0 (1 + f \cdot n_0)^{-1/2} \tag{3.10}$$

where $c_0$ - sound velocity in pure liquid, $n_0$ - volumetric bubble concentration, **f** – correction factor ($f = 1.6 \cdot 10^4$) [3.7].

The attenuation of sound waves in the two-phase mixture grows considerably with the increase of the bubble concentration and the increase of the frequency of fluctuations. Therefore, almost all above-stated methods that use integral characteristics of sound propagation, become ineffective as steam contents of more than 1-2 % and can further be applied only as indicators.

### 3.5.2 Mathematical model

In a finely dispersed flow, more than one bubble can be present in the control volume at the same time and consequently the probe changes into the mode of integrating measurement. The properties of finely dispersed flows representing sets of large quantities of bubble are described by complex laws. In general, the common character of these laws does not depend on the behaviour of an individual bubble in the flow. In this sense, there is a similarity to the movement and interaction of molecules and atoms, described by the equations of statistical physics. Naturally, in such a case, it is advisable to apply the theory of probability for the definition of the generalised parameters of the two-phase flow and to model the probe signal in case of a finely dispersed bubble flow.

The amplitude of the received signal is defined by the quantity and the diameter of the bubble, appearing in the control volume in the moment of the acoustic through-transmission. Due to the probabilistic character of the flow the number of bubbles in control volume fluctuates, and, hence, the amplitude of the received signals fluctuates also. The parameters of the flow can be extracted by an appropriate statistical processing and an analysis of the signal fluctuations.

The two spheres at the ends of the wave-guides form the control volume, the shape of which is assumed to be a cylinder with the following volume:

$$V_{con} = \frac{\pi \cdot (d_w)^2}{4} \cdot l \qquad (3.11)$$

where $l$ - distance between the ends of the wave-guides [m], $d_w$ - diameter of the wave-guides.

The amplitude of the through-transmission signal shows statistical fluctuations. According to [3.9] the through-transmission amplitude follows an exponential attenuation:

$$J = J_0 \cdot \exp(k \cdot n \cdot d^2 \cdot l) \qquad (3.12)$$

where $n$ - quantity bubbles in the control volume, $d$ - bubble diameter, $l$ - distance between the ends wave-guides, $k$ - correction factor, which is defined by the geometry of transmitter and receiver wave-guides, it depends on the shape of the acoustic field, $J_0$ - intensity of the transmitted ultrasonic signal, $J$ - received intensity.

From eq. (3.12) it is visible, that two parameters are determining: (a) the quantity of bubbles in the control volume and (b) the diameter of these bubbles. These parameters also define the random character of the dependency, since they are random values. Let us analyse the probability of the instantaneous presence of a number of bubbles in the control volume at a given constant bubble concentration in the flow. The control volume $V_{con}$ should be small in comparison to the volume $V_0$ of the flow channel. Further, we assume that the total number of bubbles $N_0$ in the volume $V_0$ roughly remains constant.

Let's also assume, that the bubbles are equally distributed over the flow channel (the real distribution of the bubble density over the cross section of the channel can be taken into account by introducing a correction factor). Then, the probability to meet some certain bubble in the control volume $V_{con}$ equals to the relation $V_{con}/V_0$, and the probability of the simultaneous appearance of n bubbles is $(V_{con}/V_0)^n$. Similarly, the probability of a bubble not being present inside the volume $V_{con}$ is equal to $(V_0 - V_{con})/V_0$, and the probability of the simultaneous absence for $N_0$-$n$ bubbles in the control volume is $\left(\frac{V_0 - V_{con}}{V_0}\right)^{N_0 - n}$. Therefore, the probability $w_n$ that precisely n bubbles are in the control volume $V_{con}$ is given by the following expression [3.2]:

$$w_n = \frac{N_0!}{n!(N_0 - n)!} \cdot \left(\frac{V_{con}}{V_0}\right)^n \cdot \left(1 - \frac{V_{con}}{V_0}\right)^{N_0 - n} \qquad (3.13)$$

where the factor determining the number of possible combinations of the choice n from $N_0$ bubbles is introduced.

An actual number n differs from of the mean value $n_m$, but in the interesting case $V_{con} << V_0$, where certainly, n is meant to be small in comparison to the total number of bubbles $N_0$. In this case it is possible to approximate $N_0! \cong (N_0 - n)! \cdot N_0^n$ and to neglect n in the power expression. In the result we get:

$$w_n = \frac{1}{n!} \cdot \left(\frac{N_0 \cdot V_{con}}{V_0}\right)^n \cdot \left(1 - \frac{V_{con}}{V_0}\right)^{N_0} \qquad (3.14)$$

Further, $N_0 V_{con}/V_0$ equals to the average number of bubbles $n_m$ in the control volume $V_{con}$:

$$w_n = \frac{n_m^{\,n}}{n!} \cdot \left(1 - \frac{n_m}{N_0}\right)^{N_0} \qquad (3.15)$$

At last, applying the well-known formula $\lim\left(1 - \frac{x}{n}\right)^n = e^{-x}$, we replace $\left(1 - \frac{n_m}{N_0}\right)^{N_0}$ by $e^{-n_m}$ at large values of $N_0$. Finally, we get the expression [3.2], which is a Poisson distribution:

$$w_n = \frac{n_m^{\,n} \cdot e^{-n_m}}{n!} \qquad (3.16)$$

From the analysis of the properties of the Poisson distribution it becomes obvious, that the determining parameter is $n_m$, which defines both the location of the probability maximum and its absolute magnitude. With other words: if $n_m$ is known, then the Poisson distribution describes completely the probability of a certain number of bubbles in the control volume.

Now we shall consider the second parameter influencing the behaviour of the probe, the diameter of the bubbles present in the control volume. For simplification we assume that the bubbles have a spherical shape and that their diameter is a random value.

Let us consider the probability distribution of this parameter. In the established two-phase flow there is an equilibrium between bubble coalescence and bubble breakdown. This gives reason to assume a normal distribution of the diameter according to a standard Gauss distribution [3.3]:

$$p(d) = \frac{1}{\sqrt{2 \cdot \pi} \cdot \sigma} \cdot \exp\left(-\frac{(d - \mu)^2}{2 \cdot \sigma^2}\right) \qquad (3.17)$$

This kind of statistical distribution of the bubble diameter was found for bubbles, which are large in comparison to the control volume, when the contact periods were evaluated. It is therefore likely that the normal distribution is a good approximation, also in case of small bubbles. The normal distribution is defined by two parameters: $\mu$ - the average diameter of bubbles and $\sigma$ - the root-mean-square deviation from the average diameter describing the width of the diameter distribution.

So, on the basis of the above stated assumptions, the maximum of the probability distribution of the probe signal, is caused by the product of two probability distributions. These are function (3.16) describing the probability of the presence of a given number of bubbles in the control volume and, function (3.17), which is the probability distribution of the bubble diameter. The measuring task consists in the extraction of the quantity and the diameter of the bubbles in the control volume from the probe signal. There are three independent parameters defining the final probability distribution of the primary signal of the gauge: $n_m$ in the Poisson distribution, $\mu$ and $\sigma$ in the Gauss distribution. We need three equations to determine these parameters from the measured signal. For this purpose the following statistical functions are used:

1. **M(xy)=M(x) M(y)** - the expectation value of the product of two mutually independent random values.
2. **D(xy)=M($x^2$) M($y^2$) – $M^2$(x) $M^2$(y)** - the dispersion of the product of two mutually independent random values.
3. **P(M(xy) = P(M(x)) P(M(y))** - the probability of a joint occurrence of independent events. Here **x** is substituted by **n** and **y** by $\mathbf{d^2}$.

$M(x) = n_m$ - is the expectation value of the distribution of the number of bubbles in the control volume, [3.4].

$$M(x^2) = n_m^{\,2} + n_m$$

$M(y) = \sigma^2 + d^2$ expectation value of the bubble diameter distribution [3.4]

$$M(y^2) = 3 \cdot \sigma^4 + 6 \cdot \sigma^2 \cdot d^2 + d^4$$

M (xy), D (xy) – are the expectation values and the dispersion of the probability distribution of the receiver signal. By solving this system of the equations, we find the required parameters of the distributions:

$$n_m = \frac{8 \cdot A^2 + 8 \cdot A - 1}{B - 8 \cdot B + 1}$$

$$\mu = \frac{\sqrt{4 \cdot A \cdot B - B + 12 \cdot A - 1 - 32 \cdot A^2}}{2 \cdot \pi \cdot P(xy) \cdot \sqrt{8 \cdot A^2 + 8 \cdot A - 1}} \qquad (3.18)$$

$$\sigma = \frac{\sqrt{B - 8 \cdot A + 1}}{2 \cdot \pi \cdot P(xy) \cdot \sqrt{8 \cdot A^2 + 8 \cdot A - 1}}$$

where $A = M(xy) \cdot P^2(xy) \cdot \pi^2$ and $B = 8 \cdot D(xy) \cdot P^4(xy) \cdot \pi^4$.

## 3.6 Computer interface

For the operation of the measuring device the computer program "ACOUSTIC" was elaborated, the task of which is the performing of the calculations according to the statistical methods described above. The program owns a convenient and modern graphical interface for the work with the system.

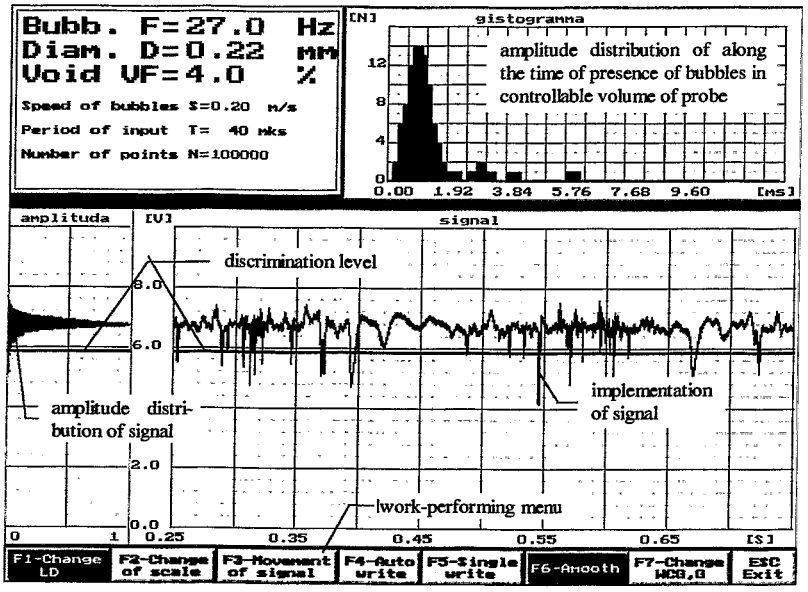


*Fig. 3.4 Screen of the monitor, example of a measurement with the Program ACOUSTIC*

The personal computer acts as a signal acquisition unit. The primary probe signal is displayed graphically. The statistical evaluation is performed almost in real-time. The choice of the signal processing method (large/small bubble evaluation) is carried out automatically by the software. The decision, which of the two methods has to be applied is taken on the basis of the statistical characteristics of the stored signal. The results of the calculations are displayed at the screen (Fig. 3.4)

The program "ACOUSTIC" allows the setting of the working parameters, such as period of transmitter pulses, measuring period, it is possible to store and to accumulate results as digital files and to perform the statistical evaluations in order to determine the steam fraction, the mean bubble diameter and the standard deviation of the bubble diameter.

## 3.7 Test of the gas fraction measurement in case of large bubbles

### 3.7.1 Integral measurements at the two-phase flow test loop (MTLoop)

Experiments were carried out in the vertical test section of the two-phase flow test loop MTLoop in Rossendorf. The local ultrasonic probe was placed into the test section with the sensitive tip in the centre of tube. The loop was operated with air-water mixture at room temperature and nearly atmospheric pressure. As reference device for measuring the gas fraction, an electrical wire mesh sensor was used. The main parameters of the tests are summarised in table 3.1.

The electrical wire-mesh sensor was equipped with 2 x 16 electrode wires of 0.12 mm diameter. The electrode pitch was 3 mm, the distance between both electrode grids was 1.5 mm. The sensor was operated at a measuring rate of 600 frames per second. The applied superficial velocities of both air and water were varied according to a test matrix shown in Fig. 3.5. Approximately 75 % of the points of a ma-

trix of 220 different combinations of air and water flow rate were realised in the tests. The signal was recorded by a 12-bit Analogue-Digital Converter (ADC) connected to a laptop via parallel printer interface. The measuring rate was 1000 Hz. Signal sequences of 10 s were recorded.

For comparison of the local gas fraction reading delivered by the ultrasonic probe with the wire-mesh sensor signal, the local instantaneous gas fraction measured by the four central crossing points of electrodes of the sensor were extracted and averaged over a measuring period of 10 s. The signals of the local probe were first evaluated according to eq. (3.1) and using a threshold of 50 % of the signal change between plain water and pure gas. The calibration values were taken from measurements, where the loop was either completely filled with air or with water. The result is shown in Figs. 3.6 and 3.7.

Table 3.1: Parameters of tests with the local ultrasonic probe in MTLoop

| No | Parameter | Sign | Unit | Value |
|---|---|---|---|---|
| 1 | inner tube diameter | $D_i$ | mm | 51.2 |
| 2 | air injection 1, number x inner diameter of capillaries | $D_{i1}$ | mm | 19 x 0.8 |
| 3 | air injection 2, number x diameter of orifices | $D_{i2}$ | mm | 36 x 1 |
| 4 | air injection 3, number x diameter of orifices | $D_{i3}$ | mm | 8 x 4 |
| 5 | elevation air injection 1 | $H_{i1}$ | mm | 2326 |
| 6 | elevation air injection 2 | $H_{i2}$ | mm | 2376 |
| 7 | elevation air injection 3 | $H_{i3}$ | mm | 2426 |
| 8 | temperature | T | °C | 30 |
| 9 | superficial air velocity | $J_G$ | m/s | ≤12 |
| 10 | superficial water velocity | $J_L$ | m/s | ≤ 4 |
| 11 | elevation electrical wire-mesh sensor | $H_{wm}$ | mm | 5495 |
| 12 | elevation ultrasonic mesh sensor | $H_{us}$ | mm | 5540 |
| 13 | elevation local ultrasonic probe | $H_{pr}$ | mm | 6533 |

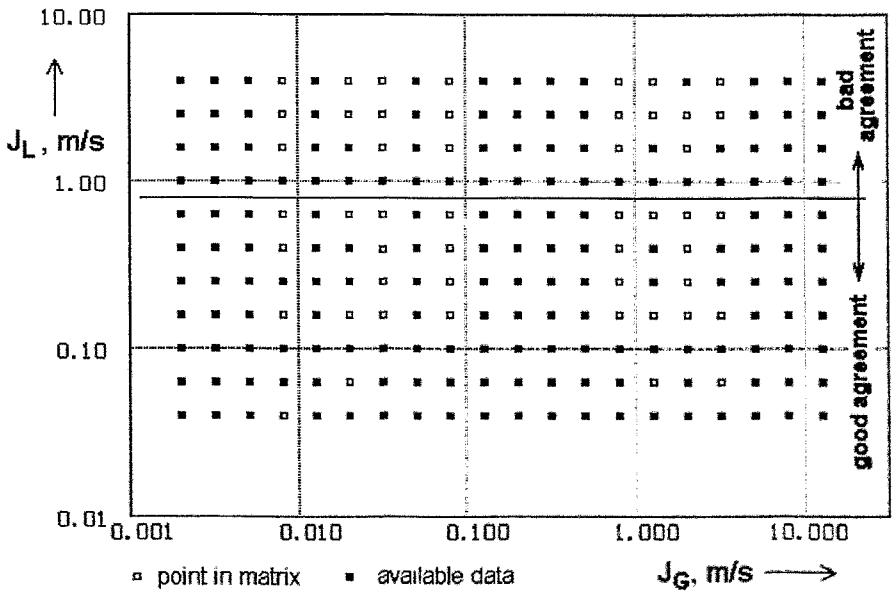


*Fig. 3.5 Test matrix for the comparison between electrical wire-mesh sensor and local ultrasonic probe in MTLoop*

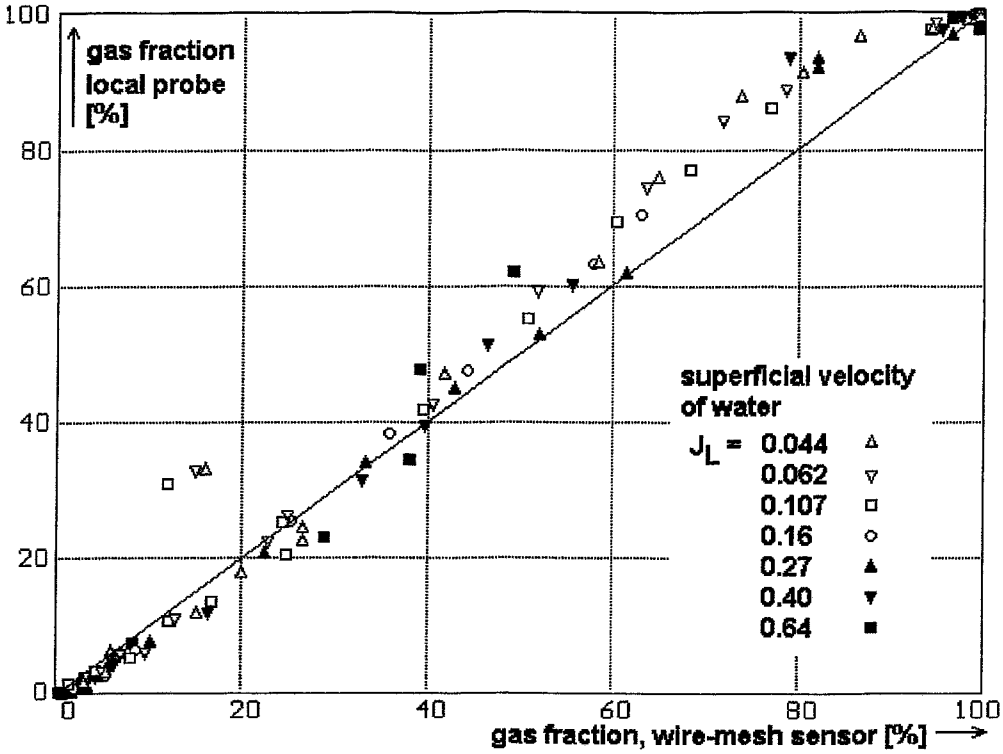


*Fig. 3.6 Comparison between electrical wire-mesh sensor and local ultrasonic probe for superficial water velocities below 1 m/s, threshold 50 %*

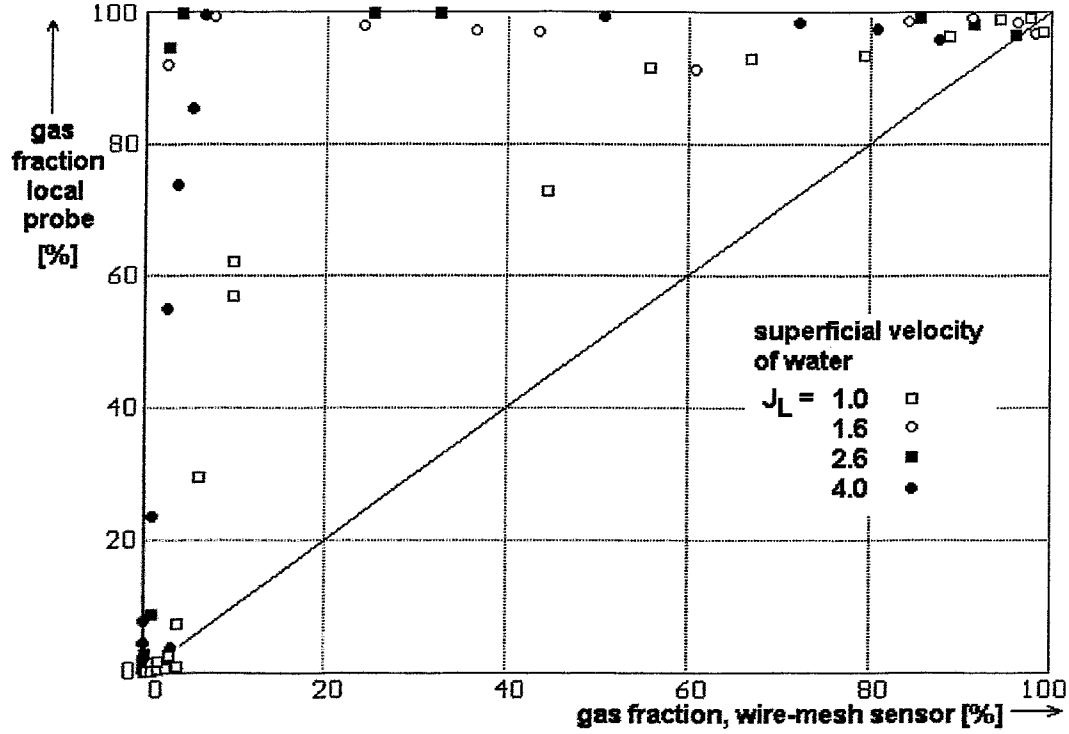


*Fig. 3.7 Comparison between electrical wire-mesh sensor and local ultrasonic probe for superficial water velocities greater than 1 m/s, threshold 50 %*

In the range of superficial water velocities from 0.044 - 0.64 m/s the agreement between wire-mesh sensor and ultrasonic probe is satisfactory. There is an overestimation of about 10 % (absolute gas fraction error) at gas fractions between approximately 70 - 90 %. The result is independent from the superficial air velocity, which was varied from 0.0024 to 12 m/s (related to normal conditions). There is some decrease of the superficial air velocity (up to -20 %) caused by the pressurisation of the loop at growing air flow rate, but this is implicitly taken into account, because the wire-mesh sensor as well as the local ultrasonic probe are both sensible to the actual volumetric void fraction in the test section.

The agreement between wire-mesh sensor and local ultrasonic probe can be improved by using the linear formula to calculate gas fractions, eq. (3.4) and (3.5), see Fig. 3.8.

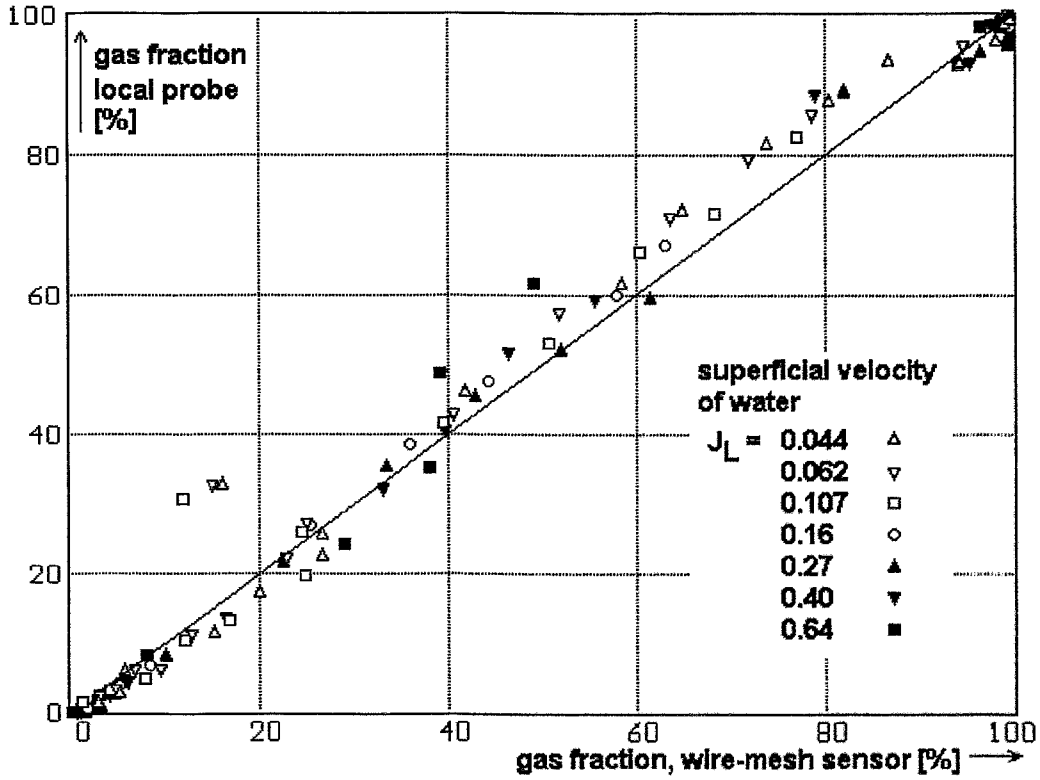


*Fig. 3.8 Comparison between electrical wire-mesh sensor and local ultrasonic probe for superficial water velocities below 1 m/s, linear formula, eq. (3.4, 3.5)*

The overestimation of the void fraction in the upper region is less pronounced. The disagreement observed at the superficial water velocities above 1 m/s are nevertheless not eliminated. We believe, that an accumulation of a stationary air bubble in the wake of the ends of the wave-guides takes place at higher velocities. This bubble causes an attenuation of the ultrasound transmission. In the result, a too high gas fraction is measured. These are perhaps physical limits of the probe, which may be overcome only by a further miniaturisation.

Some examples of time sequences of the local instantaneous gas fraction measured by the probe are shown in Fig. 3.9. Here, at a constant water flow ($J_L$) the superficial

air velocity was stepwise increased. The transition from bubble to slug flow is clearly reflected by the signals:

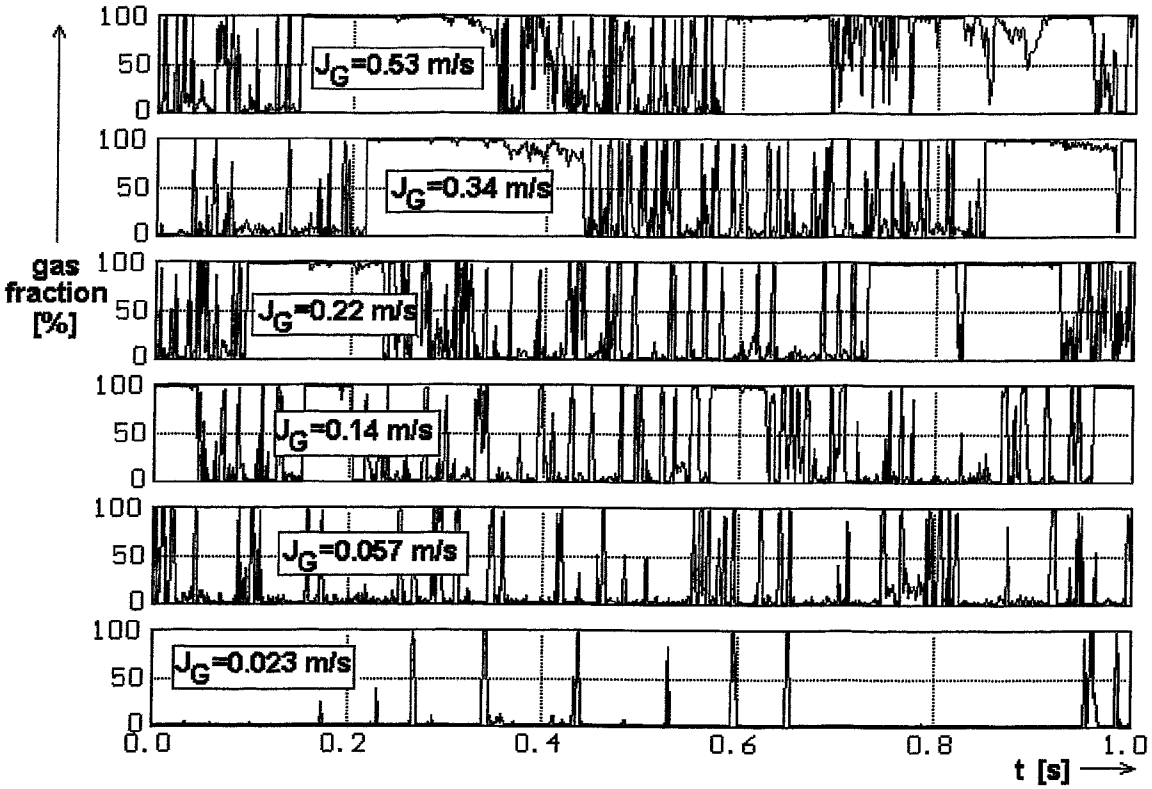


*Fig. 3.9 Instantaneous gas fractions obtained by the linear method (eq. 3.4) from the ultrasonic probe signal, superficial water velocity: $J_L$ = 0.4 m/s*

### 3.7.2 Test in a refrigerant

The operation of the local ultrasonic waveguide probe in a non-aqueous fluid was tested at the DESIRE loop (Fig. 3.10) at the Interfaculty Reactor Institute (IRI) of the Delft University of Technology, Netherlands. This loop models the internal coolant circuit of a boiling water reactor with natural circulation. Scaling considerations led to the use of a refrigerant (R12) as a model fluid, substituting the water coolant of the original reactor. R12 has a very low electrical conductivity, which makes it impossible to use neither needle-shaped conductivity probes nor the electrical wire-mesh sensors developed by FZR. For this reason, it was decided to test the local ultrasonic void probe in this fluid.

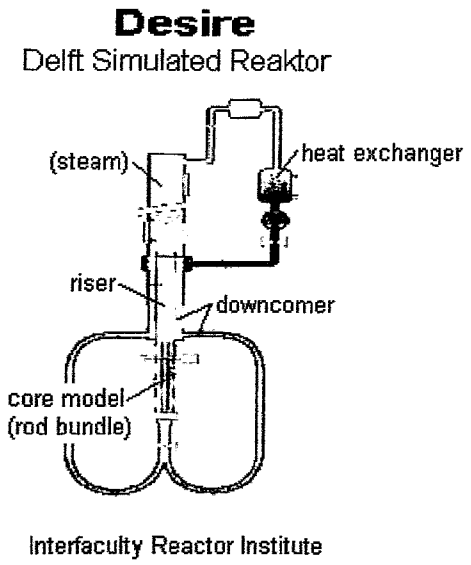


*Fig. 3.10 DESIRE - model of a boiling water reactor with natural circulation of IRI Delft*

The probe was placed into the upper plenum of the test facility above the riser section. The signal was recorded by a 12-bit Analogue-

Digital Converter (ADC) connected to a laptop via parallel printer interface. The measuring rate was 1000 Hz. Signal sequences of 10 - 200 s were recorded.

In the experiments, the electrical core power was varied. Unfortunately, all conventional measuring data (temperatures, pressures etc.) were lost because of a computer failure. It was not possible to repeat the tests. Any interpretation are therefore limited to tendencies expected when the core power changes.

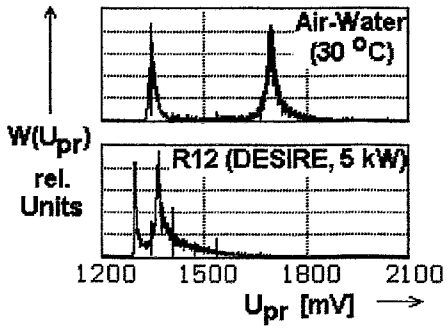


*Fig. 3.11 Histograms of the ultrasonic probe signal for water and R12*

At first, it was observed that the signal amplitude, i.e. the difference between the signal levels characteristic for liquid and for gas, is much lower in the case of the refrigerant in comparison to water at room temperature (Fig. 3.11). This is caused by a worse adaptation of the acoustic impedance of the steel wave-guides to the refrigerant R12, which is more compressible than water. The sound propagation velocity is therefore less in R12 than in water.

Nevertheless, the quality of the probe signals is sufficient for a gas fraction measurement. In Fig 3.12, the change of the signal histogram in dependence of the core power is shown. A slight decrease of the peak characteristic for the liquid phase with growing core power was observed, while the location of the gas peak is unchanged. This can be explained by an increase of compressibility of the liquid with growing temperature.

Using eq. (3.3), average gas fractions shown in Fig. 3.13 were calculated from these histograms. The tendency clearly shows an increase with growing core power. A quantitative information about the accuracy cannot be presented due to the lack of reference measurements.

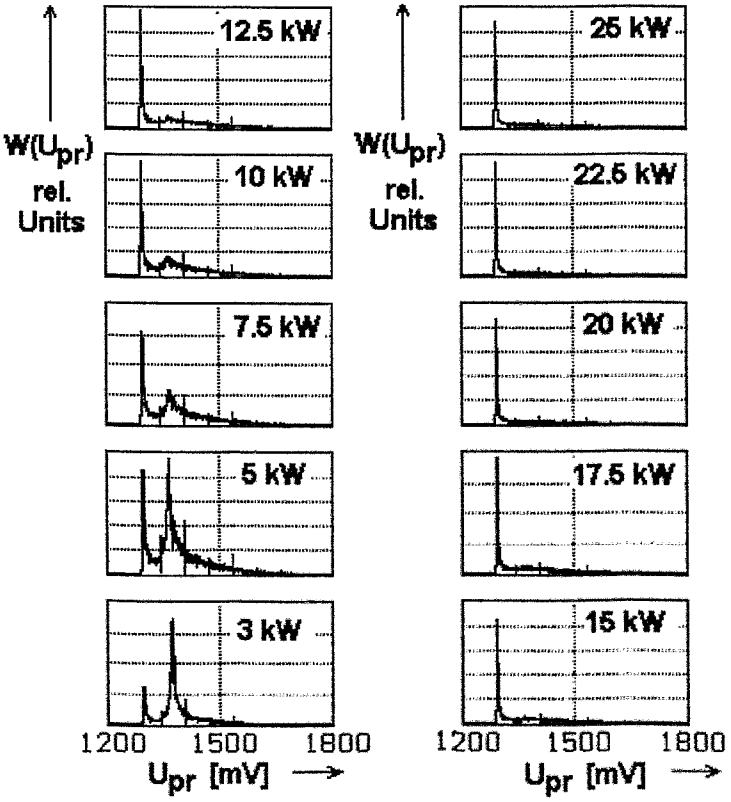


*Fig. 3.12 Histograms of the ultrasonic probe signal in DESIRE at different core power*

Finally, the DESIRE facility was brought into an

unstable state with oscillations of the coolant mass flow. These oscillations are reflected by the probe signal, which has shown gas fraction oscillations with a period of about 5 s (Fig. 3.14).

Summarising the results, it was found that the local ultrasonic probes can be applied to a flow of boiling refrigerants. This allows us to expect, that the ultrasonic mesh sensors can also be used in these fluids, because they are based on a similar working principle.

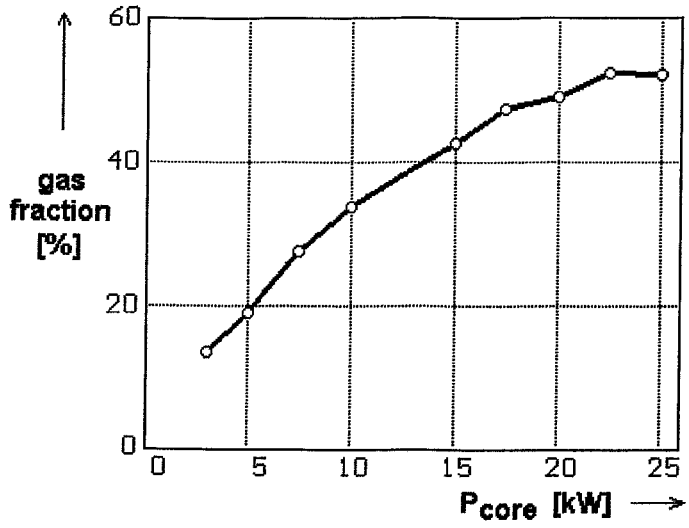


*Fig. 3.13 Gas fraction as a function of core power*

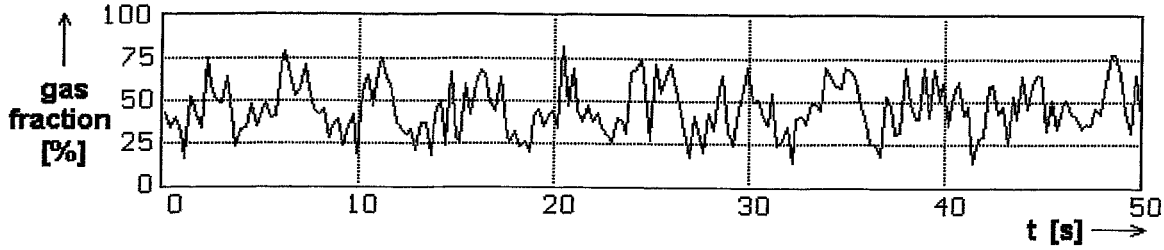


*Fig. 3.14 Gas fraction oscillations in DESIRE at a core power of 23.5 kW*

### 3.7.3 Comparison with high-speed camera recordings

The impact of individual bubbles with the local ultrasonic probe was studied by a high-speed video observation, which was synchronised with the signal acquisition of the probe. The imaging rate of the video system was 2000 frames per second. In these experiments, the pulse rate of the probe was 8 kHz, i.e. each fourth sample of the probe signal corresponds to one frame of the video device. The recording of both probe signal and video sequence was started by a synchronisation signal generated by the data acquisition computer of the probe and supplied to the high-speed video device via RS232c interface.

The tests were carried out in a rectangular perspex channel, which allowed to observe both probe and bubble from aside. The bubbles were generated by a steel nozzle, located below the probe. It was taken care to generate streams of individual bubbles by supplying very small air flow rates. The fluid was varied, beside water experiments were also carried out with glycerine and benzine.

A typical result is shown in Fig. 3.15. It confirms the principle character of the signal described in chapter 3.1, Fig. 3.1. The analogue signal starts to reflect the approach of a bubble still before the bubble has come into contact with the ends of the wave

guides. Before the output signal starts to decrease to the level characteristic for the gas phase, an oscillation is observed with a significant maximum, which reaches values well above the level characteristic for the liquid phase. This confirms that the cut of the local instantaneous gas fraction according to eq. 3.5 is necessary to avoid unrealistic negative gas fractions. The threshold method seems to be more appropriate than the linear evaluation formula, because the latter delivers contributions to the gas fraction already when the bubble has not yet contacted the probe. Nevertheless, the differences seem not to be very significant, as it was shown by the measurements at MTLoop, discussed in the previous chapter.

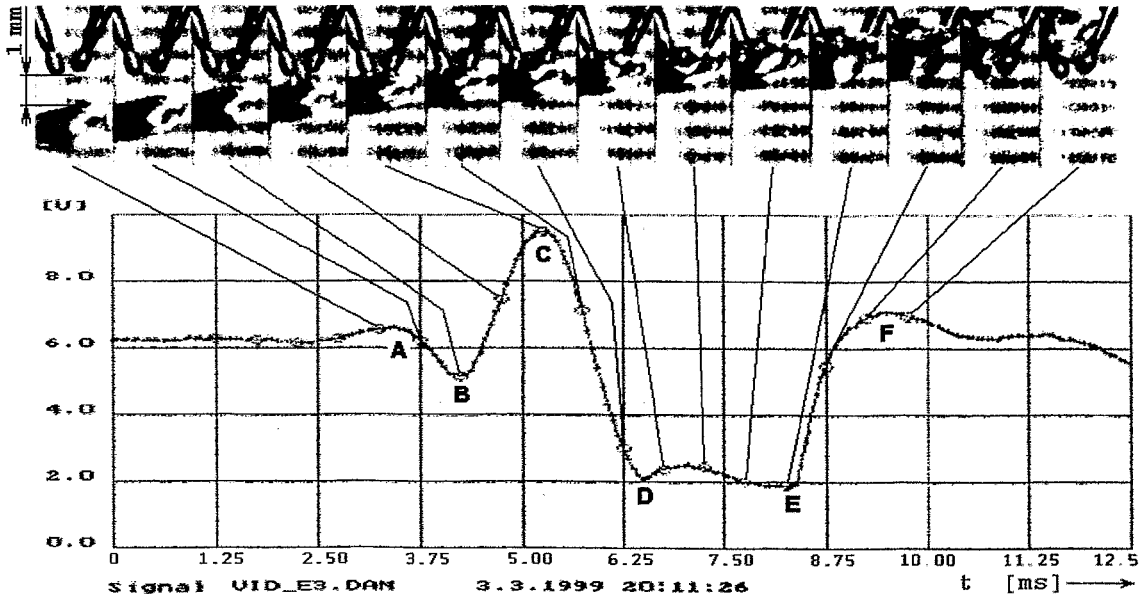


*Fig. 3.15 Comparison of a probe signal with a sequence high-speed video frames, air bubble rising in water*

The chronology of characteristic events can be described as follows: At a distance of more than 1.5 mm, the probe does not sense the approaching bubble. A maximum of the signal (**A**) is observed, when the distance between bubble and wave-guides is approximately 1 mm. It was found that the next maximum **C** corresponds to the moment, when the bubble comes into contact with the wave-guides. The previous maximum **A** is caused by a positive superposition of the direct ultrasound wave propagating from one probe tip to the other with the signal reflected at the bubble surface. Minimum **B** results from an anti-phase superposition of the two waves. The decrease towards minimum **D** is clearly caused by the covering of the sphere-shaped ends of the wave-guides. The rising slope between points **E** and **F** is connected with the successive re-wetting of the probe. Some subsequent signal fluctuations are the result of the gas-liquid boundary moving along the cylindrical parts of the wave-guides. The amplitude of these fluctuations is less than the oscillations during the approach of the bubble.

### 3.7.4 Bubble velocity measurement

The evaluation of the time difference between the maximums **A** and **C** can be used to determine the bubble velocity. This was done for an ensemble of several bubbles. The velocity found as a quotient of the sensible distance (1 mm) divided by the time

difference was compared to a velocity obtained by evaluating the high-speed video frames (Fig. 3.16). The bubble rise velocity was varied by using liquids with different viscosity.

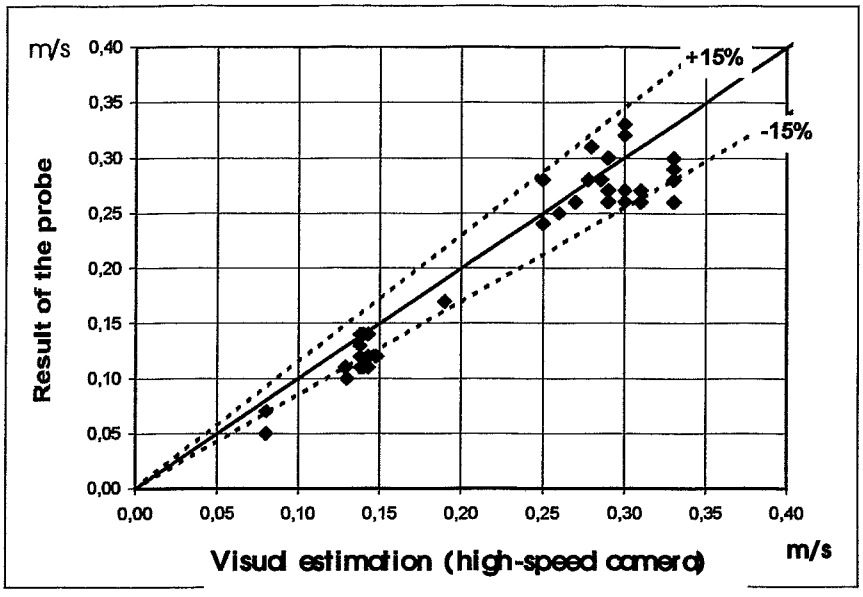


*Fig. 3.16 Comparison between bubble velocities obtained optically and by the probe*

### 3.7.5 Bubble size estimation

From the measured bubble velocity and the contact period, the bubble size can be estimated. This was done for an assembly of bubbles. The result was compared by bubble diameters obtained from the high-speed video frames (Fig. 3.17). We assume that the measuring error of 15 % is caused by the deformation of the bubbles, which obtain an elliptical instead of a spherical shape.

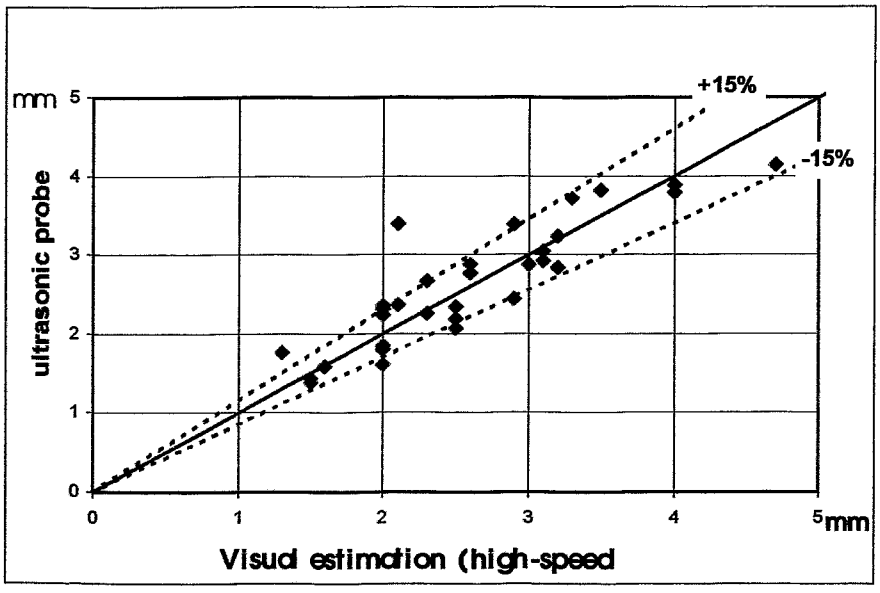


*Fig. 3.17 Comparison of bubble diameters*

## 3.8 Test of the gas fraction measurement in case of small bubbles

For these tests, a special bubble generator was designed and constructed, which is able to produce small bubbles with diameters down to several µm. It is based on the saturation of water with air in a pressure vessel at a pressure of about 6-7 bar. The saturated liquid is depressurised through a small nozzle. Due to the pressure decrease, the degassing process starts and swarms of very small bubbles appear in the liquid.

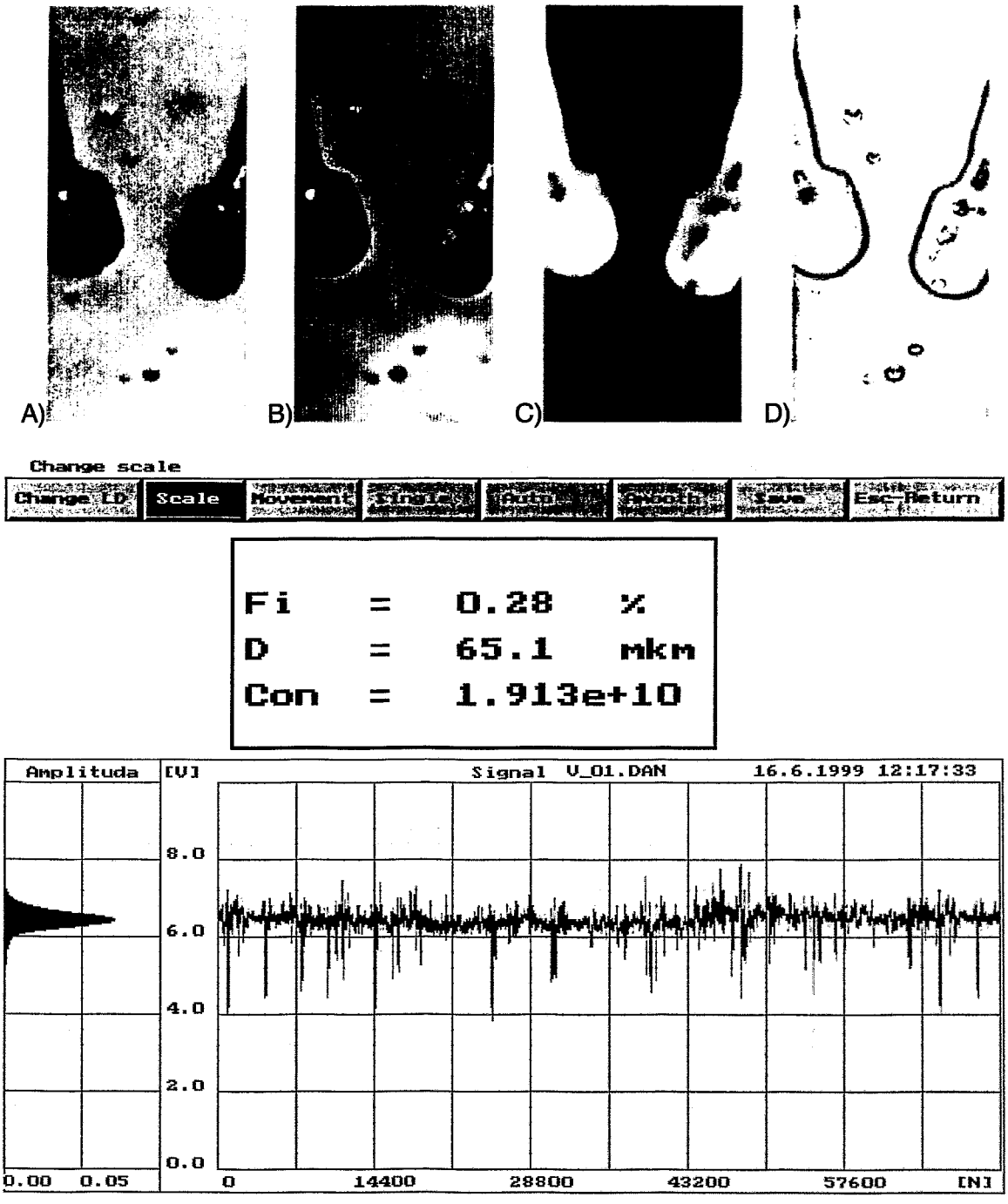


*Fig. 3.18 Screen dump and high-speed video frame for a two-phase flow with a low quantity of small bubbles*

The interaction of the small bubbles with the probe was at first studied by high-speed video observation (Figs. 3.18 and 3.19). The video frames (A) are processed to increase the contrast by image processing methods (contour extraction), the result is shown in frame D. A comparison is given between video frames and the measuring result. The latter is presented in form of screen dumps of the measurement control screen. Here, **Fi** denominates the gas fraction, **D** the mean bubble diameter and **Con** the particle concentration [1/m³], calculated according to the theory in chapter 3.5.2.

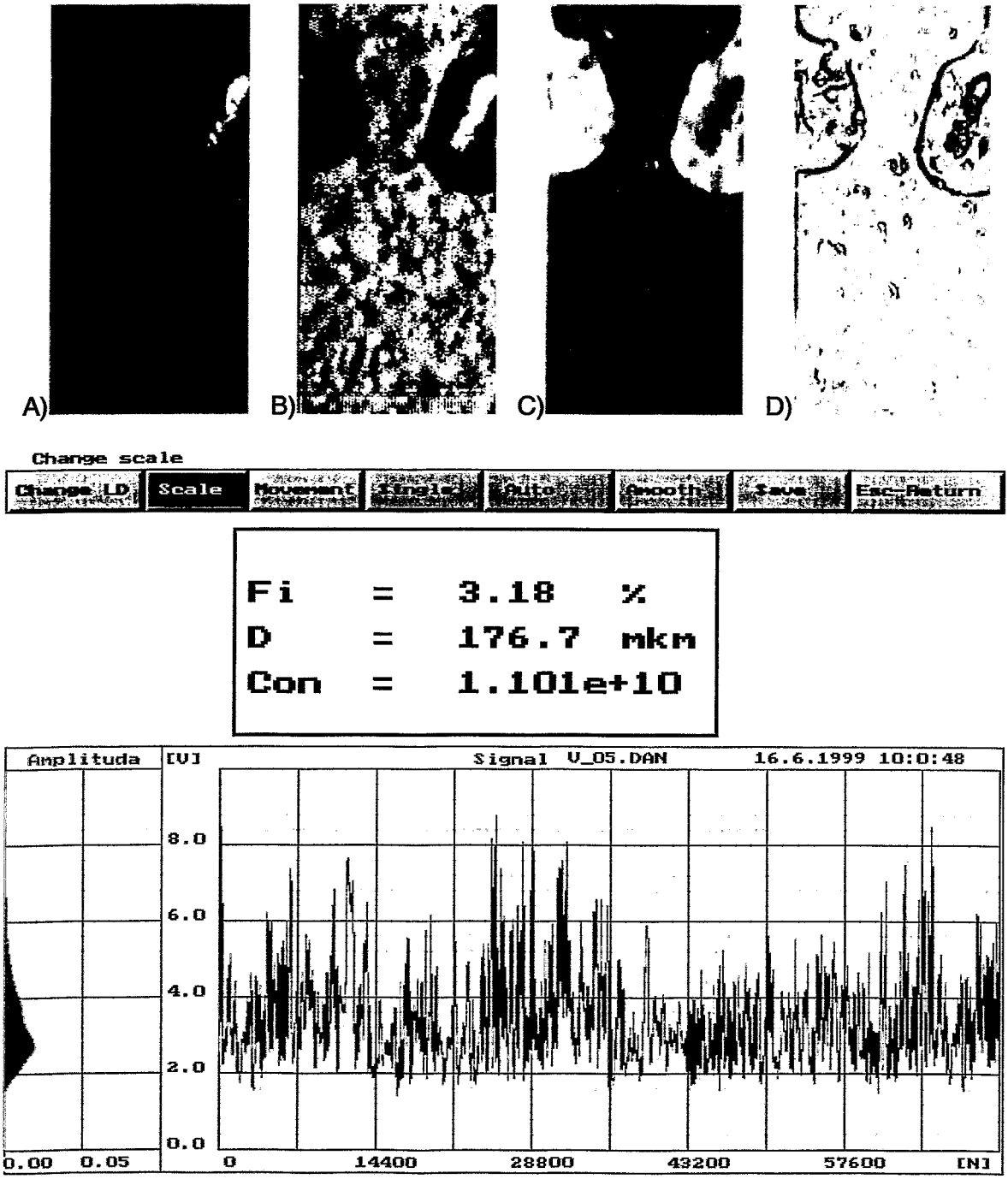


*Fig. 3.19 Screen dump and high-speed video frame for a two-phase flow with large quantity of small bubbles*

A quantitative check of the accuracy was performed by comparing the measured mean bubble diameters with the results of measurements of a Phase Doppler Particle Analyser (PDPA). For this purpose, the air-saturated water was injected into main water flow of the vertical test section of the two-phase flow test loop MTLoop. In the result, a two-phase flow at a well-defined water velocity with very small bubbles was generated. The channel was equipped with a 100 mm high observation window made of a transparent perspex tube. The PDPA was applied through the perspex wall. The results of the comparison is given in Fig. 3.20.

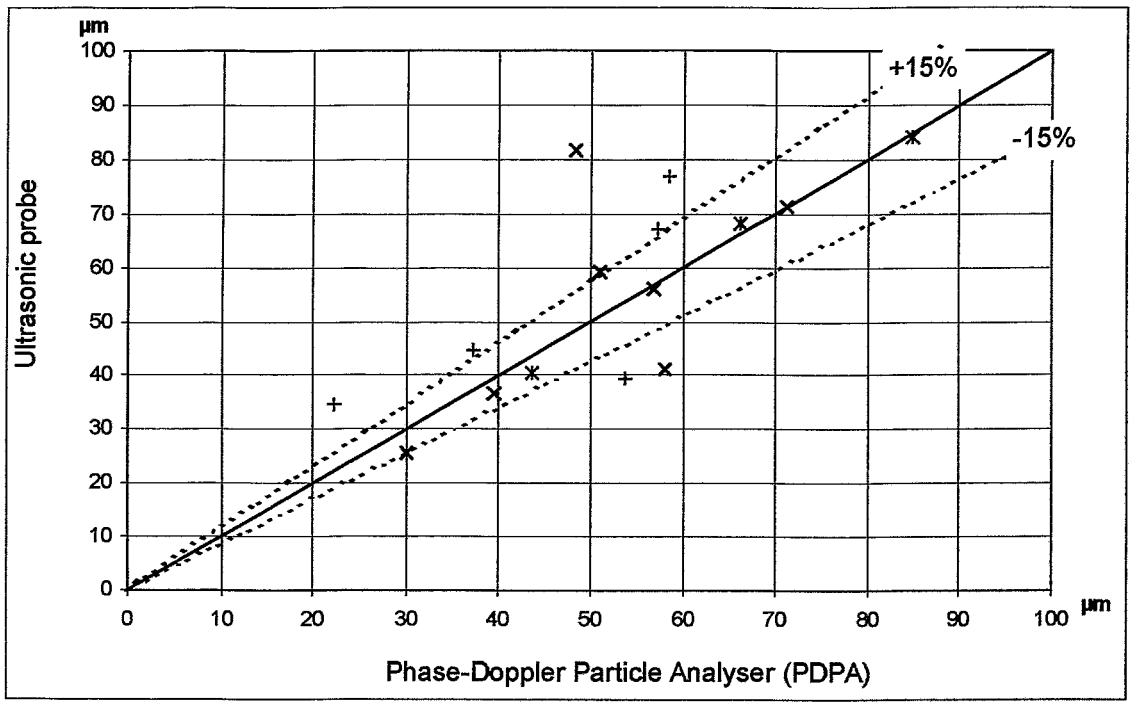


*Fig. 3.20 Comparison between mean bubble diameters obtaind by the local ultrasonic probe and the PDPA*

## 3.9 Nomenclature

| | | | | | |
|---|---|---|---|---|---|
| a | - | weight coefficients | q | $1/m^2$ | effective cross-section |
| c | m/s | velocity | T | s | total time of measurement |
| d | m | diameter | V | $m^3$ | volume |
| f | $m^3$ | correction factor | w | - | probability |
| J | $Wt/m^2$ | ultrasonic signal intensity | $\varphi$ | - | average steam fraction |
| k | $1/m^3$ | correction factor | $\alpha$ | - | local volumetric gas fraction |
| l | m | length | $\gamma$ | $m\ s^2/kg$ | compressibility |
| N | - | quantity of bubbles | $\mu$ | m | average diameter |

| | | | | | |
|---|---|---|---|---|---|
| n | - | quantity bubbles | $\rho$ | $kg/m^3$ | density |
| $n_0$ | $1/m^3$ | bubble concentration | $\sigma$ | - | root-mean-square |
| p | - | probability | $\tau$ | s | time |

### 3.10 Indices

| | | | |
|---|---|---|---|
| bub | bubble | L | liquid |
| con | control volume | lin | linear |
| G | gas | m | mean |
| os | oscillation | w | wave-guide |

### 3.11 References


[3.1] Melnikov V.I., Usinin G.B., Acoustic methods of diagnostics of two-phase coolants in NPP. Moskow. Energoatomizdat, 1987.

[3.2] Landau L.D., Livshiz E. M., Statistical physics. Moskow. Science.1964.

[3.3] Bocharov P.P., Pechinkin A.V., The theory of probabilities. Moskow. Science. 1994.

[3.4] Gmurman V.E., A management to the decision of tasks on the theory of probabilities and mathematical statistics. Moskow. Higher school. 1989.

[3.5] Lependin L.F., Acoustics. Moskow. Higher school. 1978.

[3.6] Gavrilov A.R., The contents of free gas in a liquid and acoustic methods of his measurement. Acoustic magazine. 1989. N3.

[3.7] Levkovskiy O.L., Structure turbulence of currents. Leningrad. Shipbuilding. 1988

[3.8] Machin V.A., Melnikov V.I., Chatrov B.A., An estimation of accuracy of measurement steam considers by a method of acoustic sounding. Industrial Heatengineering. 1981.N 4

[3.9] Isakovish I.P., Common acoustics. Moskow. Science. 1973.

# 4. Single point probe

This part of the report deals with the development of high frequency immersing probes for the measurement in fluids of high parameters, using longitudinal waves. A single point probe is used in active and passive working modes. A special technology to produce wave-guides results in an increase of the working frequency into ranges up to 10 MHz. The single point probe can be used for the measurement of gas fractions or the velocity of the gas-liquid inter-phase surface as well as velocity measurements in single phased liquids. The theoretical basics of probe design including wave-guide, piezoelectric crystal and radiating-receiving surface are described. As an example, test measurements of the velocity of a liquid sodium flow are described. These tests were performed at the sodium loop NATAN of FZR (Dept. of Magnetohydrodynamics).

## 4.1 Functioning of the single point probe

The process of wave spreading in wave-guide is dominated by the resonance phenomena, which is defined by the relation between geometrical dimensions and frequency. For the description, the dispersion of longitudinal waves must be taken into account. It depends on the physical properties of the wave-guide material, the geometrical parameters, the wavelength and the wave propagation velocity (speed of ultrasound). The wave equation for waves travelling along the axis of a wave-guide are solved by the function:

$$\exp [\, j( \gamma z - \omega t ) \,], \tag{4.1}$$

where: z - coordinate; $\gamma = 2\pi/\lambda = \omega/c$ - constant of speed; $\lambda$ - wavelength; c - phase wave velocity; $\omega$ - ultrasound frequency; t - time. In case of a cylindrical wave-guide, an exact solution of the wave propagation equation can be found. Axis-symmetrical longitudinal waves are described by the Pohgamer equation:

$$2\alpha/a \, ( \beta^2 + \gamma^2 ) \, J_1 (\alpha a) J_1 (\beta a) - (\beta^2 - \gamma^2)^2 \, J_0(\alpha a) \, J_1 (\beta a) - 4\gamma\alpha\beta \, J_1(\alpha a) \, J_0(\beta a) = 0 \tag{4.2}$$

where: $\alpha^2 = (\omega/c_l)^2 - \gamma^2$ ; $\beta^2 = (\omega/c_\tau) - \gamma^2$ ; $c_l = \sqrt{(2\mu + \lambda/\rho}$ - propagation velocity of longitudinal waves; $c_\tau = \sqrt{\mu/\rho}$ - propagation velocity of flexural (bending) waves; a - radius of wave-guide; $\mu$, $\lambda$- Lame constant; $\rho$ - wave-guide material density; $J_0$, $J_1$ - Bessel's functions.

The dependence between constant of spread $\gamma$, frequency and geometry of the wave-guide are determined by the dispersion coefficient. Thereby the dependency between phase wave velocity and frequency are determined. The dispersion coefficient for longitudinal waves is shown in Fig. 4.1.

For the description of a wave-guide with rectangular cross-section, the theory of wave propagation in an infinite plate is used, the width of which is greater than the wavelength. The dispersion equations for longitudinal and flexural normal waves are:

$$\frac{thj\beta h}{thj\alpha h} = -\frac{4\gamma^2\alpha\beta}{(\gamma^2 - \beta^2)^2}; \tag{4.3}$$

$$\frac{thj\beta h}{th\alpha h} = -\frac{(\gamma^2 - \beta^2)^2}{4\gamma^2\alpha\beta}. \qquad (4.4)$$

Where, h is the thickness of the plate.

Graphs of the dispersion of longitudinal and flexural waves in endless plates are presented in Fig. 4.2. The behaviour of dispersion lines for the plate and for cylindrical wave-guides are analogous. A maximum of dispersion (the dependence velocity of acoustical waves from frequency) in field of low frequency is observed. For the bad waves of higher order, attenuation is increased after increasing the cross-section size and the working frequency. Beginning from a certain working frequency, the quantity and direction of the irradiated energy is increased in comparison to a cylindrical wave-guide.

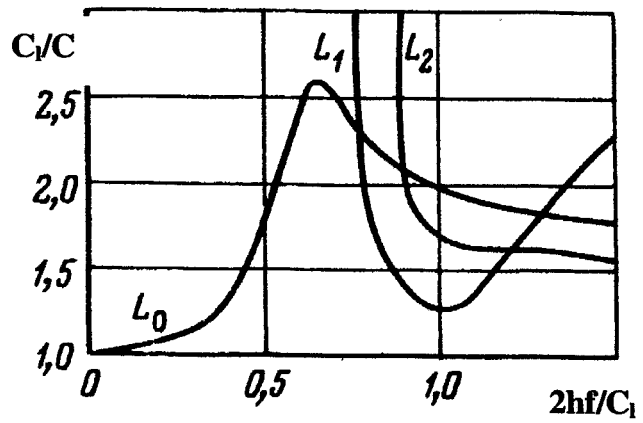


*Fig. 4.1 Dispersion of longitudinal waves*

*$L_0, L_1, L_2$ - longitudinal waves of 0, 1, 2 orders*
*$C_l$ – velocity of longitudinal wave in fine rod*

## 4.2 Design of coiled wave-guide sensor

An infinite plate has some advantages in the region of high frequency. Therefore, a new type of wave-guide was developed. The so-called coiled wave-guide consists of a thin foil of stainless steel, which is wrapped to form a cylindrical rod of a certain diameter much larger than the thickness of the foil. The latter approximately equals the wavelength. The acoustic sensor on basis of such a coiled wave-guide is shown in Fig. 4.3. Each layer of foil forms an individual wave-guide, which works independently from the other layers. The waves are in phase, the irradiated acoustical energy is a result of a positive superposition of the waves in each layer.

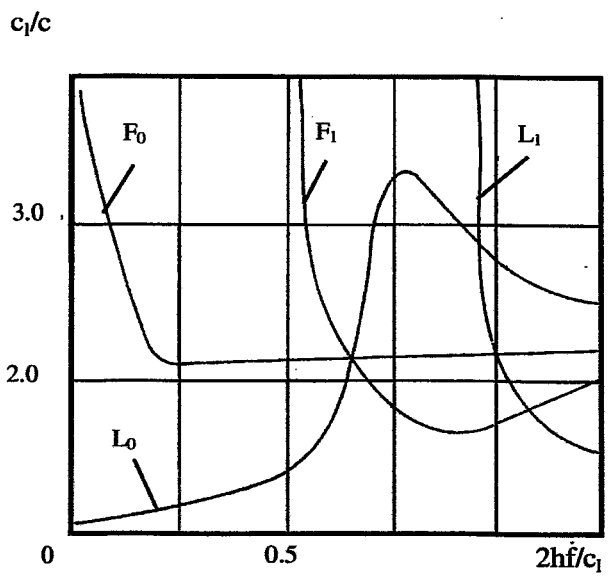


*Fig. 4.2 Dispersion of the wave propagation velocity in an endless plate of 0.3 mm thickness*
$F_0, F_1$-bending wave; $L_0, L_1$-longitudinal wave

For effective radiation into the measuring fluid, the radiating surface is formed by a large number of layers. For the hermetisation of the probe, the immersed part of the wave-guide is put into a protective top and fixed with the top by welding. In order to protect it from mechanical damage, the probe is placed into a protective case. The main technical characteristics of the single point probe are shown in Fig. 4.4. The main parameters are: maximum of working temperature - 400 $^0$C; maximum pressure 15 MPa; material of wave-guide - steel 08CrNiTi18.10; diameter of wave-guide - 7 mm; working frequency - 4 MHz; angle of radiation - $90^0$; angle of beam widening - $1.7^0$; near area - 25 mm; attenuation coefficient in the electric-acoustical line - 7. The sensor is calibrated in impulse mode.

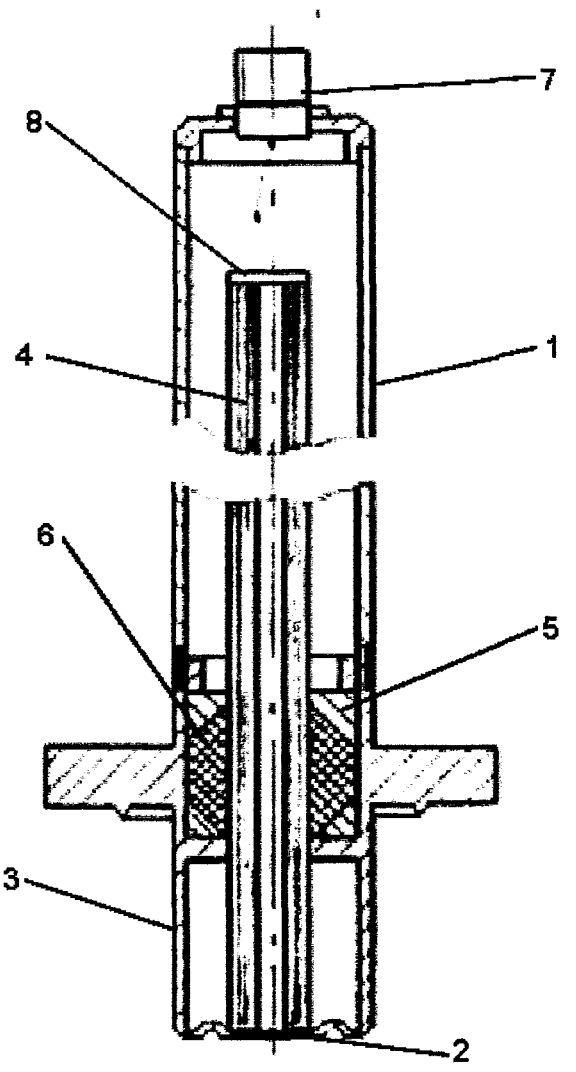


*Fig. 4.3 Design of single point probe with coiled wave-guide*

1 - case; 2 - radiation area; 3 - protective top; 4 - wave-guide; 5 - distance element; 6 - rubber-plug; 7 - connector; 8 - acoustic converter

## 4.3 Example of application

The single point probe was connected to an ultrasonic test monitor of the SONY company and tested in reflection mode. The velocity profile of a liquid sodium flow was measured in the sodium loop NATAN. Previously, the main characteristic of single point probe were determined in a water flow in the laboratory of TUNN. After that, the single point probe was mounted into the sodium circuit of Rossendorf. It was placed into the test channel under an angle of $70^0$ to the axis of the cross-section. The working temperature of the liquid sodium was 200 $^0$C. The velocity of liquid sodium was varied in range from 0.2 to 1.0 m/s. Some experimental data of velocity profile variations in the cross-section of the channel are showed in Fig. 4.5.

## 4.4 Conclusions

The new type of coiled wave-guide allows to design sensors, which can work on a higher frequency, than traditional wave-guide sensors. This is an important result for non-intrusive high-temperature applications, where a direct mounting of the piezoelectric crystal to the surface of the experimental or industrial facility is not possible.

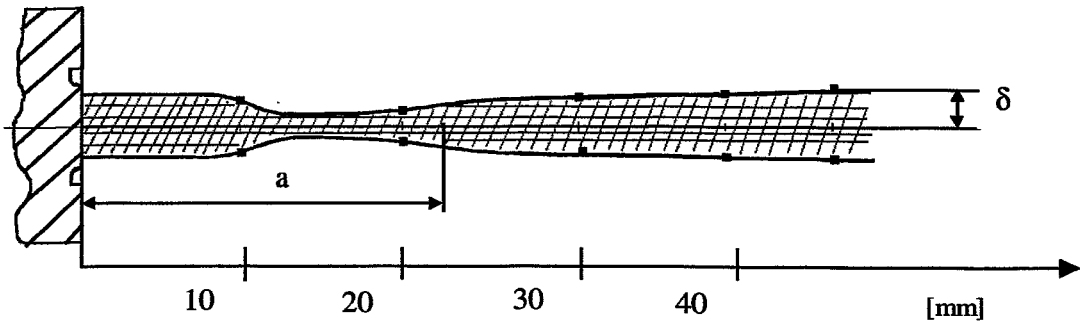


*Fig. 4.4 Acoustical beam shape of the single point probe*

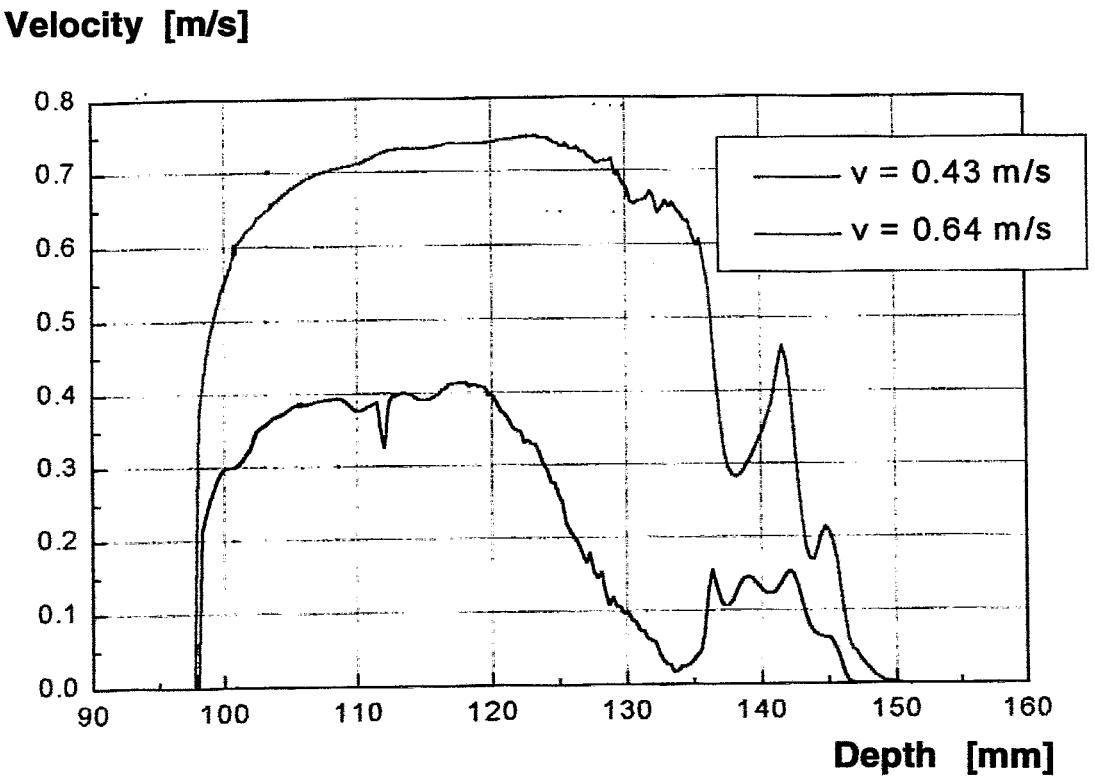


*Fig. 4.5 Measured velocity profile at the FZR sodium loop*

# 5. Non-invasive through-transmission sensors

This part of the report deals with the development of non-invasive sensors for gas phase measurements in pipelines, based on an ultrasonic through-transmission technique. Special wave-guide transducers are flanged to the outer wall of the pipe. This allows to apply the sensor in case of high temperatures inside the pipeline. It can be used for gas fraction as well as gas phase velocity measurements. The theoretical basis of the sensor design and two types of devices with their technical characteristics are presented. It will be furthermore reported about test measurements at the two-phase flow test loop MTLoop in Rossendorf and at the Pilot Plant Pipework (PPP) facility of UMSICHT in Oberhausen.

## 5.1 Working principle of the non-invasive sensor.

The function of the sensor is based on the excitation of bending waves (transversal waves) in the wall of the pipeline. These transversal waves generate ultrasound sources, when they arrive at the inner surface of the pipe wall. The ultrasound beam is irradiated under a well defined angle $\Theta$ to axis of pipeline and can be received by a sensor of identical design at the other side of the tube (Fig. 5.1). In this respect, the wall of the pipe acts as wave-guide. At the parallel contact surface with the fluid inside the pipe, a mode transformation takes place and the final longitudinal ultrasonic wave is generated.

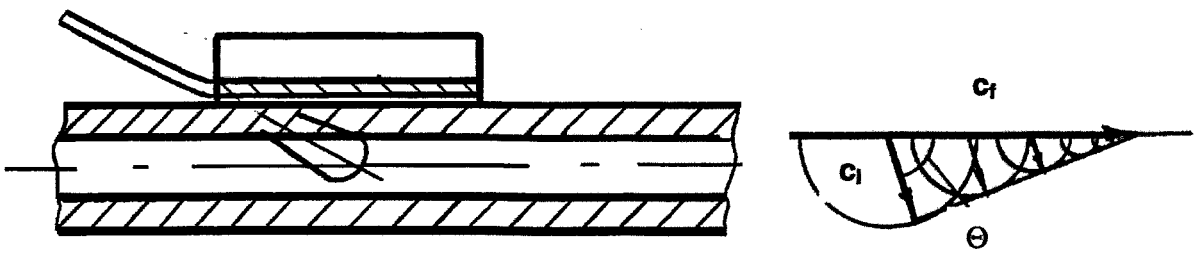


*Fig.5.1 Working principle of the non-invasive sensor, mode transformation at the inner wall surface*

When we assume that the liquid is non-viscous and energy losses in the wave-guide material are neglected, the attenuation of the bending waves in the flat wave-guide is only caused by the irradiation of sound into the liquid. An approximate expression for the coefficient of attenuation of flexural waves (for the case kh>>1) is:

$$\alpha = \frac{\rho_l \cdot c_l}{\rho \cdot h \cdot \sqrt{c_p h \omega - 2c_l^2}} \qquad (5.1)$$

where:

h - wave-guide thickness; $c_p$ - propagation velocity of longitudinal waves in the wave-guide at $f \rightarrow 0$; $\omega=2\pi f$; f - ultrasound frequency; $\rho_l$ - density of the liquid; $\rho_f$ - density of wave-guide; $c_l$ - speed of sound in the liquid; k - wave coefficient, l - length of wave-guide.

In case that $\omega h c_p > 2c_1^2$, the coefficient $\alpha$ is real and sound is irradiated into the liquid. The propagation velocity of bending waves depends on the frequency in the low-frequency range:

$$c_f = \sqrt{\frac{c_p h \omega^2}{2}}. \qquad (5.2)$$

Operational frequency and wave-guide thickness are determined by functions (5.1) and (5.2). The angle $\Theta$ between the wave vector and axis of the pipe is determined by the ratio between the speed of sound in the liquid and the propagation velocities of the bending waves:

$$\Theta = \text{arctg}\frac{c_l}{c_f}. \qquad (5.3)$$

The radiation angle depends on the frequency, since the speed of sound in the liquid and the propagation velocity of the bending waves are functions of the frequency, too. The attenuation of an acoustic wave in the wave-guide immersed in liquid is determined as follows:

$$A = A_0 \exp(-\alpha l). \qquad (5.4)$$

## 5.2 Functional elements and physical characteristics of the sensor

The non-invasive wave-guide sensor consists of three functional parts: electrical-acoustic converter, wave-guide communications line, radiating-receiving element.

The acoustic converter with piezo-crystal disc and lap was designed to generate bending waves. The piezo-crystal converter is attached to the lateral surface of the wave-guide (Fig. 5.2). The dimensions of the piezo-crystal converter and the steel lap heights and their position determine the amplitude-frequency characteristics of converter.

The amplitude-frequency characteristic of a bending waves converter with a wave-guide of rectangular cross-section of 2.5×1.5 mm made from steel X6CrNiTi18.10 and a piezo-crystal converter with a height of 0.9 mm made from zirconate-titanate of lead and a lap made from steel X6CrNiTi18.10 is presented on Fig. 5.3.

The operating frequency is 400 kHz, the propagation velocity of the bending waves in the wave-guide is 3000 m/s. With a piezo-electric converter attached at the distance $\lambda/2$ (where-$\lambda$ is length of waves) from the free end of the wave-guide (it is equal to 2.5 mm), a maximum width of the operational frequency range is realised. The transmission coefficient of this converter reaches 0.4-0.5. The relative width of the operational frequency range (6 dB) is between 0.3-0.4.

An elastic hermetic covering of the piezo-crystal - lap system expands the amplitude-frequency characteristics by 20-30%. In this case the resonance frequency of the converter is decreased by 5-7 % and the transmission is decreased by 15-20 %.

Another method of bending waves generation is based on transformation of longitudinal waves into bending waves at the contact surface between wave-guide and outer pipe surface. In this case, the piezo-electric converter located at the back face of the wave-guide generates longitudinal waves (Fig 5.4). At the sharp 90 deg bend of the wave-guide nearly 70 % of the energy of the longitudinal waves is converted into bending waves.

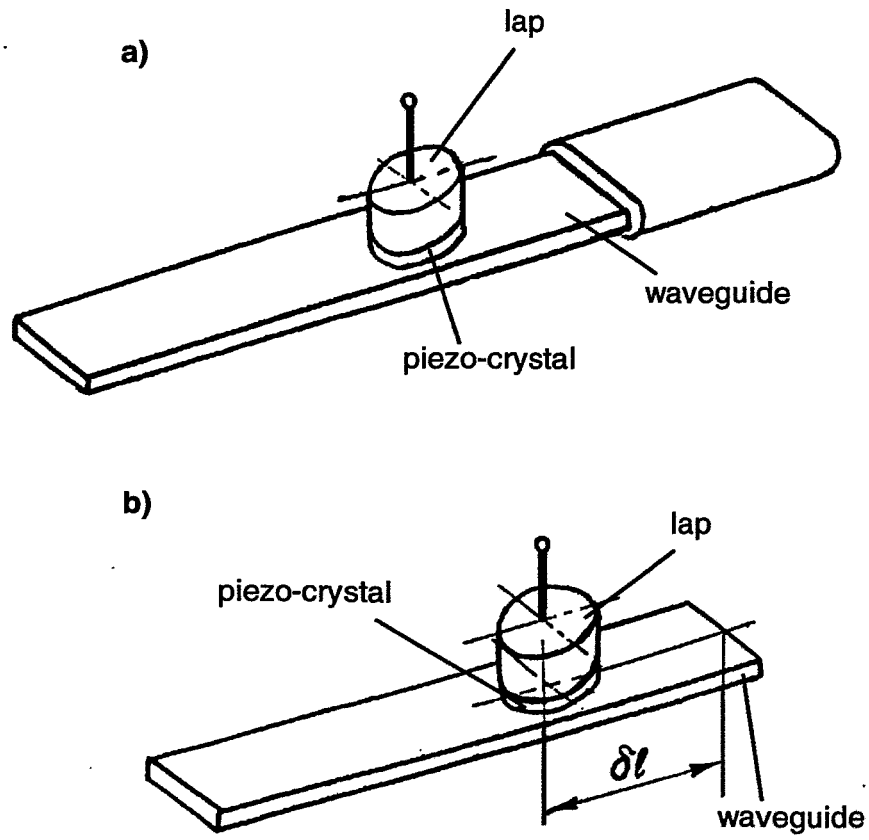


*Fig. 5.2 Acoustical converter generating bending waves*

*a) - with elastic hermetic covering of the wave-guide end*

*b) - without elastic hermetic covering of the wave-guide end*

The amplitude-frequency characteristics of converter with a rectangular cross-section of 2,5×1,5 mm made from zirconate-titanate of lead-19 located on the free end of wave-guide with an equal cross-section made from steel X6CrNiTi18.10 is shown in Fig. 5.5. The operating frequency is 500 kHz, the relative band width is 0.7. The transmission coefficient of this converter reaches 0.4.

Cylindrical wires, stripes, rods of rectangular cross-section can be used for the manufacturing of wave-guides. Two rubber plugs are used for the support of short (< 0.5 m) wave-guides.

The radiating-receiving element having form of core approximating along pipe axis and location on the internal surface was produced. The acoustical contact is provided by using of polish on the location place and by using of contacting layer from soft metal (copper, lead...).

The radiation direction field of the radiating-receiving element with a rectangular cross-section of 2.5×1.5 mm and a length 60 mm mounted onto a pipeline of 40 mm outer diameter of 40 mm and 4 mm wall thickness is given in Fig. 5.6. The material of the radiating-receiving element and the wall of the pipeline is identical (steel X6CrNiTi18.10),

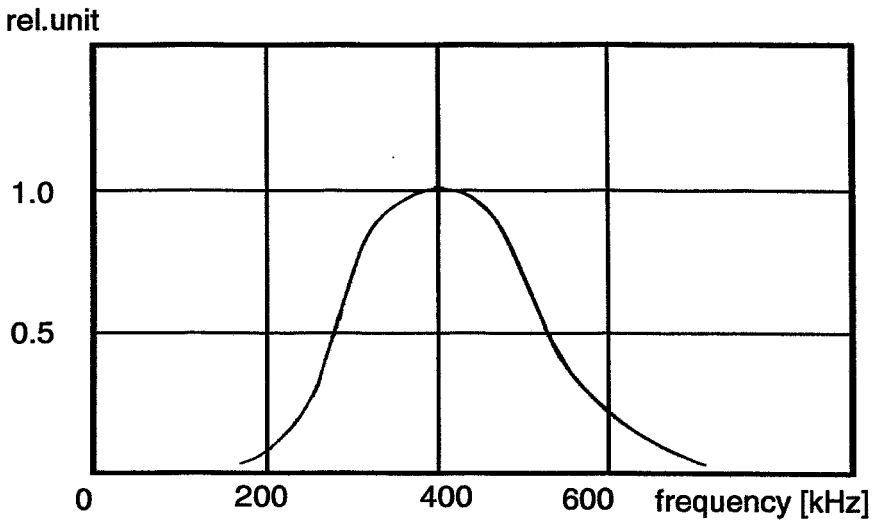


*Fig. 5.3 Amplitude-frequency characteristic of the acoustical converter working in bending waves mode*

the operating frequency is 400 kHz. The fluid is water under normal conditions. By measuring the radiating direction field it was shown that the experimental angle of inclination of the main lobe is 38 degree. This is in good agree with the theoretical angle (32 deg). Depending on the operation frequency the angle of inclination is changed. The effective radiating point is located at a distance 10-12 mm from the front edge of the radiating-receiving element. This is equal to 1.5-2 lengths of bending waves. The radiating direction field was received under normal condition in water, as well as in acetone and hexane. At room temperature, the latter liquids have the same acoustic properties as saturated water at a pressure of 4.4 and 8.5 MPa, respectively, and were used as model liquids for pressurised water.

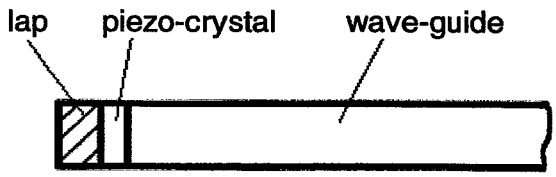


*Fig. 5.4 Acoustical converter for longitudinal waves*

The thickness of the radiating-receiving element must be adapted to the wall thickness of the pipeline by using the following expression:

$$h \leq 2\text{-}3\lambda_{total}; \tag{5.5}$$

where: $\lambda_{total}$ - total length of wave system consisting of radiating-receiving element + pipeline wall. For the formation of an acoustical field with a maximum radiation energy the length of the radiating-receiving element is selected according to

$$l \geq 2\text{-}3\lambda_{total}. \tag{5.6}$$

Contact paste is used to press the radiating-receiving element to the pipe surface, because the bending oscillations of the wave-guide are not symmetrical. The paste provides an acoustical "soft" fastening (non-hindrance of micro-moves).

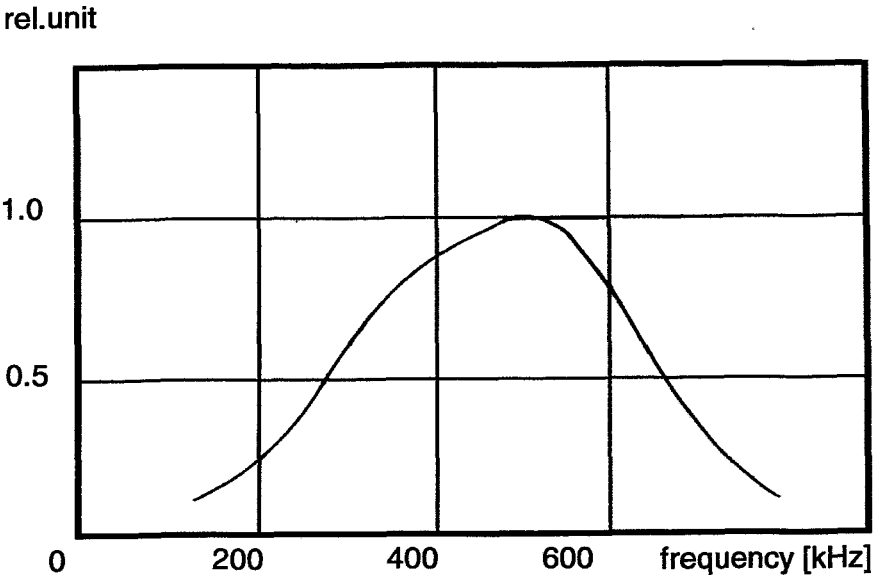


*Fig. 5.5 Amplitude-frequency characteristic of the converter for longitudinal waves*

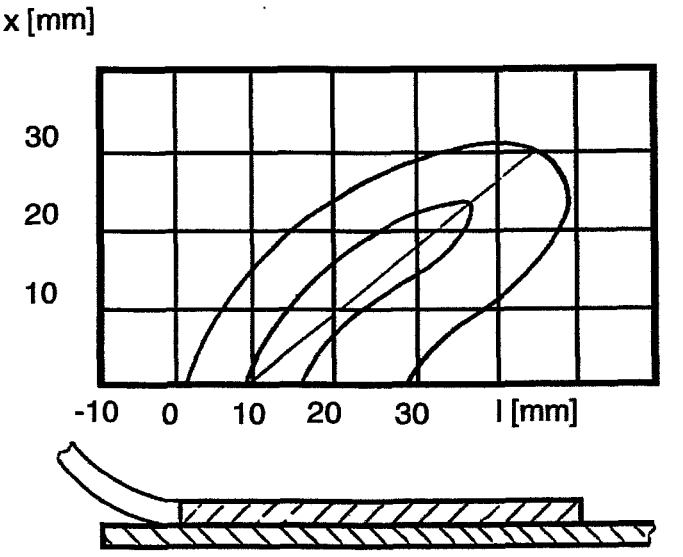


*Fig. 5.6 Acoustical field of the radiating-receiving element*

## 5.3 Design and field of application.

Two design versions of the non-invasive through-transmission sensors are shown in Fig. 5.7 and Fig. 5.8. In case of Fig. 5.7 the radiating-receiving element has a rectangular cross-section of 2.5×1.5 mm and a length of 10 mm. It is pressed to the pipe surface by copper screws (M6). The wave-guide communications line has a length of 350 mm. It is placed into a protective tube of 10 mm diameter and a wall thickness of 4 mm by using heat-resistant rubber plugs. The disk-shaped piezo-crystal converter is made from zirconate-titanate of lead-19 and has a diameter of 2.5 mm and a thick-

ness of 0.8 mm. It is soldered to the face of the wave-guide back end. The free surface of the piezo-crystal and the wave-guide is covered by silicon sealing compound. The amplitude-frequency characteristic of the converter shows a single resonance with a central frequency of 400 kHz. The bandwidth (6 dB) is 250 kHz. The connection with the electrical communication line and the protection from electromagnetic disturbances is realised by a differential transformer. The sensor works as follows: The electro-acoustic converter generates ultrasonic pulses of the required frequency and duration. They propagate along the wave-guide to the radiating-receiving element, exciting oscillations in the radiating-receiving element and the pipe wall. In the result, an ultrasonic wave is irradiated under the angle Θ. In dependence from the measuring tasks one or more sensors can be operated in the regime "transmission-receive", or two sensors can be applied, one in transmitter the second in receiver mode.

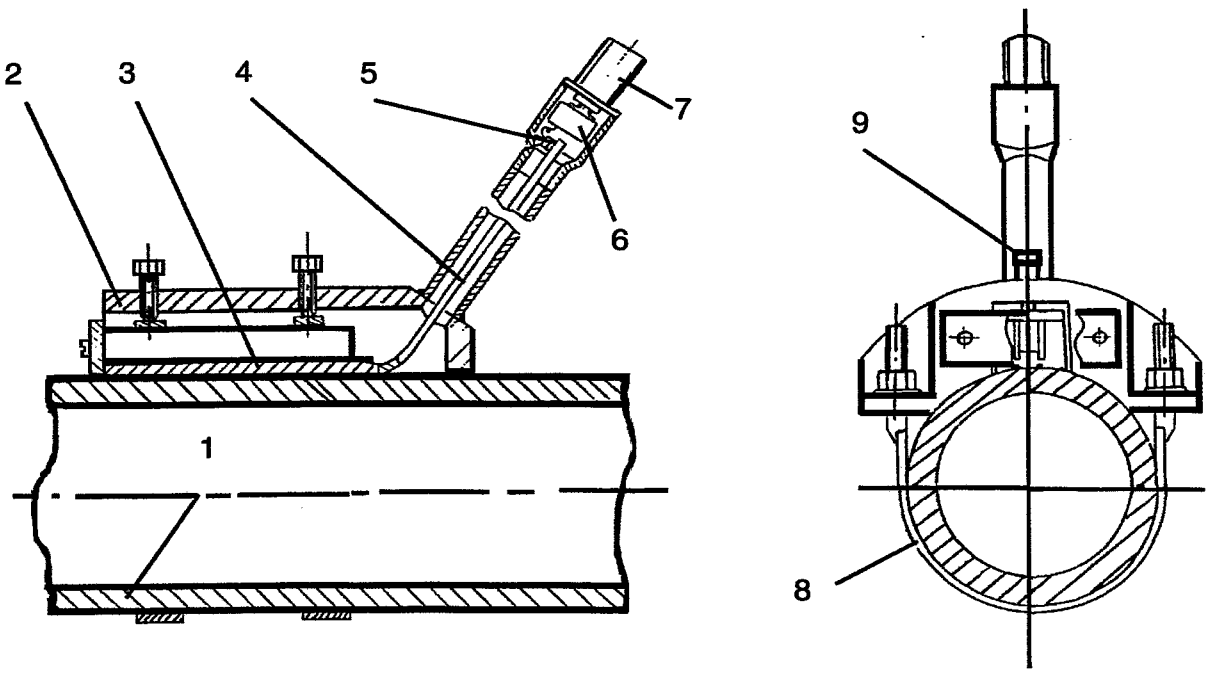


*Fig. 5.7 Design of non-invasive sensor*

*1 - pipeline; 2 - case; 3 - radiating-receiving element; 4 - wave-guide; 5 - piezo-crystal*

In the design given in Fig. 5.8 the radiating-receiving element is pressed to the pipe surface using a pressing nut. This allows to separate the body of sensor from the collar, which mounted on the pipe. This technical decision allows to use the same sensor for different pipe diameters by changing the dimensions of the collar.

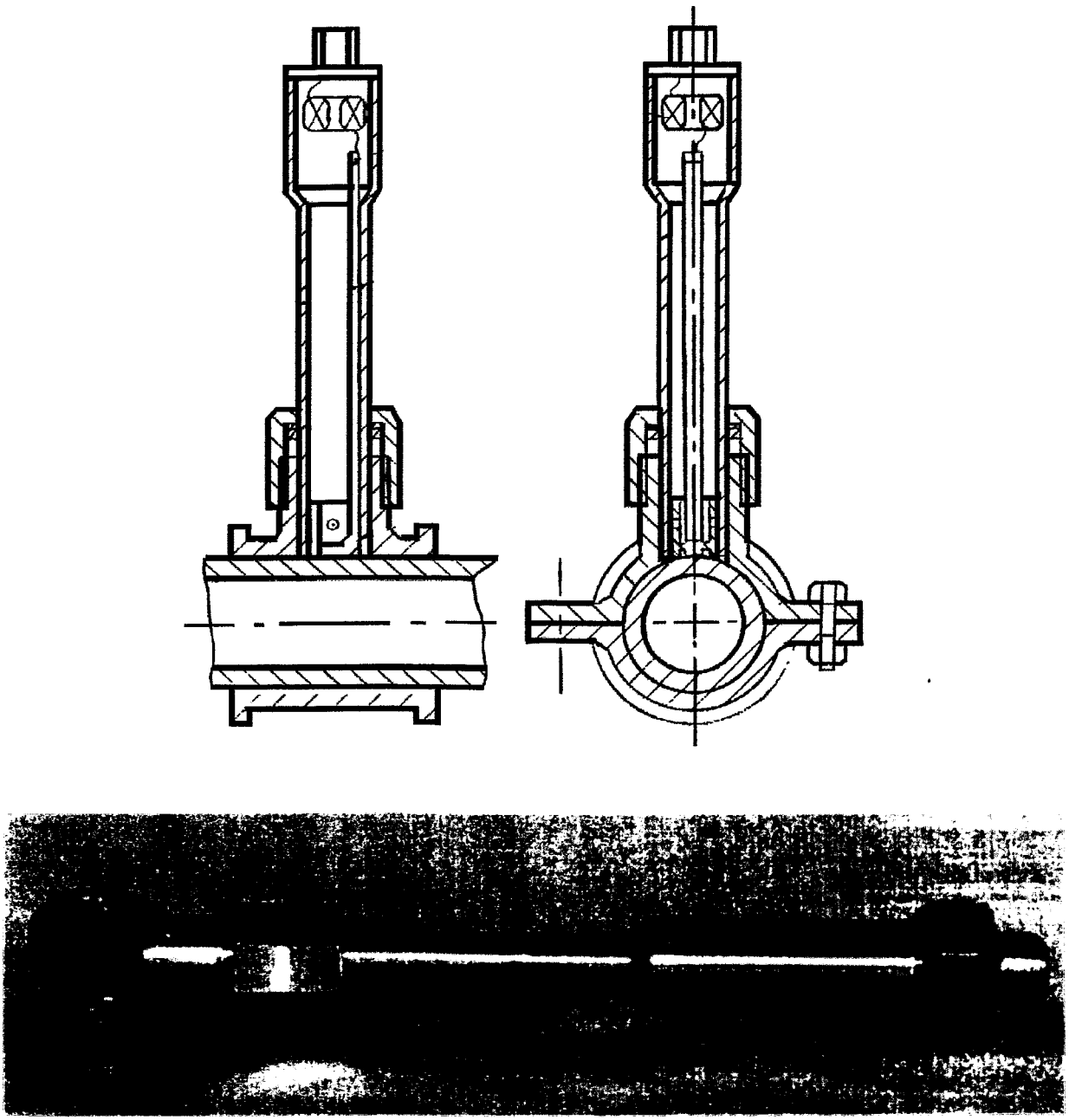

*Fig. 5.8 Design of separable non-invasive sensor*

*1 - pipeline; 2 - case; 3 - radiating-receiving element; 4 - wave-guide; 5 - acoustical converter; 6 - differential transformer; 7 - connector; 8 - collar; 9 - screws*

## 5.4 Signal acquisition

The signal acquisition is carried out similarly to the function of the signal acquisition unit used in case of the local wave-guide probes (chapter 3.3), i.e. the received pulse is analysed by a peak detector circuit, which is activated by a strobe pulse derived from the excitation trigger. The delay between excitation and rising edge of the strobe as well as the duration of the strobe must be set up according to the time total delay of the ultrasound in the wave-guides, the pipe walls and the measuring fluid.

For operating a single sensor in transmission/receive mode, the excitation pulse and the receiver cascade are connected to the same piezo-converter. This mode is similar to the pulse-echo mode of ultrasonic testing devices. For a through-transmission, a separate crystal is used to receive the ultrasound after propagating through the measuring fluid. In this case, excitation output and receiver input are separated from each other.

The signal acquisition unit delivers a voltage signal in a range between 0 and 5 V. This signal reflects the amplitude of the received ultrasonic energy with a measuring rate equal to the repetition rate of the excitation pulse. It contains information about the acoustical properties of the measuring fluid. For void fraction measurements, it must be calibrated by comparison to another reference method.

The voltage signal is digitalised by an AD converter and processed by a micro-controller MC68340. Four channels are connected to one micro-controller. The controller is linked to a data acquisition PC via serial interface. A view of the sensor together with the signal acquisition unit and the processor unit is given in Fig. 5.9.

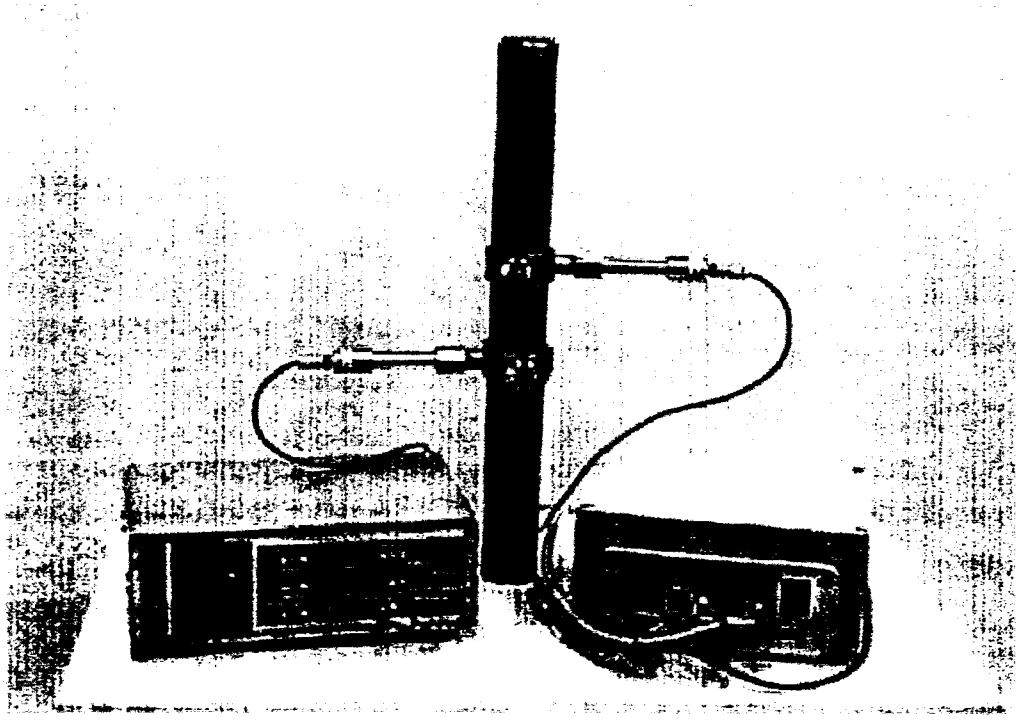

*Fig. 5.9 View of the non-intrusive ultrasonic probes mounted on a 50 mm test tube together with signal acquisition unit (left) and processor unit (right)*

## 5.5 Calibration

A calibration was carried out at the two-phase flow test loop MTLoop in a vertical upwards air-water flow. The output voltage of the ultrasonic device was compared to the readings of an electrical wire-mesh sensor. For the purpose of a direct comparability, the two-dimensional gas fraction distributions measured by the wire mesh sensor were used to calculate average values along the through-transmission chord of the non-invasive ultrasonic wave-guide sensors.

At first, signals of both pulse-echo mode and through-transmission mode were recorded for different combinations of the superficial velocities of air and water in the test section. The superficial velocities were varied in the ranges of 0.0024 m/s $\leq J_{air} \leq$ 12 m/s and 0.044 m/s $\leq J_{water} \leq$ 4 m/s respectively. Fig. 5.10 presents the output voltage in through-transmission mode, averaged over a measuring period of 120 s, plotted against the linear average of the wire-mesh data, which was averaged over 10 s.

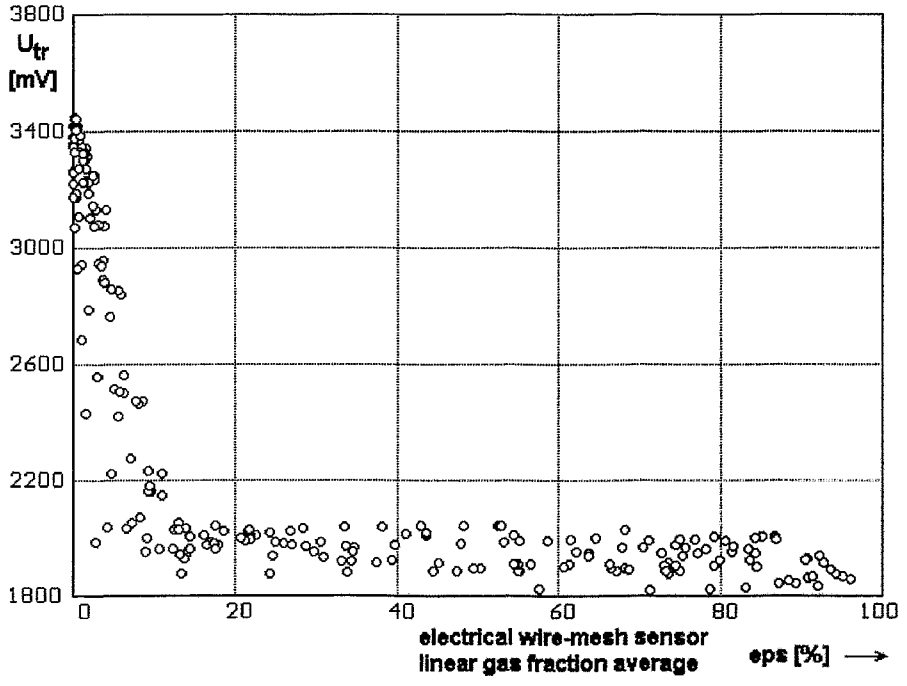


*Fig. 5.10 Amplitude of the ultrasonic through-transmission signal compared to the gas fraction measured by the electrical wire-mesh sensor*

A significant dependency between gas fraction and ultrasound amplitude, which is worth calibrating, can be found only in the range of gas fractions below 12-13 %. In this range and at velocities below 2.5 m/s, the following linear expression can be used to obtain gas fractions:

$$\varepsilon \approx \frac{3400\ \text{mV} - U_{tr}}{1600\ \text{mV}} \cdot 12.5\ \% \qquad (5.7)$$

Using this method, the test points lie in an error band of ± 0.02 (absolute gas fraction error ± 2 %), which means an approximate relative error of ± 16 % related to the range of $0 \leq \varepsilon \leq 0.125$ (maximum gas fraction 12.5 %), which is the validity range of

eq. (5.7). This result is illustrated in Fig. 5.11. The test points obtained at a higher velocity have shown a faster decrease of the ultrasound amplitude with growing gas fraction. We believe that this is caused by a significant change in the bubble diameter, which decreases with growing velocity.

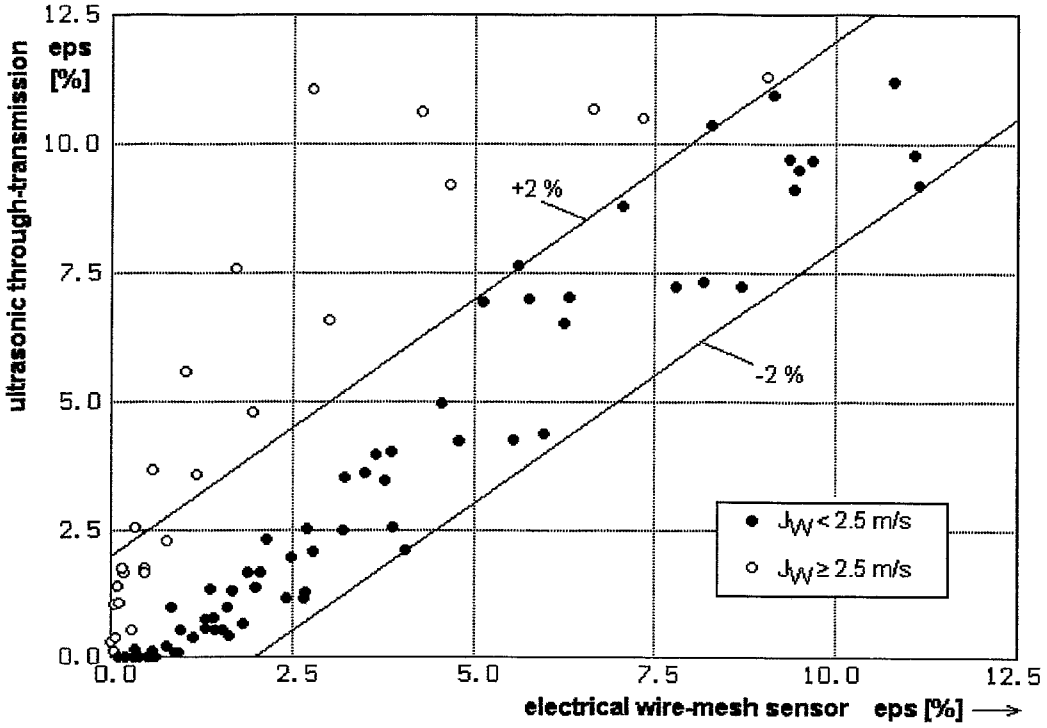


*Fig. 5.11 Accuracy of Eq. (5.7) in the void fraction range below 12.5 %*

Concerning the gas fractions above the limit of 12.5 %, the high damping of the ultrasound makes an application impossible. When the density of bubbles is too large, the ultrasound beam is completely interrupted and a further increase of the gas fraction is not reflected by the signal. Summarising we can state that the described ultrasonic through-transmission method can be used to asses the volumetric gas fraction in the range of low gas fractions. It can be used to detect the onset of bubble generation. Due to the low accuracy it is rather a warning device for bubble detection than a gas fraction meter.

In Fig. 5.12, the result of the pulse-echo measurements is shown. In this case, an unequivocal dependency from the volumetric gas fraction cannot be found. The pulse-echo mode was therefore not used for practical measurements.

## 5.6 Application in water hammer experiments

In the frame of a joint research with Fraunhofer UMSICHT Oberhausen in the frame of a project funded by BMBF [5.1], the through-transmission sensors were applied to detect a cavitation bubble behind a fast acting flap-valve in a pipeline. Two test pipelines with inner diameters of 54.3 mm respectively 108 mm were used. They were operated with water at ambient conditions. The ultrasonic energy was only sufficient to record signals on the 54.3 mm pipeline. In the tests, the growing cavitation bubble was observed by a sharp decrease of the ultrasonic signal, occurring when the gas

phase reached the position of the corresponding through-transmission device. An example of the obtained results is shown in Fig. 5.13.

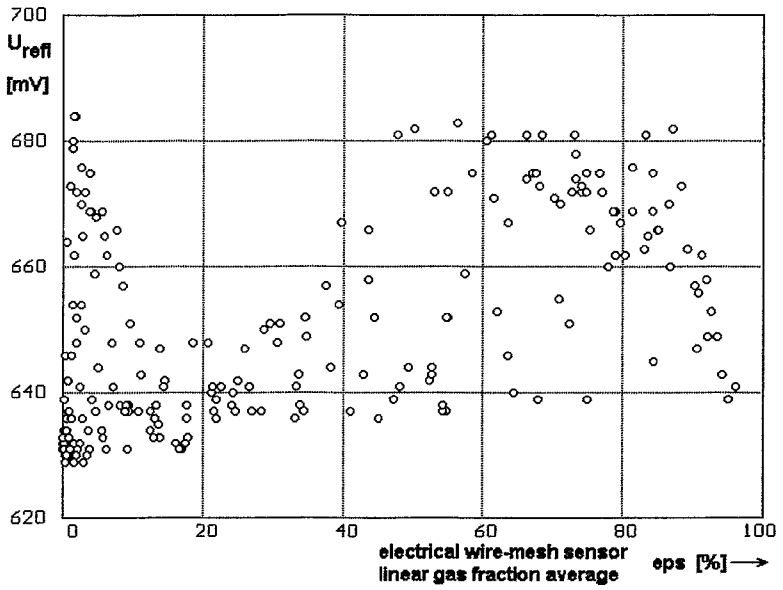


*Fig. 5.12 Amplitude of the reflected ultrasonic signal compared to the gas fraction measured by the electrical wire-mesh sensor*

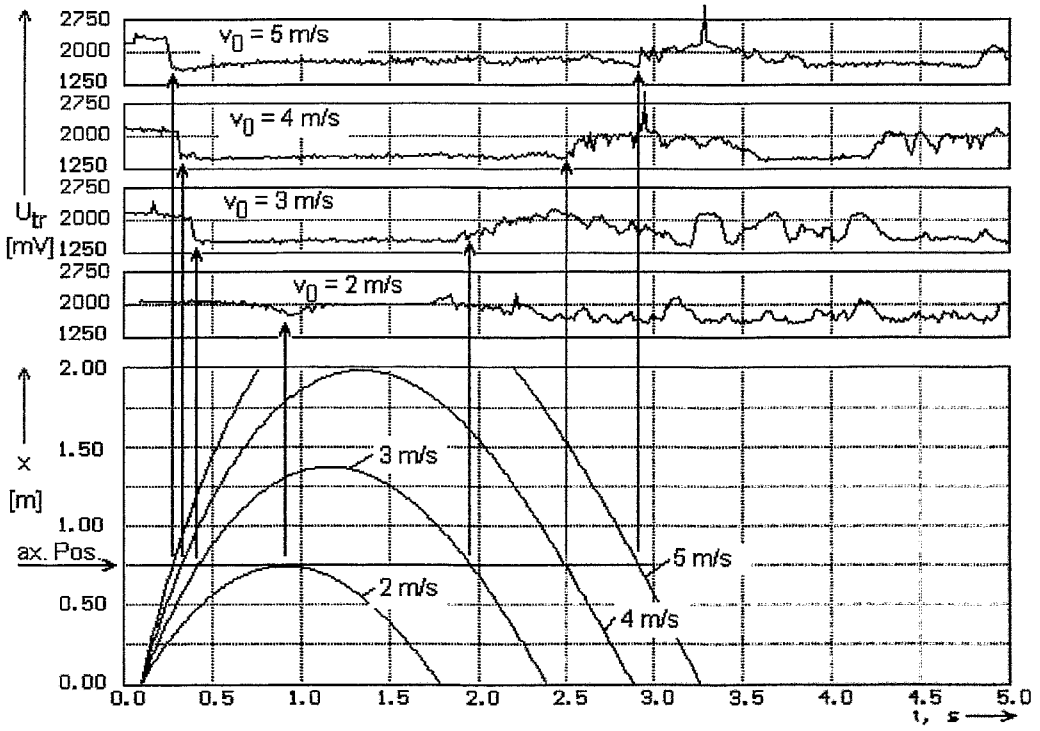


*Fig. 5.13 Example for a cavitation bubble detection by a non-intrusive ultrasonic sensor located 0.75 m downstream the fast acting valve at the Pilot Plant Pipework test facility of Fraunhofer UMSICHT [5.1]*

The sensor was mounted at a distance of 0.75 m downstream of the fast acting flap valve, which was activated at t=0. After the closing tome of approximately 100 ms the cavitation bubble occurred. The length of the bubble is a function of time (x(t)) shown in Fig. 5.13. The maximum length depends on the initial water velocity, which is the parameter in the figure. The indications of the ultrasonic device about arrival and vanishing of the bubble are in good agreement with a theoretical model predicting a time dependency of the length close to a parabolic law.

## 5.7 Reference

[5.1] H.-M. Prasser, A. Böttger, J. Zschau: Entwicklung von Zweiphasenmeßtechnik für vergleichende Untersuchungen zur Beschreibung von transienten Strömungen in Rohrleitungen, Abschlußbericht FZR-233 zum BMBF-Vorhaben 11ZF9504/1, August 1998.

# 6. An ultrasonic mesh sensor for two-phase flows visualisation

This part of the report presents an ultrasonic mesh sensor for the visualisation of transient two-phase flow in pipes. Design and operating conditions of the device are described in detail. Special emphasis is given to the first experimental tests of the ultrasound system. The results of a quantitative and qualitative comparison between the ultrasonic mesh sensor and the electrical wire-mesh sensor developed by FZR are discussed. The advantages and disadvantages of the ultrasound device are outlined.

## 6.1 Working principle of ultrasonic mesh sensor

Based on the positive results of the local ultrasonic wave-guide probe (see chapter 3), the idea was born to develop a mesh sensor similar to the electrical wire-mesh sensors of FZR. For this purpose, the electrodes of the wire-mesh device were replaced by wave-guides. The local instantaneous presence of the liquid phase is detected by the intensity of the ultrasound transfer from a transmitting wave-guide to a receiver wave-guide instead of the measurement of the local electrical conductivity. The new device is therefore based on the measurement of the acoustic conductivity of the two-phase mixture in local points, which are equally distributed over the cross section of the flow.

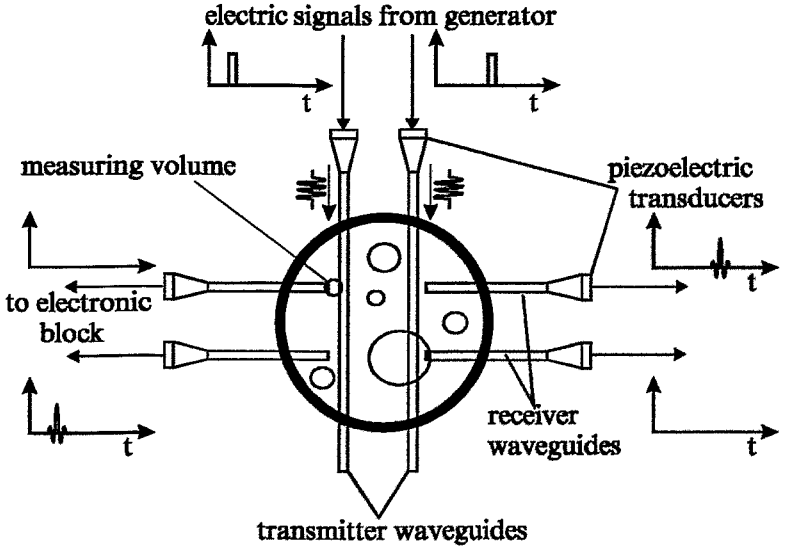


*Fig 6.1 Simplified scheme of an ultrasonic mesh sensor with six wave-guides*

The sensor consists of two groups of ultrasound wave-guides. The wave-guides of the first group (transmitter wave-guides) are used to irradiate acoustic waves into the two-phase mixture. The ultrasound wave-guides of the second group (receiver wave-guides) receive the acoustic waves transmitted through the measuring fluid in the control volumes. The simplified six-wave-guide scheme of the ultrasound wave-guide sensor is shown in Fig. 6.1. The transmitter wave-guides are cylindrical rods, which are excited by piezo-crystals fixed to their ends outside the measuring cross section. Ultrasonic waves are irradiated into the fluid from the lateral surface of these wave-guides. If there is liquid (e.g. water) in the measuring volume, the attenuation of ultrasound propagating through the measuring volume is insignificant. In the result, the waves reach the end of the receiver wave-guide, which are oriented towards the transmitter rod. After transformation into electric signals by a piezo-crystal, fixed to the outer end of the receiver wave-guide, the amplitude of the received waves is registered by the electronic block. If the control volume is filled with gas or vapour, the ultrasound is not irradiated due to the bad matching of the acoustic impedance of steel and gas. The signal does not

appear at the receiver wave-guides. During a measuring cycle, the transmitter wave-guides are activated in a successive order. During the excitation of a selected single transmitter wave-guide, the signals of all of the receiver wave-guides are recorded simultaneously. After the last transmitter wave-guide has been activated, a two-dimensional matrix of electric signals is completed that reflects the acoustic conductivity of the two-phase mixture in all local control volumes formed between both groups of ultrasonic wave-guides.

The ultrasonic mesh sensor is connected to an electronic block (signal acquisition unit). The operation of the device is controlled out by means of a personal computer, which is connected to the electronic block. A schematic view of the ultrasound wave-guide system is shown in Fig. 6.2.

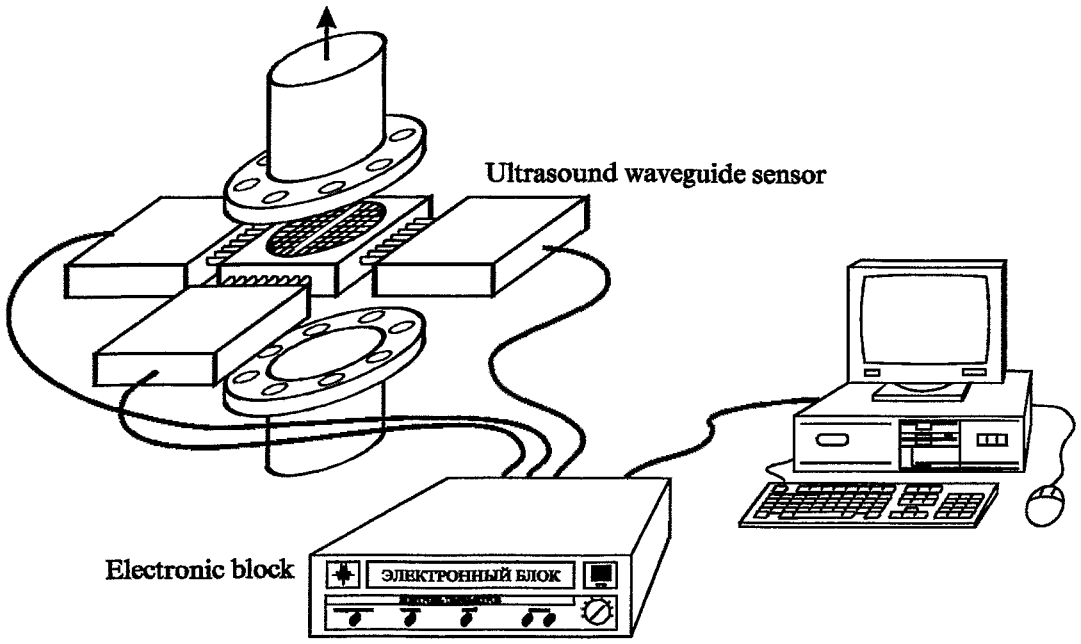


*Fig. 6.2 Schematic view of the ultrasonic mesh sensor*

Before experiment, during the calibration procedure, data of two extreme situations are stored in the memory of the PC - matrix of values of signals in gas phase and matrix of values of signals in liquid phase. According to these values the levels of discrimination for different gas fraction distributions are established.

## 6.2 Sensor design

Two types of sensors have been developed (Fig. 6.3). The first sensor (prototype № 1) consists of a metallic frame where the transmitter and receiver wave-guides are fixed (Fig. 6.4). Design and layout of the wave-guides are such, that 48 sensitive points are formed, which are equally distributed over the cross section of the pipeline (nominal diameter 50 mm).

The control volumes are formed between cylindrical transmitter wave-guides and perpendicularly located receivers. For the receiver wave-guides wires with a diameter of 0.8 mm are used, the transmitter wave-guides consist of capillaries with a diameter of 1.1 mm. The free end of the receiver wave-guide is oriented to the lateral surface

of the transmitter wave-guide. The gap between them is 1.0 mm wide. Thin-walled capillaries were chosen as transmitter wave-guides to increase the irradiation of ultrasound energy into the two-phase mixture. There are independent receiver wave guides for either the left and the right half of the cross section.

The described design has two important advantages: (1) it guarantees a high sensitivity of the sensor, because of control volumes of an optimal geometry, (2) pairs of transmitter wave-guides, coupled to independent sides of the receivers, which allows to increase time resolution by factor two. This sensor has been used successfully in a number of experiments.

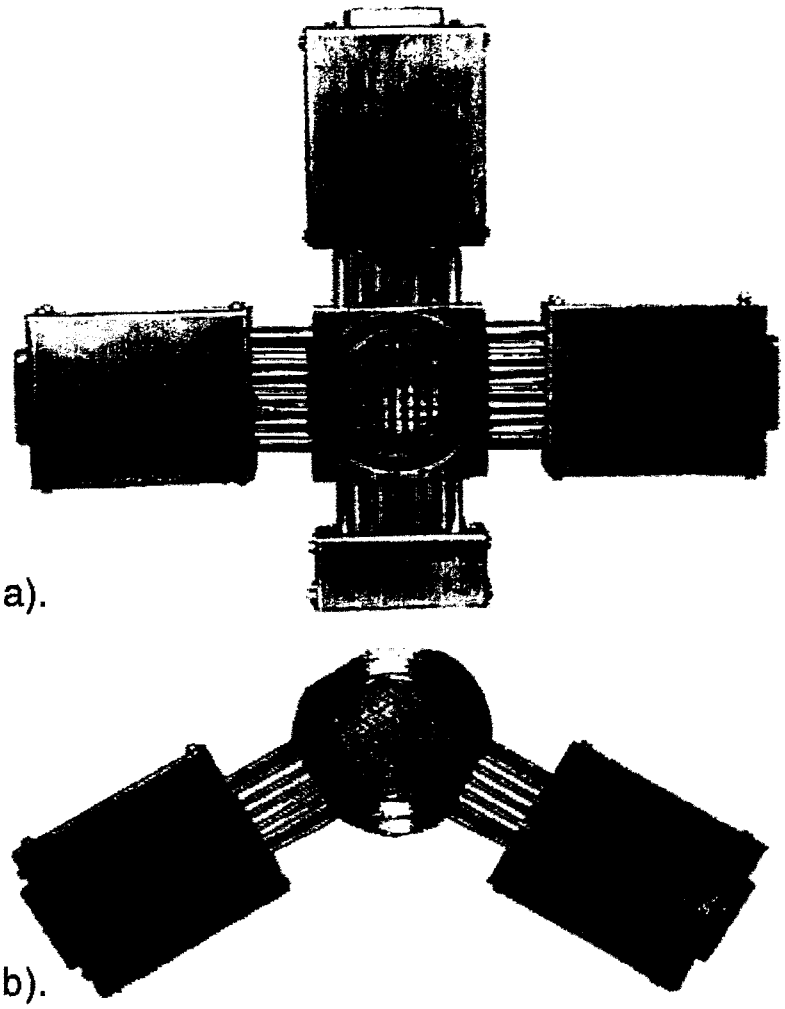


*Fig. 6.3 Two types of ultrasonic mesh sensors*
a) Prototype №1 (48 sensitive points)
b) Prototype №2 (37 sensitive points)

In order to simplify the complicated design of the prototype № 1 and to reduce the dimensions of the wave-guides for decreasing the feedback to the flow, a second type of sensor was developed (Fig. 6.3b, Fig. 6.5). It consists of two planes of wire grids with 7 wires of a diameter of 0.8 mm. This results 37 sensitive points over the cross section (nominal diameter 50 mm). The wave-guides of the first plane are transmitters, the wave-guides of the second plane work as receivers. The angle between the wave-guides of both planes is 120 deg, the distance - 1.0 mm. The wave-guides of both types have special concavities (Fig. 6.5, view-*I*) to increase the sensitivity of the sensor.

In case of the first sensor, the irradiation of acoustic energy is carried out due to radial fluctuations of the transmitter wave-guides, i. e. only longitudinal waves are used. In contrast to that, prototype № 2 uses flexural waves. The mode transformation is realised by the small concavities, which act as punctual sources and receivers of ultrasound.

The main advantage of the second prototype compared to the first one is the simplicity of the construction. Furthermore, the sensor of the second design is more reliable in operation, it is more suitable to the large mechanical loads. In addition, the simplified design makes it more easy to adapt the sensor to larger pipe diameters than 50 mm. Last but not least, the reduced dimensions of the wave-guides decrease the disturbance of the two-phase flow caused by the intrusive device.

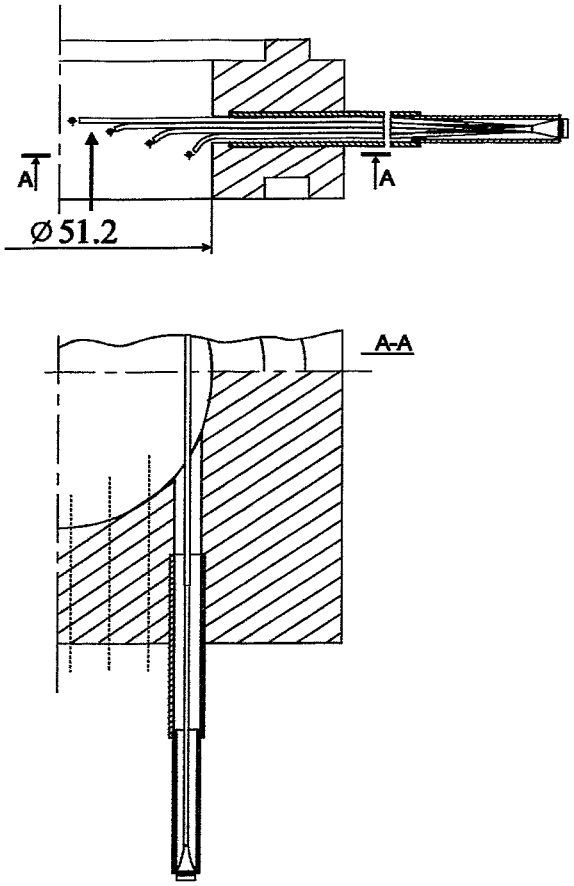


*Fig. 6.4 Sketch of the ultrasonic wave-guide sensor (prototype № 1)*

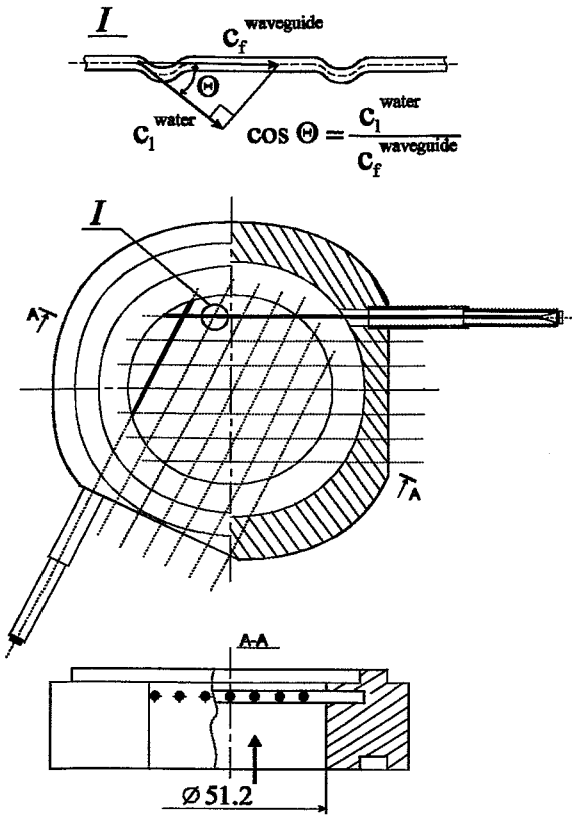


*Fig. 6.5 Sketch of the ultrasonic wave-guide sensor (prototype № 2)*

Both types of sensor are manufactured from corrosion proof steel. It allows to use the device for two-phase flow measurements even under hostile conditions, which are met in industrial facilities.

## 6.3 The peculiarities of the electronic hardware

The electronic block contains an electronic circuit for the control of the device. During the measurement cycle, the piezoelectric transducers of the transmitter wave-guides are activated by the electric pulses from the pulse generator. The basic control and measuring signals are shown in Fig. 6.6. From the diagram we can see that there are two factors putting limitations on the time resolution (i.e. the repetition rate) of the ultrasound wave-guide device:

1. The first limiting factor is the relatively low speed of sound in the wave-guides (5000 m/s for longitudinal acoustic waves, 3000 m/s for flexural acoustic waves).

2. The second limitation is given by the reverberation in the receiver and transmitter wave-guides.

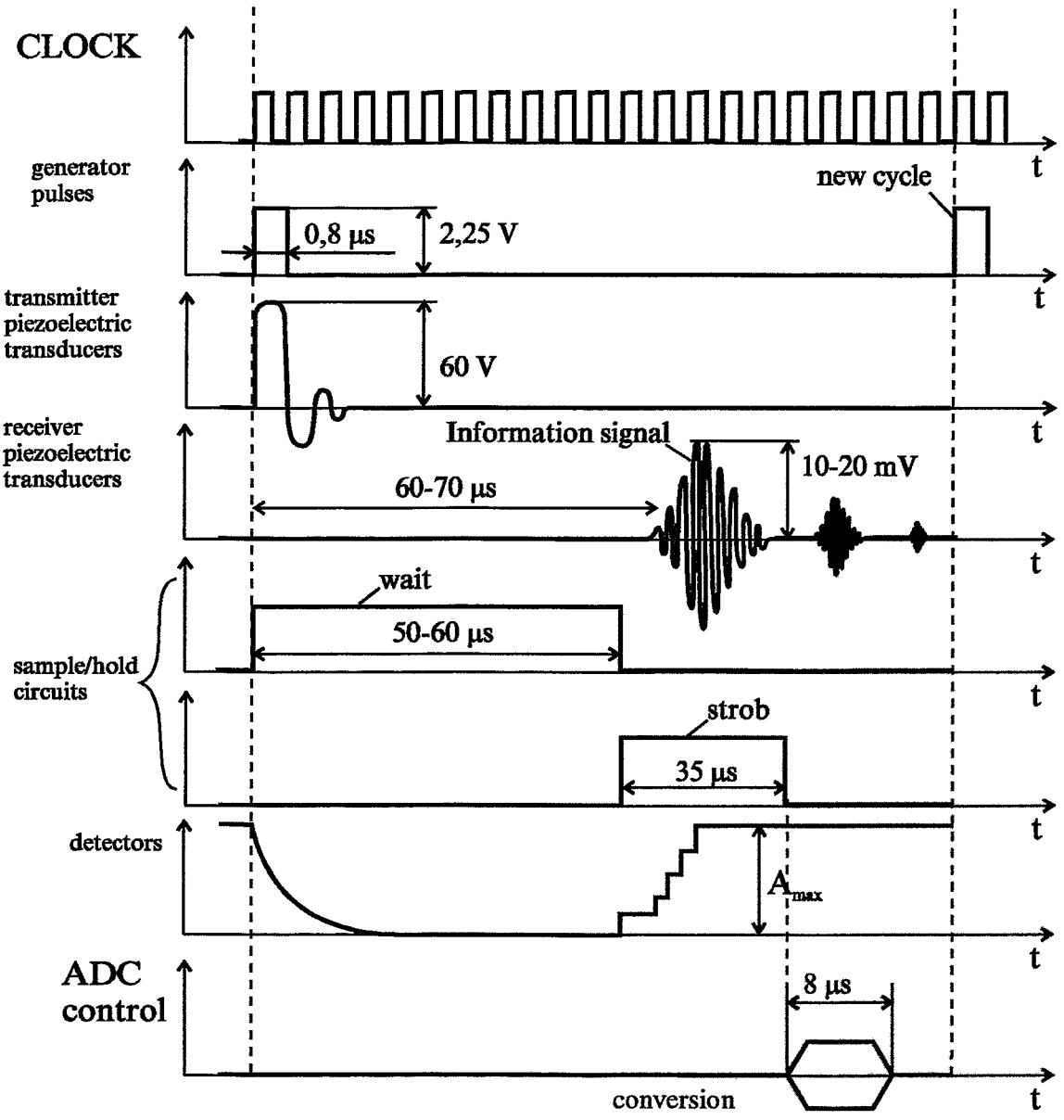


*Fig. 6.6 Diagram of the control signals and the signal acquisition*

In order to reduce the first limitation we used wave-guides as short as possible. For the reduction of the reverberation, a damping of the construction elements by thin copper wire coils was applied.

The software developed for the ultrasound wave-guide sensor is similar to that developed by FZR for the electrical wire-mesh sensor.

## 6.4 Test results in an air-water flow

Both types of ultrasonic mesh sensors were tested at the two-phase flow loop (MTLoop) of FZR. A qualitative and quantitative comparison of the measurement re-

sults obtained by the ultrasonic mesh sensor with the readings of the electrical wire-mesh sensor was carried out. The ultrasonic sensors were fixed in a vertical pipe section of the test facility, a vertical pipe of 51.2 mm inner diameter, by means of flanges. In experiments with the prototype № 1 the ultrasound sensor was placed at a distance of 45 mm behind the wire mesh sensor. In experiments with the prototype № 2 the ultrasound sensor was placed at a distance of 45 mm in front of the wire mesh sensor. Both types of ultrasonic mesh sensors have been tested at different gas fraction distributions, established by supplying the test section with well-defined flow rates of air and water. Experiments were carried out under carefully controlled conditions, at nearly atmospheric pressure and a temperature of 30 °C. The superficial velocity of air was varied within the range from 0.0025 m/s to 12 m/s. That of water was varied from 0.04 to 4.05 m/s.

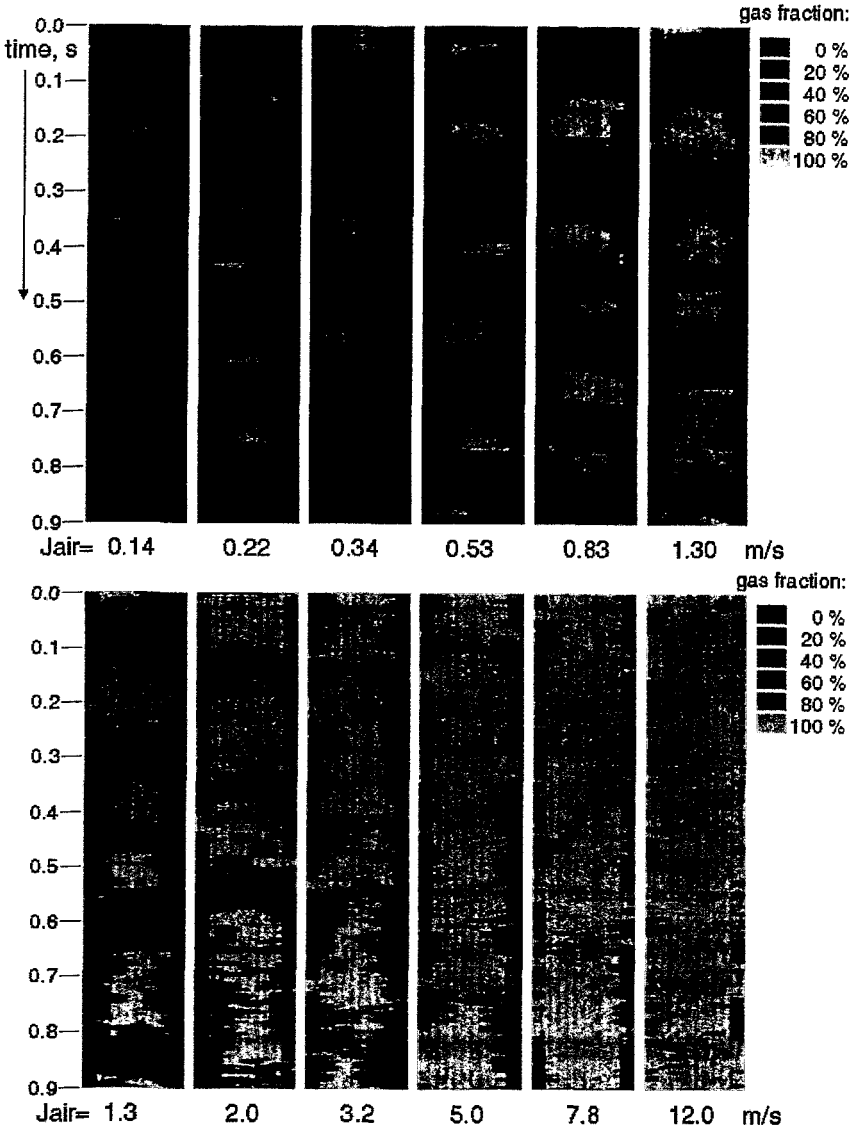


*Fig. 6.7 Virtual sectional views of the two-phase flow, transition from bubble to annular flow*
superficial water velocity: 1 m/s; sensor № 1, time resolution: 200 Hz.

Fig. 6.7 presents the results of a selected experimental tests. The measurement was carried out with the prototype № 1 of the sensor. Virtual sectional views of the flow structure were generated by taking instantaneous gas fraction distributions over the diameter of the measuring cross-section from the two-dimensional sensor data. These gas fraction distributions were transformed into colours and plotted in a column beginning from the top and moving downwards with increasing time. This procedure was realised off-line in the data evaluation computer. To increase the quality of the imaging, a linear

interpolation within the cross-sectional images was applied. The images of the gas-water flow are qualitatively similar to those obtained with wire-mesh sensor [6.2].

Fig. 6.8 shows the qualitative comparison of sequences of individual frames and of virtual sectional views recorded in a vertical plug flow with the ultrasonic mesh sensor prototype № 1 and with the electrical wire-mesh sensor of FZR with 16 x 16 sensitive points inside the cross-section.

It is clearly visible, that both methods are able to reproduce the flow structure similarily. The spatial resolution of the electrical sensor is better because of the larger number of wires in comparison to the wave-guides of the ultrasonic sensor. The time resolution is also better; in order to have a direct comparison, the electrical wire-mesh sensor was operated at a reduced measuring rate adapted to the rate of 200 frames per second, delivered by the ultrasonic device. An important observation is that the ultrasonic device often indicates too much water in the cross section. In some images, droplets sitting between the transmitter and receiver wave-guides are visible, which cause the false indication of water inside the part of the cross-section

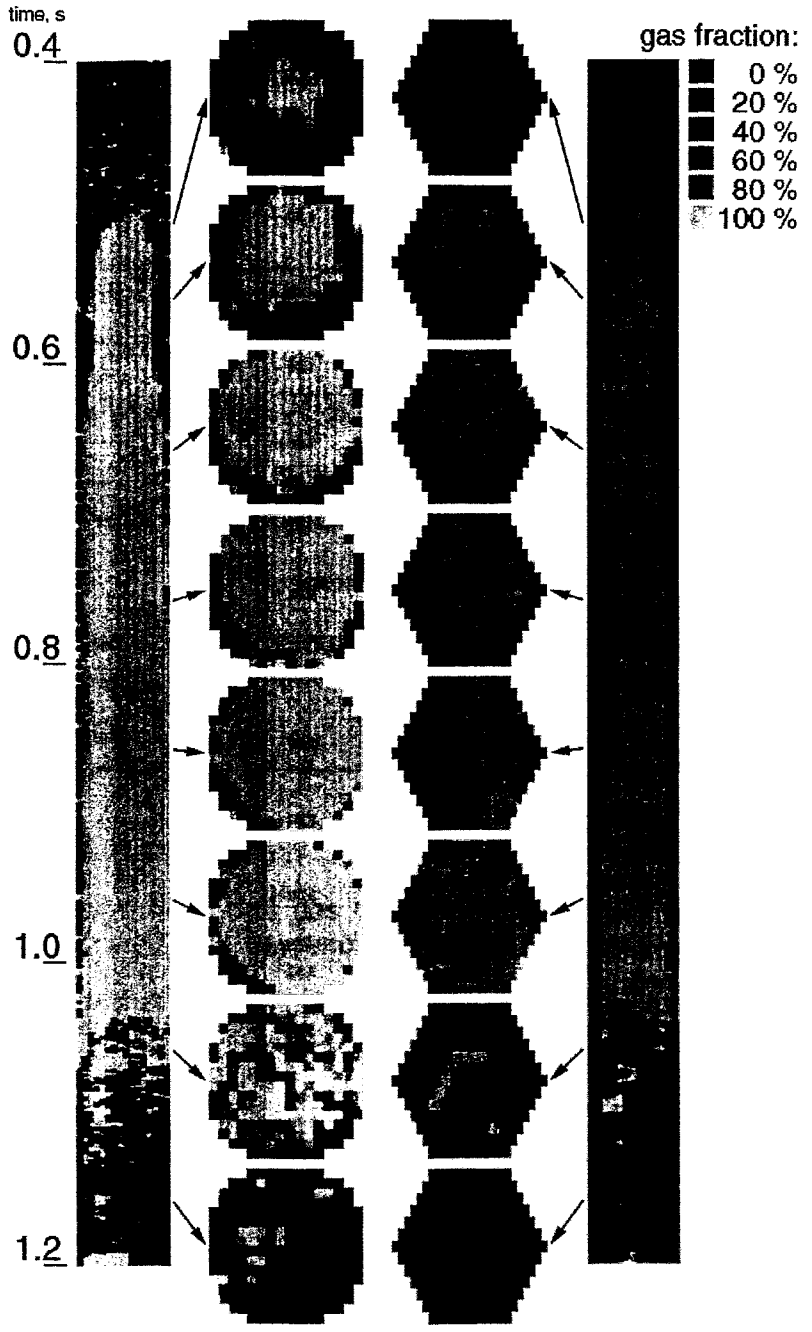


*Fig.6.8 Comparison of sequences of frames and virtual sectional views originating from a vertical plug flow*
left: electrical wire-mesh sensor
right: ultrasonic mesh sensor

which is occupied by the air plug. This is a disadvantage of the first sensor design with its rather thick wave-guides.

Fig. 6.9 shows the qualitative comparison of the virtual sectional views for bubble, plug and annular flows. The pictures obtained by the electrical wire-mesh sensor and the ultrasonic mesh sensor are slightly different. The reason of the disagreement between the results is the lower spatial and time resolution of the ultrasonic device. Another weak point is the mentioned local overestimation of the liquid fraction due to droplets captured in the gap between transmitter and receiver wave-guides. This effect is again well recognisable in the virtual side views. Nevertheless, the ultrasound wave-guide sensor was found to be well suited to flow pattern studies.

For the quantitative comparison between wire-mesh sensor and ultrasound wave-guide sensor, the average volumetric gas fractions of time and diameter were used. The measured average volumetric gas fractions for the superficial velocities of 1 m/s for water and 0-12 m/s for air is shown on Fig. 6.10.

The ultrasound wave-guide sensors produced a negative systematic error, especially in the range of bubble and small plug flows. The basic systematic errors are due to low spatial and time resolution of the wave-guide sensors. Correction for spatial resolution is needed in order to reduce these systematic errors. Except for mentioned systematic errors, there

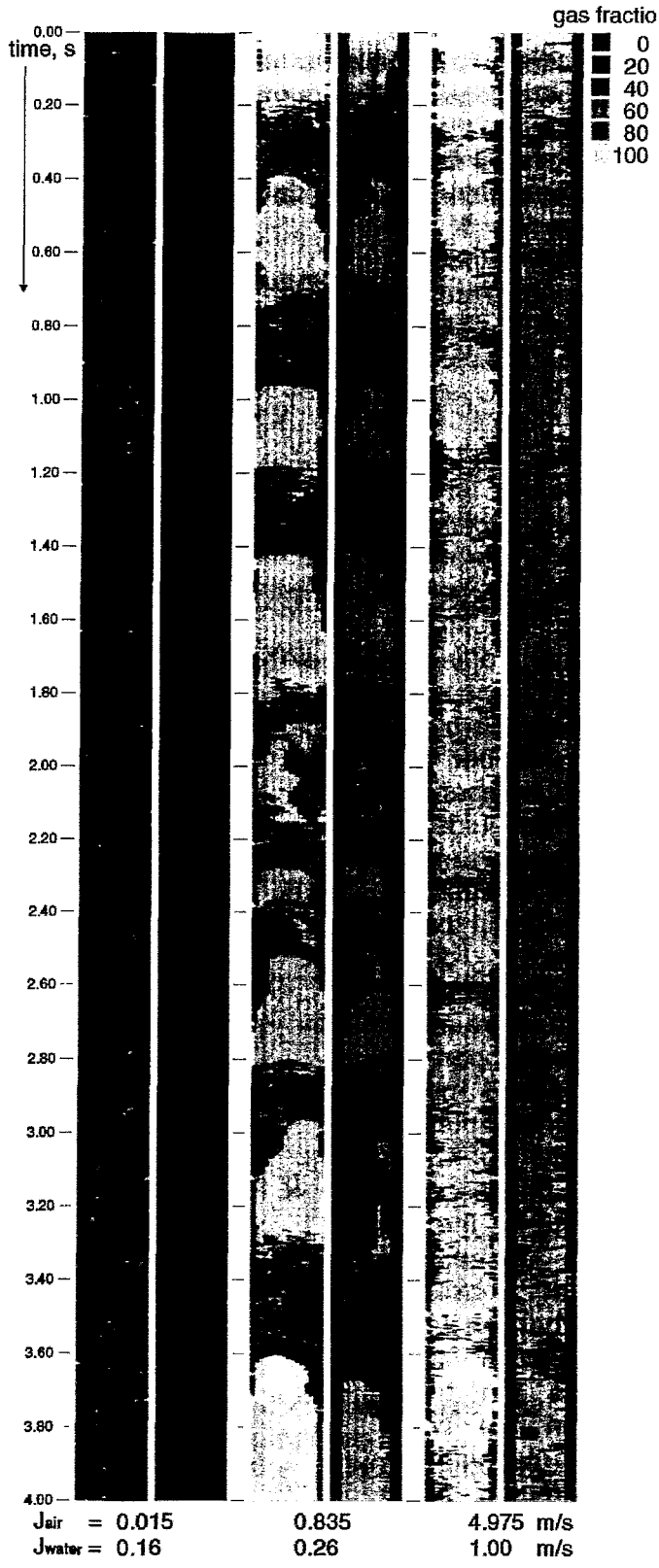


*Fig. 6.9* *Virtual sectional views for different flow regimes*
left column: electrical wire-mesh sensor
right column: ultrasonic mesh sensor

are errors due to influence of the sensors on the flow. At a low superficial velocity of water droplets accommodate between transmitter and receiver wave-guides. They have a significant effect on the reading of the ultrasound device. At a high superficial velocity of water artefacts are observed, because acoustic emission takes place in the ultrasound wave-guides. These errors can be minimised by a further optimisation of the construction of the sensors. For example, a protecting grid of metallic rods can be mounted just in front of wave-guides to eliminate the acoustic emission. To reduce the effect of the droplets on the reading of the device the distance between transmitter and receiver wave-guides should be increased.

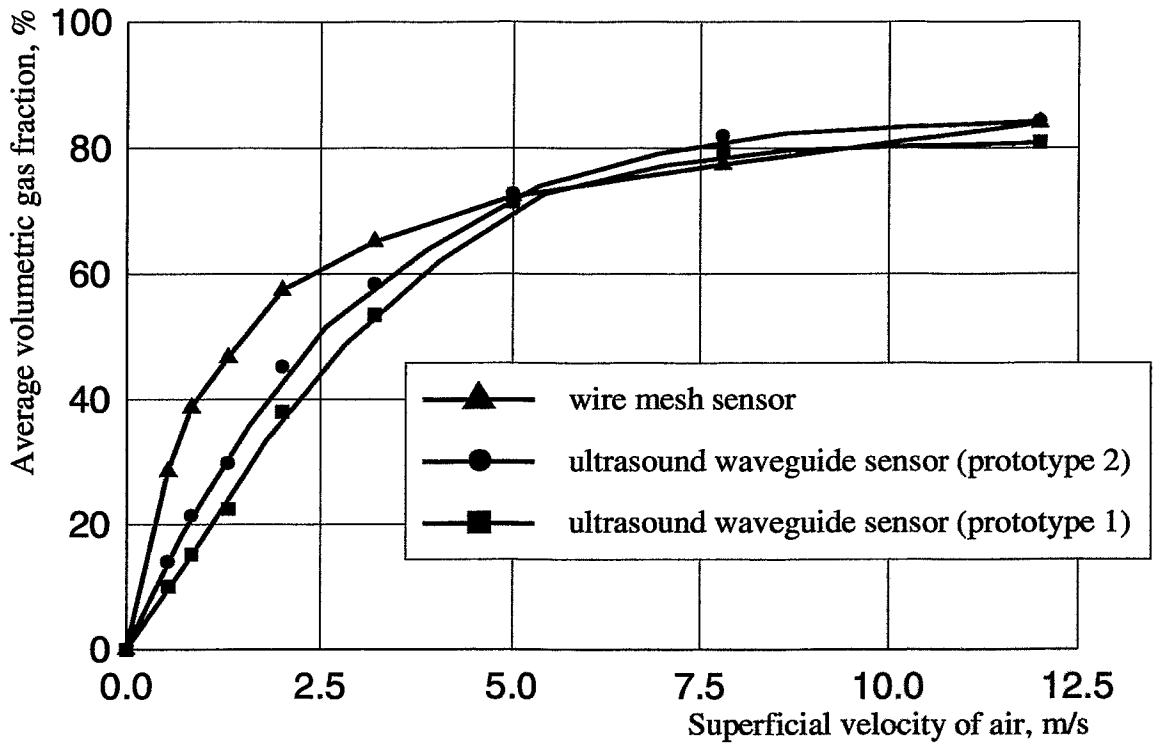


*Fig. 6.10 Comparison of average volumetric gas fractions measured by the electrical wire-mesh sensor and the ultrasound wave-guide sensors*

Diameter of the pipe: 51.2 mm; superficial velocity, water: 1.0 m/s; sensors: wire-mesh (256 sensitive points), prototype № 1 (48 sensitive points), prototype № 2 (37 sensitive points)

## 6.5 Test in a steam-water flow

The ultrasonic mesh sensor was tested in a steam-water flow in the two-phase loop MTLoop. For this purpose, the electrical heater of the loop was operated and the pressure was increased up to 25 bar. Measuring points were recorded in the range from 6 to 25 bar. The water was circulated with a superficial velocity from the range between 0 and 0.4 m/s. A heater power of 12 respectively 16 kW was used. The experiments were carried out by setting up the liquid flow and the heater power. The measurement was started, when steady-state conditions were reached, i.e. saturation pressure and temperature are the result of an equilibrium between heater power and heat losses of the test loop. Consequently, the void fraction in the vertical test

section is also a result of this equilibrium. Therefore it cannot be varied freely in a wide range, as it was done in the experiments with air injection.

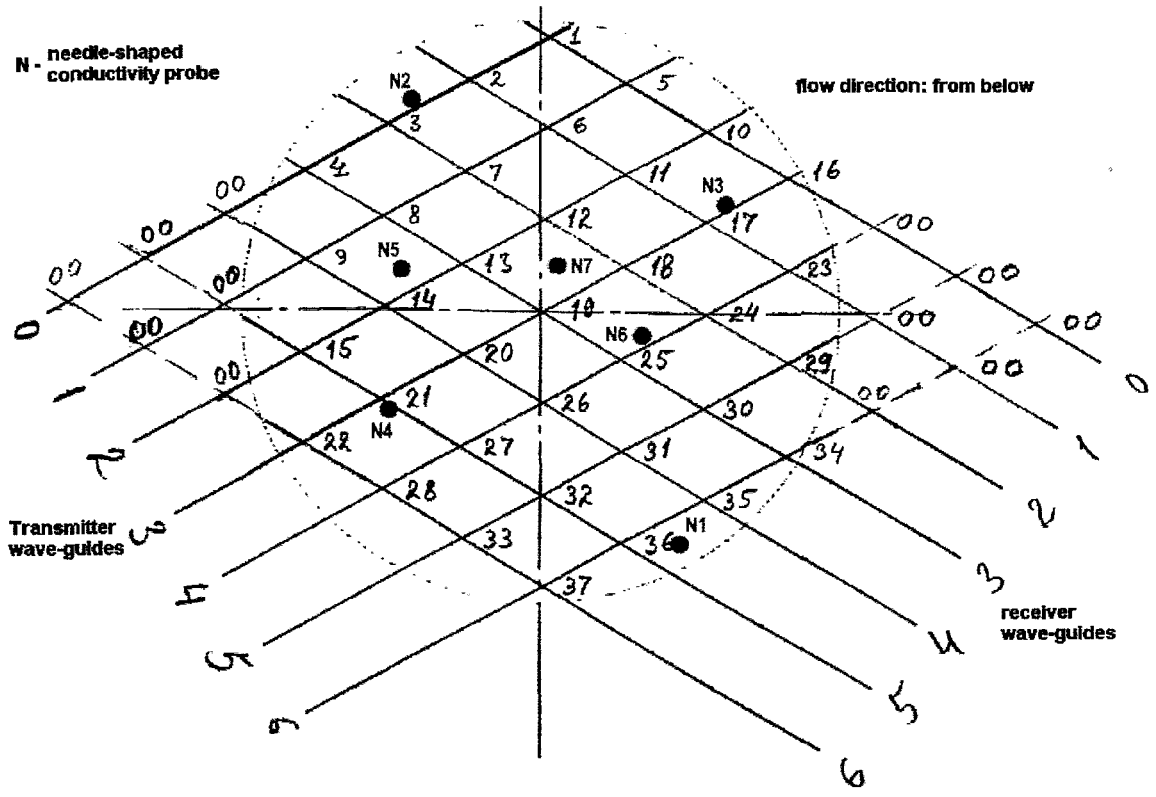


*Fig. 6.11 Location of the needle-shaped conductivity probes (N1-N7) in the measuring matrix of the ultrasonic mesh sensor*

The test of the ultrasonic mesh sensor was carried out by comparing the measuring results with reference measurements. The void fraction distribution inside the vertical test section of 51.2 mm diameter was measured by needle shaped conductivity probes, the sensitive tips of which were located at different radial positions. An averaging of the readings of all 7 probes and the calculation of a time average allows a quantitative comparison between probes and mesh sensor. Since the mesh sensor delivers two-dimensional void distributions, those measuring position inside the two-dimentional matrix were averaged, which correspond to the accurate position of the needle probes (Fig. 6.11). The result of this comparison is shown in Fig. 6.12.

The maximum void fraction reached was 13.5 %. The signals of the ultrasonic mesh sensor were evaluated by relating the amplitude of the received signals to the reference signal obtained for plain liquid and plain steam. The amplitudes for plain steam were recorded during a calibration operation before the experiment. The signal levels for plain liquid were extracted from the measuring signal by calculating power density distributions from the measuring signal. This means, the change of the physical properties of the liquid was taken into account by an adaptive calibration.

The agreement between needle probes and mesh sensor is satisfying. Unfortunately, it was not possible to set-up conditions with higher gas fraction. The flow regime was bubble flow in the transition area to slug flow. In Fig. 6.13 some examples of virtual

sectional views obtained by the ultrasonic mesh sensor are shown. At the lowest pressure and the lowest superficial water velocity, the highest void fractions were generated, and slugs are clearly visible (Fig. 6.13 A). Inside the slugs, sometimes false indications of water occur, which are caused by droplets accommodated at the the crossing wave-guides. Fig. 6.14 illustrates this effected by supplying a phase distribution over the cross section during the passage of a steam plug.

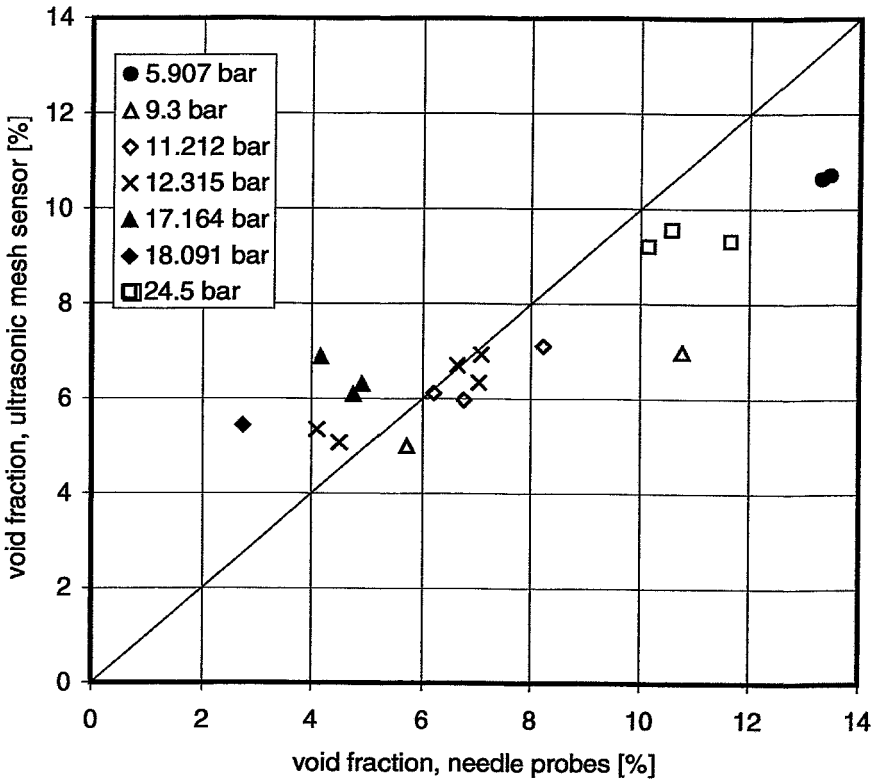


*Fig. 6.12 Comparison between average void fractions measured by needle-shaped conductivity probes and the ultrasonic mesh sensor in a steam-water flow*

*parameter: saturation pressure [bar]*

With increasing pressure and water velocity, the void fraction decreases (Fig. 6.13 B and C). In Fig. 6.13 D, results are shown obtained at nearly 25 bar. The sensor was working reliably at such parameters.

## 6.6 Conclusion

The inexpensive device for high-speed visualisation of the two-phase flows is developed which is simple to make and to operate. An analysis of the experimental results indicate that the ultrasonic mesh sensor has the spatial and time resolution which is adequate for qualitative diagnostic of the different two-phase flows over a wide range of gas fraction distributions. The device can be used to investigate the transient two-phase flows in industrial and experimental equipment. The ultrasonic mesh sensor is especially useful for the measurement in electrically non-conductive fluids. It is also employed in investigations of the high pressure and high temperature flows.

The test results show that additional work is needed to improve the precision of the device. The sensor (prototype № 2) has shown that it is capable in working under high temperature and pressure (temperature up to 225 °C, pressure up to 2.5 MPa).

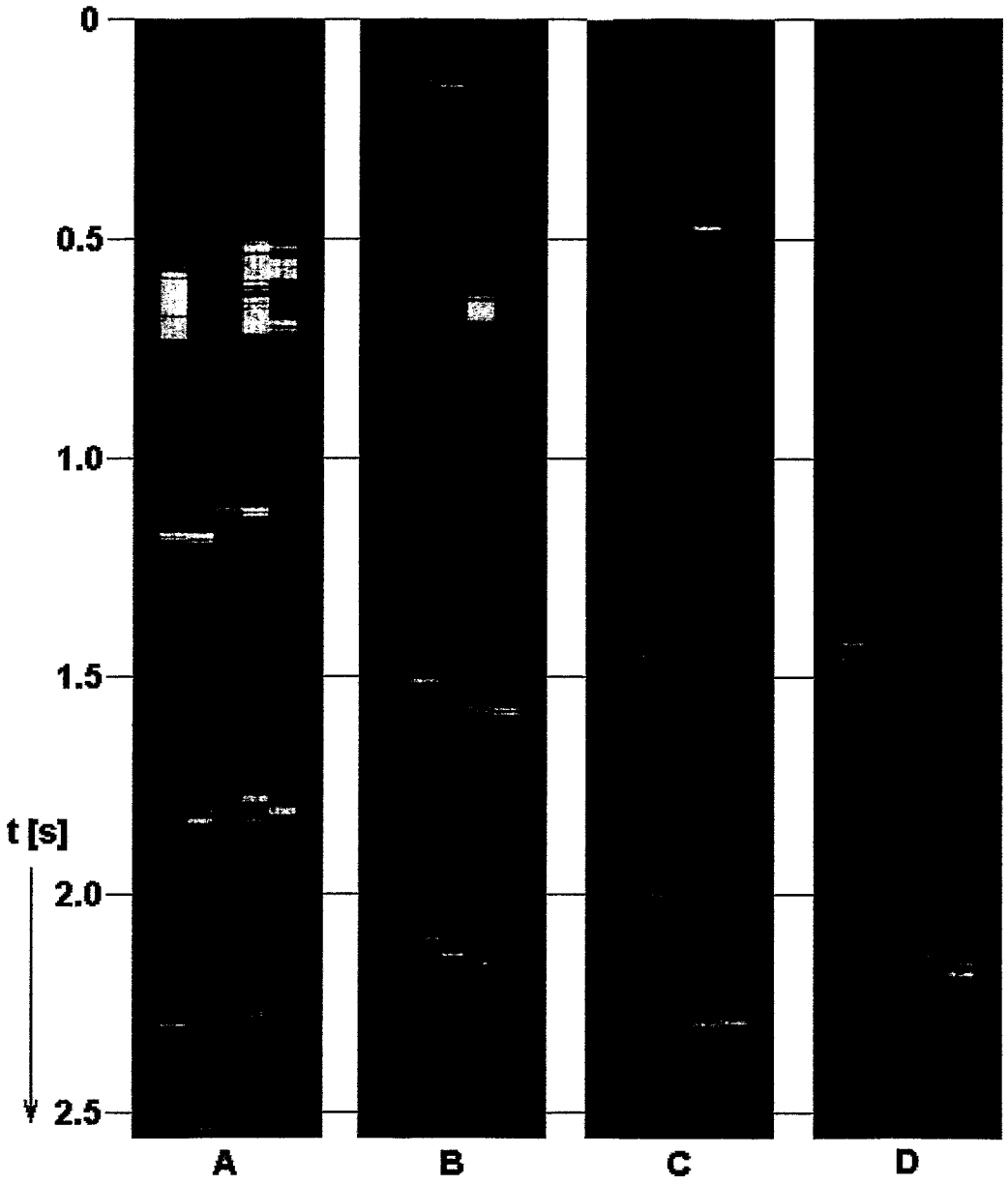


*Fig. 6.13 Virtual sectional side views of the steam-water flow in the vertical test section of MTLoop, recorded by the ultrasonic mesh sensor*

| Column | A | B | C | D |
|---|---|---|---|---|
| pressure [bar] | 5.91 | 9.34 | 18.37 | 24.73 |
| heater power [kW] | 12.34 | 12.20 | 12.10 | 16.50 |
| superficial water velocity [m/s] | 0.042 | 0.076 | 0.40 | 0.065 |

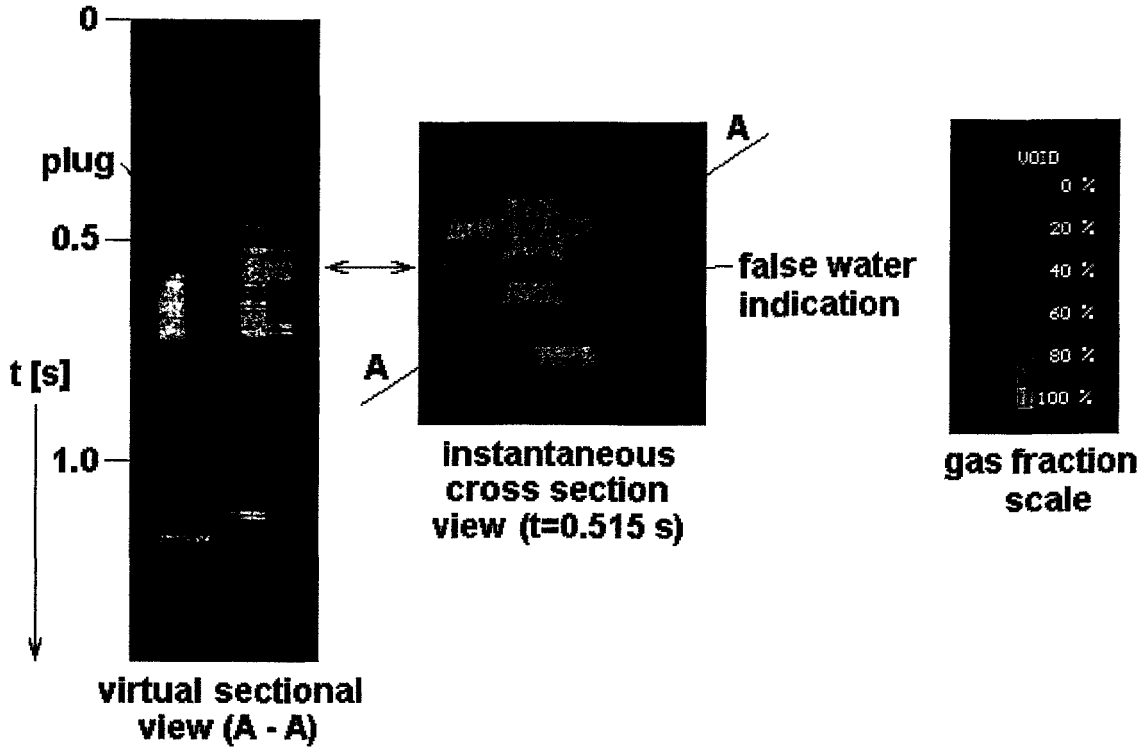


*Fig. 6.14 Instantaneous void fraction distribution with false water indication inside a slug, regime A shown in Fig. 6.13*

## 6.7 References

[6.1] Melnikov V. I., Nigmatulin B. I. The newest two-phase control devices in LWR equipment based on ultrasonic and WAT-technology. Nuclear Engineering and Design.- 1994.- № 149.- P. 349-355.

[6.2] Prasser H.-M., Bottger A., Zschau J. A new electrode-mesh tomograph for gas-liquid flows. Flow Measurement and Instrumentation.- 1998.- № 9.- P. 111-119.

# 7. Project conclusions

In the course of the project, new methods of two-phase flow instrumentation were developed and are now ready for an application in thermal-hydraulic experiments. The state of development is different for the different methods, which were investigated. Especially the intrusive local void fraction probes based on wave-guides (section 3) have reached a high degree of perfection. The experiments carried out at the test loop in Rossendorf, but also the tests at the DESIRE facility in Delft have shown that they can be successfully applied to solve the task of local void fraction measurements in different fluids: (1) high pressure and temperature water under boiling condition, (2) two-phase flows with very small bubbles (e.g. under the presence of surfactants), (3) organic liquids and refrigerants. They can directly be used for scientific purposes. The use of stainless steel for all parts of the probes which are in contact with the measuring fluid makes them robust enough even for industrial applications. It is therefore recommended to continue the development in the direction of a commercial use.

Ultrasonic mesh sensors are very promising devices for a fast two-phase flow visualisation (section 6). The main advantage is the large robustness of these sensors as well as the fact, that they can work in electrically non-conducting liquids, where the similarly fast wire-mesh sensors cannot be used. The experience has shown, that the sensors still have to be improved, especially concerning the accuracy and the stability of operation. We believe that there is large areas of possible applications in nuclear and chemical industries as well as in the field of research.

The project failed in creating a tomographic sensor based on the non-intrusive ultrasonic through-transmission technique. The non-intrusive wave-guide sensors (section 5) developed have several positive properties achieved by innovative approaches, such as high transfer of ultrasound energy through the measuring object despite of using wave-guides. The application of wave-guides allows to perform measurements on hot pipes. Unfortunately, the dependency of the through-transmission amplitude from the void fraction is very non-linear and the signal quality is poor. In the present stage of the development, the sensors can rather be used for a qualitative gas respectively level detection than for void fraction measurements. In case of void fractions above 10-12 % it is practically not possible to receive valuable signals. It is expected that the use of a new type of high-frequency wave-guide could solve this problem in the future. This type of wave-guide was tested on a liquid sodium loop for velocity measurements in single-phase flow (section 4).

The wave-guide density sensor described in chapter 2 requires further development of the electronic circuitry. It was successfully demonstrated that it is able to measure densities of single-phase liquids. Due to the small changes of the time delay, which have to be measured with a high resolution, satisfactory accuracy can be achieved only by a high-speed signal acquisition, the creation of which remained a task for the future.

Summarising, the project has succeeded in a significant progress in the field of intrusive two-phase flow instrumentation. The main innovation was achieved by the development of the ultrasonic mesh sensor, the resoluting capability of which is comparable to methods like electrical wire-mesh sensors and ultra-fast X-ray tomography, while the device itself is robust and low expensive.

# Appendix A

## MTLoop - the two-phase flow test facility of FZR

MTLoop was constructed in 1995 as a test facility for the test and the development of two-phase flow instrumentation. It was used, for example, to develop non-intrusive ultrasonic methods based on pattern recognition techniques [A1, A2], for the assessment of the accuracy of needle shaped conductivity probes [A3], for the development of the electrical wire-mesh sensors (see appendix B) [A3]. In the frame of a research project funded by the Federal Ministry of Economy (BMWi), the facility is used to study transient two-phase flow in vertical pipes.

The test loop has two experimental test sections, a 3500 mm high vertical test section and a 1000 mm long horizontal test section. In both cases, the inner pipe diameter is 51.2 mm. There are 1700 mm long segments of 29 and 81 mm inner diameter, which can be flanged into the vertical test section. The test sections as well as all other main components of the loop are manufactured from stainless steel. Flange connections in many positions make it possible to vary the position of measuring devices and the sensors to be investigated. In case of low-pressure operation, glass windows can be flanged into the loop for visual observations.

The loop (Fig. A1) can be operated either with an air-water or a steam-water mixture. For the air-water regime, the facility is quipped with four air flow meters covering the region of superficial air velocities from 0 - 12 m/s with the accuracy given in Fig. A2. The air is injected by one of three injection devices: (A) a set of 19 capillaries with an inner diameter of 0.8 mm, equally distributed over the pipe cross section, (B) 36 orifices of 1 mm diameter in the pipe wall, equally distributed over the perimeter, and (C) 8 orifices of 4 mm diameter in the pipe wall, also equally distributed over the perimeter. The air injection is located in the lower part of the vertical test section. It is also flanged into the pipe, so that the position can be changed. Another air injection device is placed at the inlet of the horizontal test section.

For the steam-water mode, the loop is equipped with an electrical heater of a maximum power of 20 kW. The heater rods are pressed to the wall of the lower pipe section of the vertical test channel from outside. The loop can be operated at a maximum pressure of 25 bar (2.5 MPa) and a maximum temperature of 225 °C. In the downcomer tube of the loop, heat exchanger tubes are installed for cooling the flow. They are connected with a cooling loop equipped with its own circulation pump and an air cooler outside the building. In case of air-water operation, the heaters and the cooling system are also used to keep the temperature on the desired level during the experiments.

The water flow is generated by a circulation pump, the revolutions of which are controlled by a frequency converter unit. The flow rate is measured by an ultrasonic flow meter and controlled by changing the pump power supply frequency and by a by-pass valve. The superficial water velocity can be varied in the range from 0 to 4 m/s. It is measured with the accuracy given in Fig. A3.

In the upper part, a cyclone separator is used to remove the gas respectively the steam before the fluid enters the downcomer pipe. The separator vessel is equipped

with a level gauge and the safety valve of the facility. Beside the mentioned flow meters and the level gauge, the facility has several thermocouples, pressure and differential pressure transducers. For void fraction calibration purposes, a gamma densitometer with a Cs-137 source (13 mCi) is available. Furthermore, LDA, PDPA and extensive video equipment can be used for measurements.

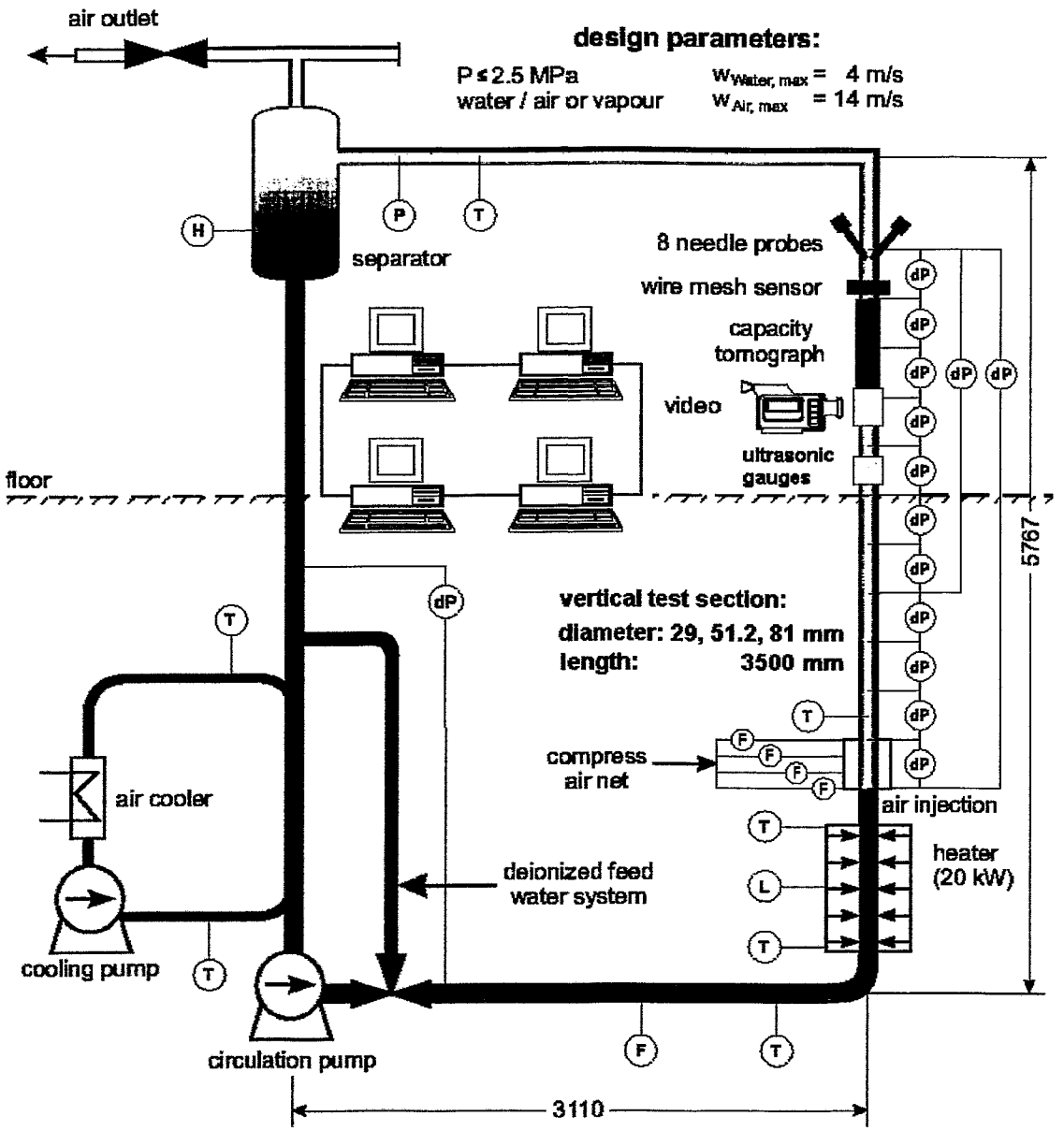


*Fig. A1 Scheme of MTLoop*

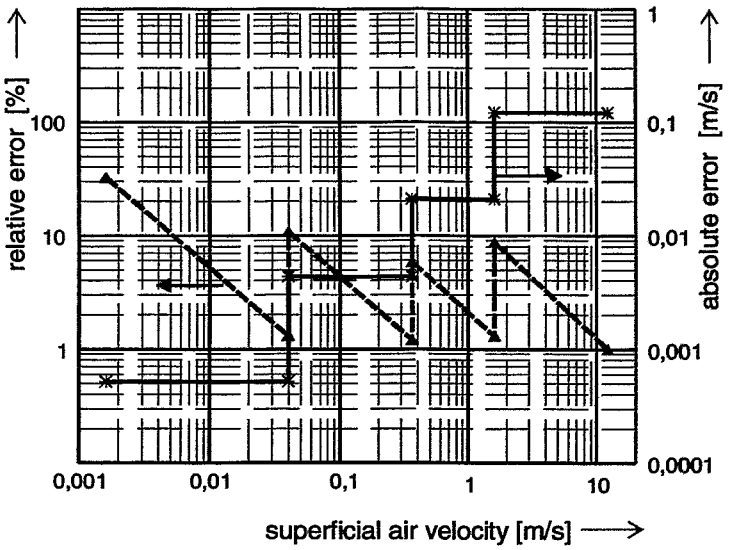


*Fig. A2 Accuracy of the air flow control of MTLoop*

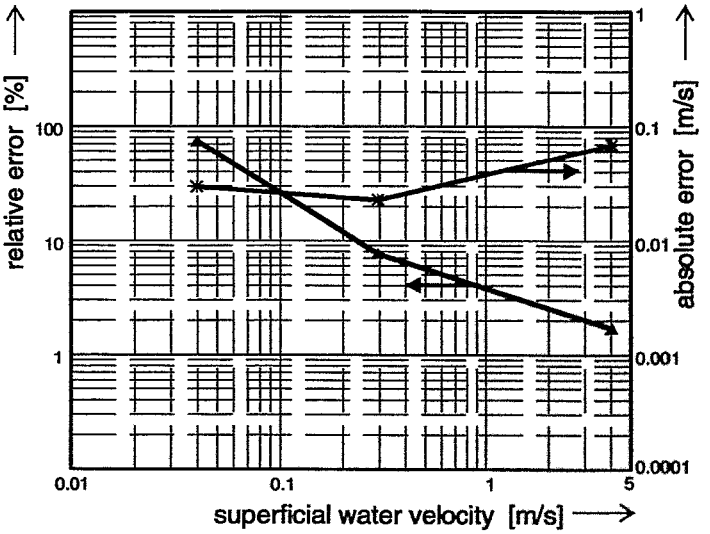


*Fig. A2 Accuracy of the water flow control of MTLoop*

## References

[A1] H.-M. Prasser, P. Schütz, N. Kossok: Berührungslose Detektion der Struktur und Messung ausgewählter Parameter von Zweiphasenströmungen durch Mustererkennungsverfahren unter Verwendung von Ultraschall als Messsonde, BMBF-Vorhaben 1500967, Bericht FZR-203, November 1997.

[A2] Prasser, H.-M., Hensel, F., Schütz, P.: Ultrasonic two-phase flow measurements based on pattern recognition techniques, Proceedings of the XIII IMEKO world congress, Torino, 5-9 September 1994, vol. 2, pp. 1112-1117

[A3] H.-M. Prasser, A. Böttger, J. Zschau: Entwicklung von Zweiphasenmesstechnik für vergleichende Untersuchungen zur Beschreibung von transienten Strömungen in Rohrleitungen, Abschlußbericht FZR- 233 zum BMBF-Vorhaben 11ZF9504/1, August 1998.

# Appendix B

## Electrical wire-mesh sensors developed by FZR

### B1 State of the art

A wire-mesh sensor for measuring the volumetric fraction of water in crude oil was first proposed by Johnson [B1]. Two planes of wire grids are placed into the flow in a short distance from each other. The angle between the wires of both grids is 90 deg. The wires of the first plane (transmitter plane) were supplied with pulses of a driving voltage. If the pulse, given to one of the transmitter wires, arrived at a certain wire of the second plane (receiver plane), it was assumed that the crossing point between the two selected wires was occupied by the conducting phase (water). This detection was performed for all crossing points of wires of the two planes by means of two multiplex circuits. The resulting binary information was evaluated by a counter circuit. In the end, the average volumetric fraction of the conducting phase was obtained by relating the number of crossing points occupied with water to the total number of crossing points.

A successful application of a wire-mesh sensor to a fast measurement of gas fraction distributions was presented by Reinecke et al. [B2]. The device consists of three planes of 29 thin wires each (diameter 0.1 mm). The wires of two successive planes are forming an angle of 60 deg. By measuring the impedance between all pairs of adjacent wires belonging to the same plane, a projection of the conductivity distribution along the direction of the wires is recorded. The impedance measurement is carried out with alternating current of high frequency (1 MHz) and the sampling of the individual pairs of electrodes is performed by a multiplex unit. This operation is performed for all three planes. In the result, three independent projections are obtained, which are afterwards transformed into the conductivity distribution within the cross section where the sensor is placed. The distribution is interpreted as the void fraction distribution. The system offers an imaging rate of 112 frames per second. The spatial resolution of the images equals the distance between two adjacent wires. Related to the cross section, this means 1000 pixels.

The transformation into the image has to be performed by applying tomographic image reconstruction algorithms. This is the main disadvantage of that solution. The conductivity measurement provides a total of 3 x (29-1) = 84 linearly independent values of average conductivities along the projecting lines. In the same time, images of the mentioned 1000 pixels are reconstructed. The system of equations to be solved for the image reconstruction is therefore highly underdetermined. The solution is stabilized by additional a-priory knowledge, for example: the local conductivity must be in the interval between the conductivities of the gas and the liquid. Nevertheless, the image reconstruction cannot a-priorily be taken to be free of artefacts. Another disadvantage is high numerical efforts for the iterative image reconstruction algorithm, which are very time consuming.

The aim of the presented work was to develop an electrode mesh device for fast cross-section imaging without the need of time consuming and inaccurate image reconstruction procedures. Further, special emphasis was given to a stable sensor design for hostile conditions in industrial facilities.

## B2 Conception of the FZR device

The idea was to use a sensor similar to the one described in [B1], with a completely new signal acquisition technique [B3]. One plane of electrodes is used as transmitter, the other as receiver plane. A simplified scheme of the device is shown in Fig. B1. During the measuring cycle, the transmitter electrodes are activated by a multiplex circuit in a successive order. The multiplex procedure is realised by closing one of the switches S1 - S4.

The data acquisition for the imaging is achieved by replacing the binary signal integration of [B1] by an evaluation of the analogue current signals from the receiver electrodes. The currents are transformed into voltages by operational amplifiers and sampled by individual sample/hold circuits. After an analogue/digital conversion the signals are recorded by a data acquisition computer connected to AD converters and stored for each receiver electrode separately. This procedure is repeated for all transmitter electrodes. In this way the distribution of the electrical conductivity over the cross section occupied by the sensor is obtained row by row. After the last transmitter electrode has been activated, a two-dimensional matrix of values of current is available that reflects the conductivities between all crossing points of the electrodes of the two perpendicular planes.

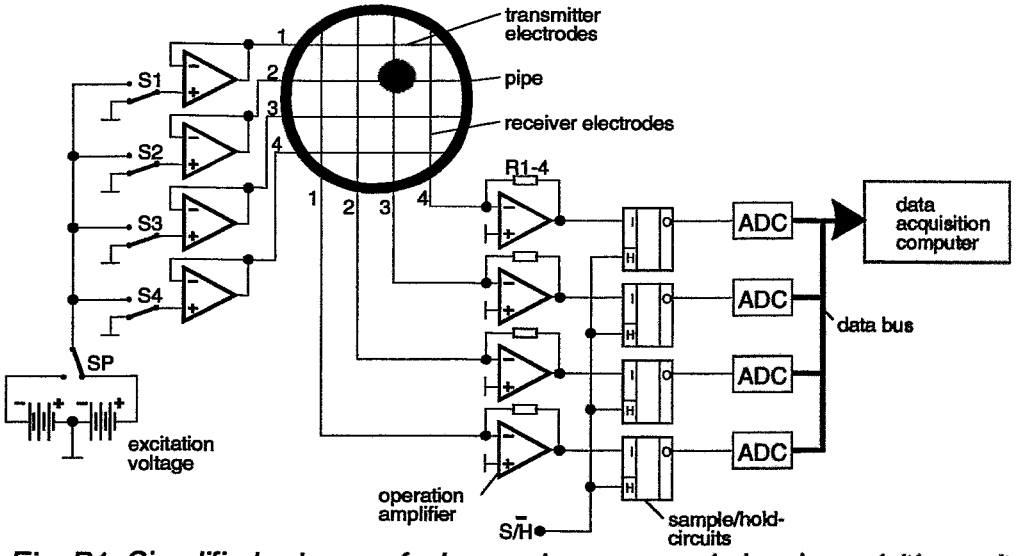


*Fig. B1 Simplified scheme of wire-mesh sensor and signal acquisition unit*

## B3 Pulse modulated driving voltage

The conductivity measurement must not be carried out with direct current, because electrolysis would cause significant measuring errors and, perhaps, may destroy the sensor. Conductometers, for example, usually apply a sinusoidal alternating voltage. Any changes of the conductivity of the fluid are causing a modulation of the sensor current. The instantaneous amplitude carrying the information about the conductivity is derived by demodulating the signal. The demodulation requires a frequency of the supply voltage that is significantly higher than the desired measuring rate.

In order to overcome these difficulties, we use a rectangular pulse to drive the transmitter electrodes. The pulse has a positive and a negative period of the same length and the same absolute amplitude. In this way, the driving voltage is free of any DC components. The excitation of a transmitter electrode results in the appearance of a received electrical current showing a transient behaviour, which is caused by the capacitance of the electrodes, the ion layers in the liquid, and the cables. Instead of a traditional demodulation, the current is sampled after the transient has settled down. This is achieved by triggering the sample/hold circuit (S/H), after the steady state has been established. In the result, the sampled signal reflects the real (i.e. DC) component of the current, that is proportional to the degree to which the area around the crossing point between transmitter and receiver wire is covered with the conducting phase.

### B4 Suppression of cross talk

Despite of arriving at the receiver electrodes, the major part of the driving current, flows from the instantaneously activated transmitter wire to the neighbouring parallel wires, which are at this time not supplied by the driving voltage. Cross talk may happen, when this fraction of current leads to a departure from zero of the potential at these not activated transmitter electrodes. In the consequence, there will be a current to the receiver electrodes from these neighbouring transmitter electrodes, too. The same happens, when the potential of receiver electrodes departs from zero due to the current arriving from the active transmitter electrode. In this case, there will be a current between parallel receiver electrodes. In both cases, the mentioned parasitic currents falsify the result. The main consequence is blurring (loss of spatial resolution) of the acquired images.

For preventing the cross talk both the outputs of the transmitter drivers and the receiver inputs were designed with an impedance, significantly lower than the impedance of the fluid. This guarantees that the potential of all transmitter and receiver electrodes cannot depart from zero, except that one of the instantaneously activated transmitter electrode. In the result, there is no driving potential difference for any electrical current between parallel receiver electrodes or between the not activated transmitter electrodes and the receiver electrodes and the spatial resolution of the sensor is identical with the pitch of the electrode wires.

### B5 Sensor design

The sensor consists of two planes of wire grids with 16 wires of a diameter of 0.12 mm each (Fig. B2). The wires are equally distributed over the diameter, the pitch in both directions is 3 mm. The distance between the two planes is 1.5 mm. In total the sensor disposes of 16 x 16 = 256 cross points. 224 of them are situated inside the circular cross section, the rest is not used.

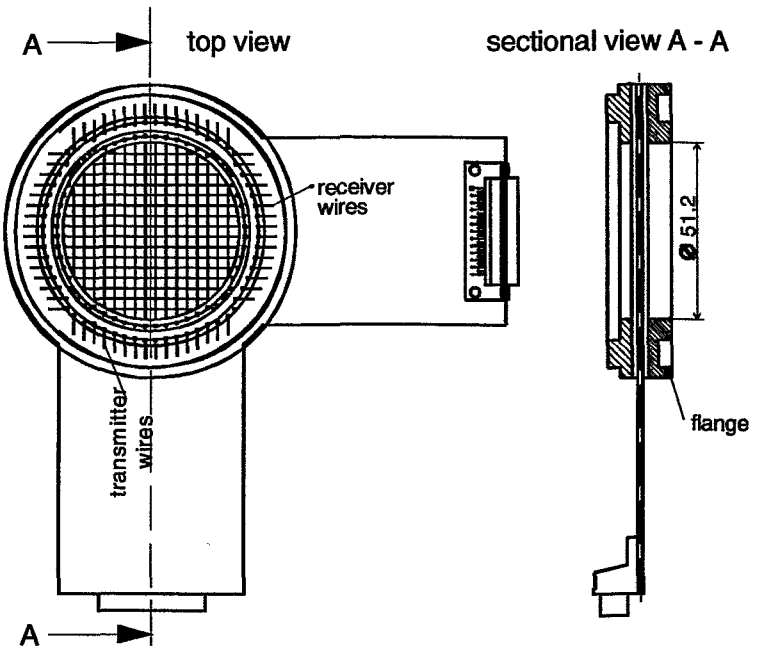


*Fig. B2 Wire-mesh sensor with 16 x 16 measuring points for a 51.2 mm tube*

## B6 Data acquisition unit

Two different signal acquisition units were developed. The first one has a maximum measuring rate of 1200 frames per second. It is closely linked to a data acquisition PC, which takes over the control of the measuring process. The unit itself does not dispose of neither a processor nor a memory block. In order to be able to optimally adapt the signal acquisition unit to the different sensors, a modular structure was chosen. One sensor module is designed for driving 16 transmitter and 16 receiver electrodes. It includes the square-pulse generator, transmitter excitation amplifiers, input pre-amplifiers, Sample & Hold circuits and AD converters. If, for example, a sensor with 32 pairs of electrodes has to be operated, two of these modules must be coupled. In this case, both sensor modules are connected to a single control module that generates the time sequence control signals and controls the data transfer to the data acquisition PC.

A control module implements communication with the data acquisition PC and the time sequence control of the measurement. The necessary logical circuits are contained in a device-specific FPGA (Freely Programmable Gate Array). For the data communication a parallel interface to the ISA bus of the PC with a bus width of 16 bit is used. A special interface card was developed, which has to be placed into the PC. The interface card is linked with the signal acquisition unit of the wire-mesh sensor over an approximately 3 m long cable.

For an increase of the measuring rate from 1200 frames/s to the desired 10 000 Hz, a second type of signal acquisition unit was developed [B6]. It was necessary to decrease the build-up time of the preamplifiers and to speed-up the data transfer from the signal acquisition unit to the data acquisition PC. It turned out, that the high quantity of data produced at 10 000 frames per second cannot be transferred on-line. In the consequence, the data acquisition module was equipped with an own

memory unit. This led to a completely new conception with the following modifications compared to the first device version. Main difference is the introduction of a DSP (digital signal processor) for the autonomous control of the entire signal acquisition procedure. The measured data (up to 170.000 frames) are stored in a buffer memory controlled by the DSP. The data transfer between signal acquisition unit and data acquisition PC is carried out via an Ethernet interface. Ethernet is a non-expensive interface for bridging large distances with quite good rates. Furthermore, the PC has not to be equipped with any special hardware but a standard network card. The transmission is done in blocks of 240 measuring values, using TCP/IP and the UDP protocol. On the analogue side, the sixteen output cascades driving the transmitter electrodes and the current-to-voltage converter cascades of the preamplifiers were put into separate functional units, which are directly plugged to the connectors of the sensor. The cables carry pre-amplified signals, which helps to reduce noise and to decrease the transient time of the amplifiers.

The reference measurements in the frame of the present project were carried out with the wire-mesh sensor of the first generation, i.e. the maximum time resolution was 1200 frames per second. In some of the tests, the measuring frequency was decreased in order to work with an integer multiple of the measuring frequency of the ultrasonic mesh sensor.

## B7 References


[B1] I. D. Johnson, (1987). Method and Apparatus for Measuring Water in Crude Oil, *United States Patent* No 4,644,263, 1987 February 17th.

[B2] N. Reinecke, M. Boddem, G. Petritsch, D. Mewes, (1996). Tomographisches Messen der relativen Phasenanteile in zweiphasigen Strömungen fluider Phasen, *Chemie Ingenieur Technik* **68,** pp. 1404-1412.

[B3] H.-M. Prasser, A. Böttger, J. Zschau (1998). A new electrode-mesh tomograph for gas-liquid flows, *Flow Measurement and Instrumentation* **9**, pp. 111-119.

[B4] A.-K. Krüssenberg, H.-M. Prasser, A. Schaffrath, A., (2000). A new criterion for the identification of the bubble slug transition in vertical tubes, *Kerntechnik*, **65/1**, pp. 7-13.

[B5] H.-M. Prasser, (1999). Measurement of gas fraction, gas velocity and volume flow by electrode mesh sensors, *Proceedings of ECCE 2 - Second European Congress of Chemical Engineering,* Montpellier, France, October 05th-07th, 1999, CDROM 11280001.pdf.

[B6] H.-M. Prasser, J. Zschau, D. Peters, G. Pietzsch, W. Taubert, M. Trepte, (2000). Wire-mesh sensor - now 10,000 frames per second, *Annual Report of Institute of Safety Research*, FZR-284, February 2000, ISSN 1437-322X, pp. 15-18.

# Appendix C

## Description of the needle-shaped void probes

### C1 Measuring principle

The local void fraction measurement is based on a local detection of the instantaneous electrical conductivity of the fluid. Each needle probe consists of a thin electrode wire, which is insulated by a small ceramic tube. At its end it is in contact with the fluid. The electrode is supplied with a small voltage. When the liquid phase is covering the tip of the probe, an electrical current is flowing from the tip towards the counter electrode, which is formed by the metallic protection tube of the probe or by the walls of the test equipment. This current is sampled with a certain rate. Any gas bubble coming in contact with the probe interrupt the current. In the result, the primary signal shows characteristic bubble pulses, Fig. C1.

The signal acquisition system performs an analysis of the signal. For a given measuring period $t_{meas}$ the maximum $I_{max}$ and the minimum $I_{min}$ of the raw signal is found. From this, a discrimination level is determined, which is used to binarise the raw signal. The level is defined as 65 % of the electrical current characteristic for the contact of the probe tip with the conducting liquid phase. It is calculated from the extreme values as follows:

$$I_{L35} = I_{max} - \Theta \cdot (I_{max} - I_{min}) \quad \text{with} \quad \Theta = 0.35 = 35\,\% \tag{1}$$

Were $\Theta$ is the threshold ratio. The binarisation is carried out by comparing the current value of the signal with the discrimination level. This results in a binary information b(t), which is set to 1 when the signal is below the level, i.e. when the decrease of the probe current has reached 35 % of the total signal amplitude (Fig. C1).

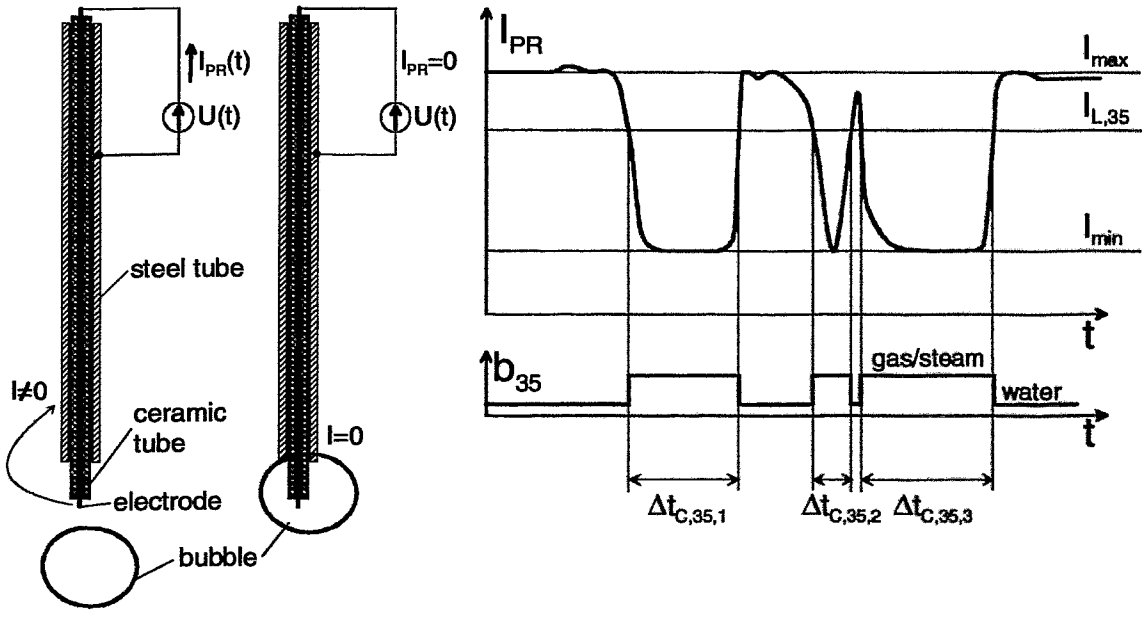


Fig. C1 Principle of function of needle-shaped conductivity probes

It is interpreted as presence of the gas phase at the probe tip. By means of counting pulses of a timer unit, the integral time of gas contact within the measuring period is obtained. Finally, the local void fraction is calculated by relating the total contact time to the measuring period:

$$\alpha_{35} = \frac{\sum t_{c,35,i}}{t_{meas}} = \frac{t_{c,35}}{t_{meas}} \qquad (2)$$

Void fraction values averaged over the measuring period according to eq. (2) are generated with a rate which is equal to the measuring period. In case of the given measuring system, the masuring period is $t_{meas} = 1$ s. Due to the fact the slopes of the probe current signal are inclined, the choice of the threshold influences the measuring result. The closer the threshold is chosen to the signal level characteristic for liquid, the higher is the measured void fraction. In order to provide information to assess this influence, a second threshold is introduced:

$$I_{65} = I_{max} - \Theta \cdot (I_{max} - I_{min}) \quad \text{with} \quad \Theta = 0.65 = 65\,\% \qquad (3)$$

With this threshold ratio, a second void fraction is determined similar to the signal evaluation shown in Fig. C1:

$$\alpha_{65} = \frac{\sum t_{c,65,i}}{t_{meas}} = \frac{t_{c,65}}{t_{meas}} \qquad (4)$$

It always holds that $\alpha_{65} < \alpha_{35}$. The difference between these two results can be used to assess the measuring error caused by the slopes of the signal. Usually, it is assumed that the threshold, which is closer to the signal level characteristic for the liquid phase ($I_{L35}$), delivers better results.

Additionally to the determination of time-averaged local void fractions, the signal acquisition unit stores an information about each individual phase change. For this purpose, a counter variable is increased at each sampling action. In the following cases an entry is made into a buffer memory together with storing the current value of this counter (clock): (1) when the probe current becomes less than $I_{L65}$ (signal changes to "gas/steam"), (2) when the probe current becomes greater than $I_{L35}$ (signal changes to "liquid"). These entries can be used to obtain advanced information about the flow structure. The difference between both thresholds is playing the role of a hysteresis band, which prevents the generation of false phase change entries caused by signal fluctuations (noise), when the signal is crossing the threshold level.

The signal evaluation according to Fig. C1 is carried out digitally in the signal acquisition unit. The raw probe current is transformed into a voltage by analogue input cascades with logarithmic characteristics. The resulting voltage is sampled with a frequency of 8192 Hz by a 12 bit ADC. The AD result is an integer number in the range between 0 and 4095. In one measuring period are therefore recorded 8192 AD results, which are stored in a buffer. It corresponds to the input voltage of the ADC in [mV], because the reverence voltage is 4.095 V.

$$U \cong C_{ln} \cdot \ln(I_{Pr}/I_0) \qquad (5)$$

Where $I_0$ and $C_{ln}$ are constants characterising the logarithmic amplifier. Due to the logarithmic characteristic of the analogue cascades, the threshold must also be converted into a logarithmic value.

$$U_{L35} = C_{ln} \cdot \ln(e^{\frac{U_{max}}{C_{ln}}} - \Theta \cdot (e^{\frac{U_{max}}{C_{ln}}} - e^{\frac{U_{min}}{C_{ln}}}) \quad \text{with} \quad \Theta = 0.35 = 35\ \% \tag{6}$$

and for the 65 % threshold respectively:

$$U_{L65} = C_{ln} \cdot \ln(e^{\frac{U_{max}}{C_{ln}}} - \Theta \cdot (e^{\frac{U_{max}}{C_{ln}}} - e^{\frac{U_{min}}{C_{ln}}}) \quad \text{with} \quad \Theta = 0.65 = 65\ \% \tag{7}$$

With these voltage thresholds, the discrimination of the AD results (eq. 5) is identical to the discrimination of the probe current by the probe threshold defined in eq. (1) and (3).

$U_{min}$ and $U_{max}$ are obtained from the stored AD results by a digital peak detection procedure. The raw signal U is low-passed by a digital filter with a time constant of 4 ms before the peak detection in order to suppress the influence of signal noise to the peak values.

## C2 Probe assembly

The assembly consists of 8 needle-shaped conductivity probes. The probes were placed into the vertical test section of MTLoop in a way, that their sensitive tips were located at the same elevation but on different radial postions. For this purpose, the probes were put into a cone-shaped support with 8 tapholes equally distributed over the perimeter. The angle between the probes and the flow direction was 45 deg. Table C1 gives the angles and the radial positions of the probes:

*Table C1 Needle probe co-ordinates in MTLoop*

| Probe | Angle [deg] | Radius [mm] | Distance from the wall [mm] |
|---|---|---|---|
| 1 | 0 | 23.6 | 2 |
| 2 | 180 | 21.6 | 4 |
| 3 | 270 | 18.6 | 7 |
| 4 | 90 | 15.6 | 10 |
| 5 | 135 | 12.6 | 13 |
| 6 | 315 | 8.6 | 17 |
| 7 | 225 | 4.6 | 21 |
| 8 | 45 | 0 | 25.6 |

A view of the probe assembly is shown in Fig. C2. Probe 1 turned out to be not available during the measurements with the ultrasonic mesh sensor, because the insulation resistance of this probe was too low.

## C3 Assessment of the accuracy of the probes

The accuracy was assessed by comparing the readings of the probes with an integral void fraction measurement using a gamma-densitometer. The

measurements were carried out with the set of 8 needle probes in the regime of an air-water flow in the following range of superficial velocities: $0 < J_{Air} < 12$ m/s, $0 < J_{Water} < 4$ m/s. The reference gamma-densitometer was equipped with a Cs-137 source of $4.8 \cdot 10^8$ Bq (13 mCi). It is shown in Fig. C3. The part of the vertical test section with probes, ultrasonic mesh sensor and gamma-device is shown in Fig. C4.

Since the gamma-device delivers void fractions averaged over the gamma beam, the comparison with the probes was carried out on the basis of a calculated line average of the local void fractions measured by the probes. It was found that the probes underestimate the void fraction by a maximum absolute deviation of 10 % at void fractions around 50 %, Fig. C5.

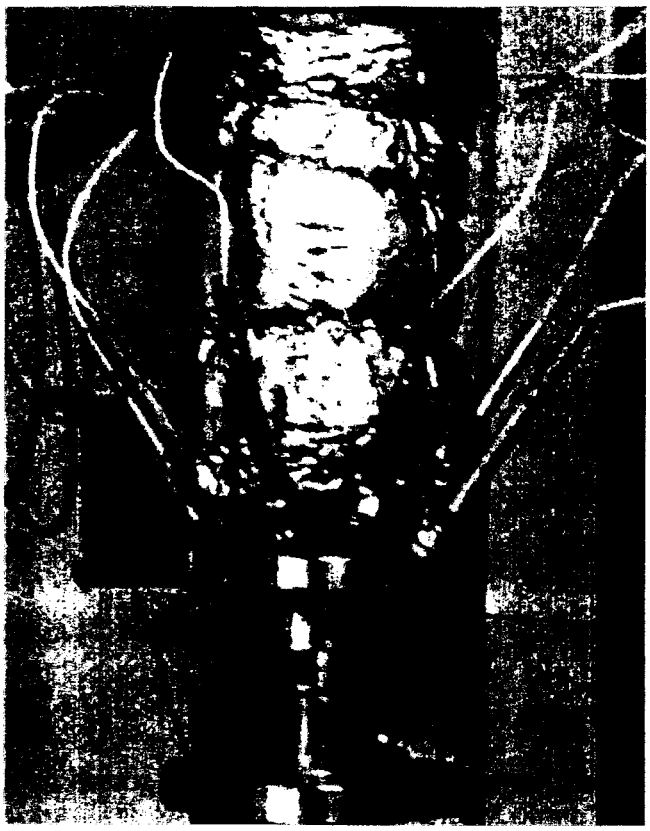

*Fig. C2 Assembly of needle-shaped conductivity probes at MTLoop*

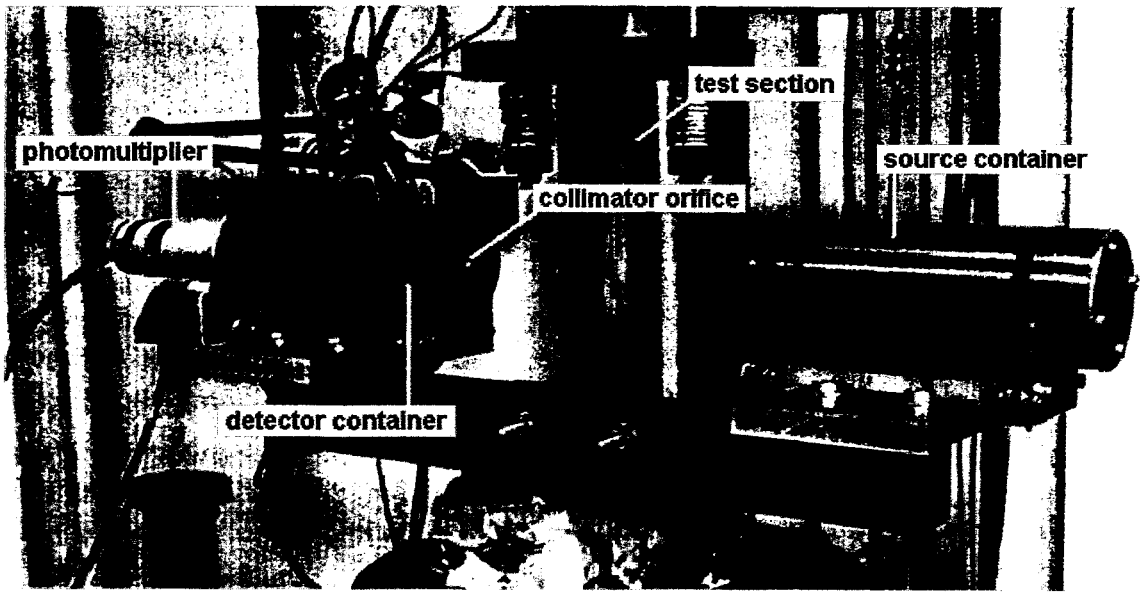


*Fig. C3 Gamma-Densitometer at MTLoop*

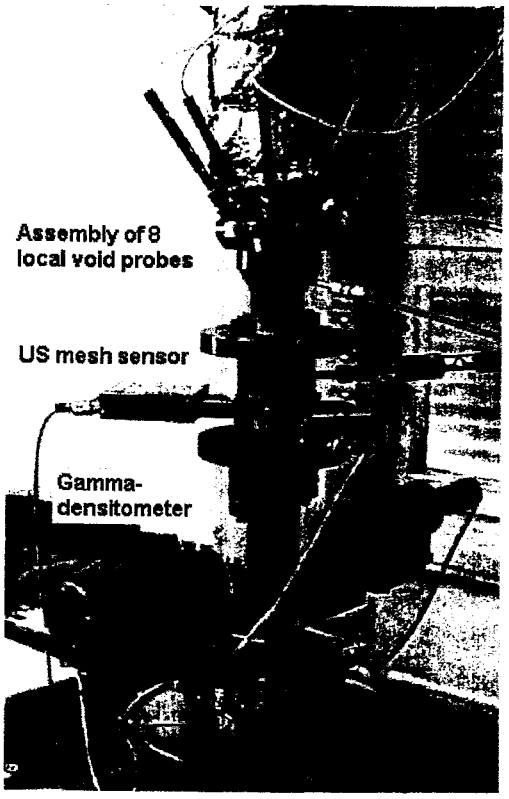


*Fig. C4 Upper part of the vertical test section of MTLoop*

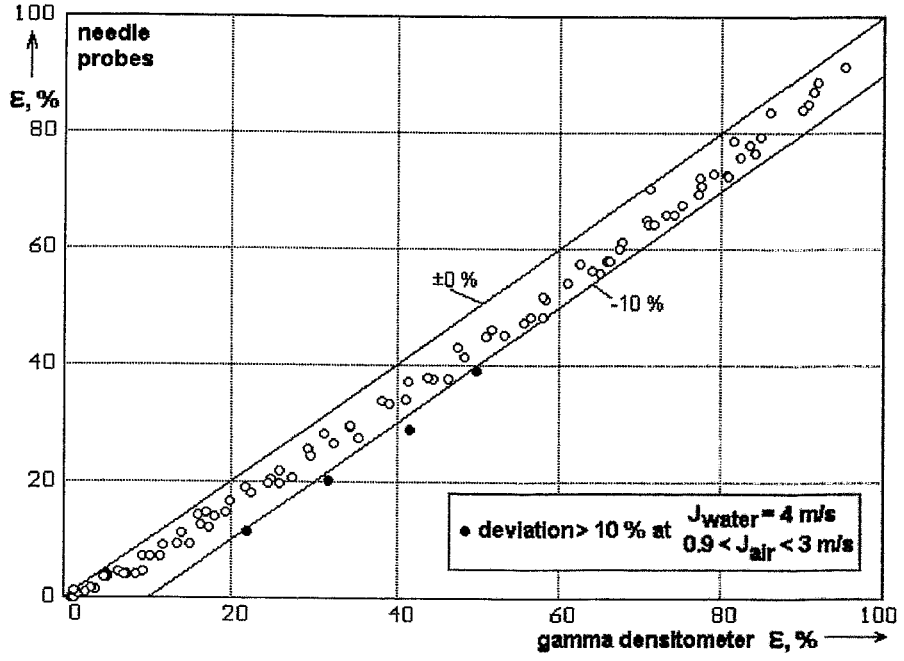


*Fig. C5 Comparison between needle-shaped void probes and a gamma-densitometer*

## Appendix D

## List of Figures

## Appendix E

## List of Tables